Electronic Supplementary Information

for the manuscript entitled

Visible Light Mediated Photocatalysis by Lanthanide Metal-Organic Frameworks: Enhanced Specificity and Mechanistic Insights

Ruchika Gupta,[a] Aashish,[a] Upma,[a] Shubhangi Majumdar,[b] Pramit K. Chowdhury[b] and Rajeev Gupta*[a]

[a] Department of Chemistry, University of Delhi, Delhi-110007 (India)
[b] Department of Chemistry, Indian Institute of Technology – Delhi, Delhi-110016 (India)

Contents

Experimental section

Materials

All chemicals, reagents and solvents of analytical grades were used without any purification unless otherwise stated. The precursor, methyl(*E*)-3-(4-aminophenyl)acrylate was synthesized as per the literature report.[1]

Synthesis

Synthesis of ligand

$H_2L^{p\text{-}COOMe}$ (**L**). Pyridine-2,6-dicarboxylic acid (1.00 g, 5.98 mmol) and methyl-(*E*)-3-(4-aminophenyl)acrylate (2.12 g, 11.96 mmol) were taken in 10 mL pyridine and the resulting mixture was refluxed with stirring for 30 min at 85 °C. Triphenyl phosphite (4.08 g, 13.16 mmol) was added drop-wise over 10 min to the aforementioned reaction mixture. The reaction mixture was finally stirred at 100 °C for 8 h. After cooling to room temperature, a colourless precipitate resulted that was filtered and washed with ice-cold water, followed by diethyl ether, and dried under vacuum. Yield: 2.78 g (96 %). ^{1}H NMR spectrum (400 MHz, DMSO-d_6) δ 11.20 (s, 2H), 8.44 (d, J = 7.7 Hz, 2H), 8.36 – 8.31 (m, 1H), 8.05 (d, J = 8.4 Hz, 4H), 7.81 (d, J = 8.4 Hz, 4H), 7.61 (d, J = 15.9 Hz, 2H), 6.53 (d, J = 16.0 Hz, 2H), 3.60 (s, 6H). ^{13}C NMR spectrum (100 MHz, DMSO-d_6) δ 168.23, 162.24, 149.10, 143.87, 140.60, 140.30, 130.60, 129.49, 126.07, 121.30, 118.59, 47.06. FTIR spectrum (selected peaks, ν/cm^{-1}): 3366 (N–H), 1702 ($COOCH_3$), 1511 (C=O). Anal. Calc. for $C_{27}H_{23}N_3O_6$: C, 66.80; H, 4.78; N, 8.66. Found: C, 66.42; H, 4.58; N, 8.42 (Figs. 1 – 3, ESI†).

Synthesis of metalloligand

$Na[Co(L^{p\text{-}COOMe})_2]$ (**1^P**). Ligand **L** (100.00 mg, 0.20 mmol) was dissolved in a N_2 flushed DMF (10 mL) and treated with solid NaH (11.00 mg, 0.45 mmol). After stirring the resultant mixture for 30 minutes at room temperature, solid $Co(OAc)_2.2H_2O$ (25.65 mg, 0.10 mmol) was added. After 30 minutes, dry O_2 was purged for 10 minutes to the above reaction mixture and the reaction mixture was stirred for further 4 h. The reaction mixture was filtered followed by the removal of solvent under the reduced pressure. The crude product was isolated after washing with diethyl ether. The crude product was re-dissolved in DMF and subjected to the vapour diffusion of diethyl ether which afforded a crystalline product within 3-4 days. Yield: 190.00 mg (90 %). ^{1}H NMR spectrum (400 MHz, DMSO-d_6) δ 7.95 (d, J = 3.5 Hz, 1H), 7.61 (d, J = 7.7 Hz, 2H), 7.43 (d, J =

16.0 Hz, 2H), 7.27 (d, J = 8.3 Hz, 4H), 6.67 (d, J = 8.3 Hz, 4H), 6.45 (d, J = 16.0 Hz, 2H), 3.68 (s, 6H). ^{13}C NMR spectrum (100 MHz, DMSO-d_6) δ 167.34, 167.05, 149.16, 144.99, 140.18, 138.67, 129.72, 128.59, 126.95, 124.18, 116.46, 51.81. FTIR spectrum (selected peaks, ν/cm^{-1}): 1684 ($COOCH_3$), 1532 (C=O). Anal. Calc. for $C_{54}H_{42}CoN_6NaO_{12}$. Calc: C 63.22; H 4.13; N 8.19. Found: C 63.25; H 4.05; N 8.18 (Figs. 4 – 6, ESI†).

Na[Co($L^{p\text{-}COOH}$)$_2$] (**1**). The metalloligand **1** was obtained after the base-assisted hydrolysis of **1^{P}**. The compound **1^{P}** (100.00 mg, 0.47 mmol) was dissolved in a mixture of THF/H_2O (3:1, v/v) and treated with 4 equiv. of NaOH (77.00 mg, 1.91 mmol). The said reaction mixture was stirred for 8 h at room temperature. The resulting solution was neutralized using 4 N HCl. Removal of THF under vacuum resulted in the precipitation of a product which was filtered and air-dried. This product was recrystallized from DMSO-H_2O, which produced a highly crystalline product within 4−5 days. Yield: 88.00 mg (93 %). ^{1}H NMR spectrum (400 MHz, DMSO-d_6) δ 8.01 (s, 1H), 7.66 (s, 2H), 7.39 (s, 2H), 7.26 (s, 4H), 6.72 (s, 4H), 6.36 (s, 2H). ^{13}C NMR spectrum (100 MHz, DMSO-*d6*) δ 168.22, 167.10, 156.41, 148.90, 144.40, 140.16, 129.94, 128.45, 127.01, 124.28, 117.84. FTIR spectrum (selected peaks, ν/cm^{-1}): 1554 (C=O). Anal. Calc. for $C_{50}H_{34}CoN_6NaO_{12}$. Calc: C 61.93; H 3.53; N 8.67. Found: C 61.88; H 3.48; N 8.52 (Figs. 7 – 9, ESI†).

Synthesis of lanthanide MOFs

*[{(**1**)Tb(DMSO)(H_2O)$_3$}·8H_2O·DMSO]* (**1-Tb**). An aqueous solution of Tb(CF_3SO_3)$_3$ (60.61 mg, 0.10 mmol) was layered over a DMSO solution of metalloligand **1** (50.00 mg, 0.05 mmol) with an intermediate layer of *tert*-butanol. Dark green coloured, needle shaped crystals were obtained in a week which were filtered, washed with diethyl ether and dried under vacuum. Yield: 72.00 mg (93 %). FTIR spectrum (selected peaks, (ν/cm^{-1}): 1562 (C=O), ν(H_2O): 3299, ν(S=O, DMSO): 1002. Anal. Calc. for $C_{54}H_{61}CoTbN_6O_{25}S_2$. Calc.: C, 43.94; H, 4.17; N, 5.69; S, 4.34. Found C, 43.81; H, 4.14; N, 5.68; S, 4.23. Absorption spectrum (solid state, λ_{max}/nm): 625, 433.

*[{(**1**)Eu(DMSO)(H2O)$_2$}·2H_2O]* (**1-Eu**). **1-Eu** was synthesized following a same procedure as mentioned for **1-Tb**; however, using Eu(CF_3SO_3)$_3$ (59.92mg, 0.10 mmol). Green colored, needle shaped crystals were obtained after 4-5 days which were filtered, washed with diethyl ether and dried under vacuum. Yield: 60.00 mg, 91.00 %. FTIR spectrum (selected peaks, (ν/cm^{-1}): 1564 (C=O), ν(H_2O): 3288, ν(S=O, DMSO): 1003. Anal. Calc. for $C_{51}H_{41}CoEuN_6O_{17}S$. Calc.: C 48.89;

H 3.30; N 6.71; S 2.56. Found C 48.70; H 3.05; N 6.88; S 2.68. Absorption spectrum (solid state, λ_{max}/nm): 620, 425.

General Procedure for the Photocatalytic Oxidation Reactions

Typically, 0.92 mmol substrate and 10 mg **1-Tb** were suspended in 2 ml H_2O in a 25 ml round-bottom flask for the oxidation of alcohols. Oxygen was bubbled into the mixture for 5 min using an oxygen balloon and the reaction vessel was then irradiated with a white LED lamp under magnetic stirring. The progress of the reaction was monitored by thin-layer chromatography (TLC). After the reaction was completed, catalyst was removed by centrifugation. The product(s) were isolated and characterized with the help of ^{1}H and ^{13}C NMR spectroscopy and ESI^{+} mass spectrometry. Similarly, the photocatalytic experiments for the oxidation of sulfides were carried using 0.80 mmol substrate and 10 mg of **1-Tb** suspended in 2 ml MeOH.

Physical methods

Elemental analysis data were obtained with an Elementar Analysen Systeme GmbH Vario EL-III instrument. FTIR spectra were recorded with an Agilent Cary 630 spectrometer having a diamond ATR. UV-Vis diffuse reflectance spectra were measured on a PerkinElmer Lambda-35 spectrophotometer while solution absorption spectra were recorded using the PerkinElmer Lambda-950 spectrophotometer. NMR spectroscopic measurements were carried out with a Jeol 400 MHz spectrometer. Thermal gravimetric analysis (TGA) and differential scanning calorimetry (DSC) were performed with Shimadzu DTG-60 and TA-DSC Q200 instruments, respectively at 10 °C/min^{-1} heating rate under a nitrogen atmosphere. Gas chromatography studies were performed with a PerkinElmer Clarus 580 equipped with an RTX-5SIL-MS column. X–ray powder diffraction (PXRD) studies were performed with a Bruker AXS D8 Discover instrument (Cu Kα radiation, λ = 1.54184 Å). The samples were ground and subjected to the range of θ = 5–50° at a slow scan rate at room temperature. Optical images of the crystals were taken with an OLYMPUS BX53 M optical microscope using the software OLYMPUS stream basic 2.3 (Build 16979). SEM and EDX measurements were performed with a Jeol SM 6610 LV instrument. EPR spectral studies were carried out with a Bruker A300-9.5/12/S/W instrument. X-ray photoelectron spectroscopy (XPS) studies were carried out using Kratos Analytical Axis Supra model. Fluorescence spectral studies were performed with a Cary Eclipse fluorescence spectrometer. Photoluminescence studies were performed using a QM-8450-11 Quanta master Up-conversion and down-conversion fluorescence spectrometer with a 450W Xe source lamp. ESI^{+}-MS spectra

were recorded on an Agilent G6530AA spectrometer. EIS measurements were performed using a Broadband dielectric spectrometer. The steady-state phosphorescence spectra were collected on HORIBA DeltaFlex TM spectrophotometer. Mott–Schottky measurements were conducted using a CHI 660E electrochemical workstation equipped with Pt and Ag/AgCl electrodes as the counter and reference electrodes, respectively. The working electrode was prepared on a graphite sheet while 0.2 M of Na_2SO_4 solution was used as an electrolyte and the measurements were carried out at two different frequencies (0.5 and 1.0 kHz). A 5W LED lamp (450 lumens, 35.81 cd) was used as the light source for the photocatalytic experiments.

X-ray diffraction studies

X-ray diffraction data for **1-Tb** and **1-Eu** were collected either on a Bruker SMART APEX-II CCD or a Rigaku Oxford XtaLAB Synergy-DW diffractometer equipped with a graphite monochromatic MoKα radiation (λ = 0.71073 Å). The frames were collected at 273 and 298 K for **1-Tb** and **1-Eu**, respectively. SMART was used for collecting frames of data, indexing reflections, and determining lattice parameters; SAINT was used for integration of the intensity of reflections and scaling; and SADABS was used for absorption correction.[2] The crystal structures were solved and refined by full-matrix least-squares refinement techniques on F^2 by using the program SHELXL-97 incorporated in WinGX crystallographic collective package version 1.70.[3] Further structure refinements were performed using Olex2 programme.[4] The crystallographic data collection and structure solution parameters for **1-Tb** and **1-Eu** are presented in Table 1, ESI† whereas selected bond distances and bond angles are described in Tables 2-5, ESI†. CCDC Nos. 2288468 (**1-Tb**) and 2288469 (**1-Eu**) contain the supplementary crystallographic data for this paper.

Transient absorption spectroscopy

Ultrafast transient absorption spectral measurements were conducted using a commercial one-box ultrafast Ti: Sapphire amplifier (Astrella 1K-F, Coherent Inc.) coupled to a femtosecond transient absorption spectrometer (Helios Fire UV-VIS, Ultrafast Systems). The amplified pulses of 100 fs duration were obtained after seeding with 20 femtosecond 70 nm bandwidth laser pulses obtained from an integrated oscillator (Vitara-S, 400 mW at 800 nm, 80 MHz) pumped by Verdi-G. The amplified output of central wavelength 800 nm (5mJ/pulse, 1 kHz) was divided into two parts. One part (~200 mW) was used to produce the femtosecond probe pulse by focusing it either on a

CaF_2 (for UV probe: 310 – 600 nm) or a 2-mm thick sapphire crystal for generating white light continuum (400-800 nm) while the other part (3.25 mW) was used to generate a tunable femtosecond pump pulse using an optical parametric amplifier (Coherent OPeraASolo, 290-2600 nm). After the sample, the probe beam (1 kHz) was collimated and then focused onto a fiber-optics coupled multichannel spectrometer equipped with CMOS sensor (1024 pixels). The pump power of the pump pulse used in the experiment was controlled by a variable neutral-density filter wheel and was kept at ~1 mW. Both the pump and probe beams were overlapped at the sample cuvette and the delay between the pump and probe pulses was controlled by a motorized delay stage. The pump pulses were chopped by a synchronized chopper at 500 Hz and the absorbance change was calculated with two time-adjacent probe pulses (pump-blocked and pump-unblocked).

Calculation of Band Gap

The band gap energy of Ln-MOFs (**1-Tb** and **1-Eu**) was calculated using the Tauc plot, according to the energy dependence relationship of $\alpha h\nu = (h\nu - E_g)^n$ where α and E_g are the absorption coefficient and the energy gap of a semiconductor, respectively. The value of n depends on whether the optical transition of a semiconductor is direct (n = ½) or indirect (n = 1). The band gap is then calculated by fitting linearly the plot of $(\alpha h\nu)^n$ versus photon energy ($h\nu$).[5]

Kinetic Studies

The kinetics for the photo-oxidation of benzyl alcohol and thioanisole were studied under the first-order conditions and monitored by using the gas chromatography, with respect to the concentration of a respective substrate. The rate constant (k) was calculated from the slope of the linear plot of $\ln(C_t/C_o)$ against time, where, (C_t/C_o) is the ratio of concentration of the substrate at a certain time 't' to that of initial time '0'. For these studies, a standard calibration curve was generated for the photo-oxidation of benzyl alcohol and thioanisole using phenol and dimethylsulfide, respectively.

Assay for the Detection of Hydroxyl Radicals

A 10 mg sample of **1-Tb** was suspended in an aqueous solution (containing 0.5 % MeCN) of 0.5 mM coumarin and was subjected to visible light irradiation. The hydroxyl radical concentration was measured by evaluating a change in the emission spectra for the generation of 7-hydroxycoumarin as a function of time (λ_{ex} = 350 nm).[6] The hydroxyl radical concentration for **1-Zn** was calculated in a similar manner, however, using a 2 mg sample of **1-Zn**.

Assay for the Detection of Superoxide Radicals

A 10 mg sample of **1-Tb** was suspended in a DMSO solution of 0.5 mM NBT and was subjected to visible light irradiation. The concentration of superoxide radicals was measured by evaluating a change in the absorption spectra as a function of time. The molar extinction coefficient of monoformazan in DMSO was 12×10^4 $M^{-1}cm^{-1}$.[7]

Assay for the Detection of Singlet Oxygen

To evaluate the generation of singlet oxygen by **1-Tb** upon visible light irradiation, two classical probes were employed.

(i) 9,10-Dimethylanthracene (DMA)

A 10 mg sample of **1-Tb** was suspended in an aqueous solution (containing 1 % MeCN) of 2 mM DMA and was subjected to visible light irradiation. The concentration of $^1O_2$ was measured by evaluating a change in the emission spectra as a function of time.[8]

(ii) 1,5-Dihydroxynapthalene (DHN)

A 10 mg sample of **1-Tb** was suspended in an aqueous solution (containing MeCN/MeOH (4:1), v/v) of 2 mM DHN and was subjected to visible light irradiation. The concentration of singlet oxygen was measured by evaluating a change in the absorption spectra as a function of time. The molar extinction coefficient of 5-hydroxy-1,4-napthalenedione (juglone) was 3811 $M^{-1}cm^{-1}$.[9] Additionally, rate constant (k) for the formation of juglone was calculated from the slope of the linear plot of $\ln(C_t/C_o)$ against time, where, (C_t/C_o) is the ratio of concentration (absorbance) at a certain time 't' to that of initial time '0'. All C_o and C_t values were obtained by the maximum absorption (absorbance at λ_{max}) in the entire absorption spectrum.

Detection of Hydrogen Peroxide

Two classical methods were employed to evaluate the generation of H_2O_2.

(i) By UV-Vis Spectroscopy

When an excess amount of I is added to a solution containing H_2O_2, I is oxidized to I_2 by H_2O_2. Subsequently, I_2 further reacts with the I ion to form tri-iodide ion (I_3), which shows two characteristic spectral features at ca. 300 and 350 nm in its UV-Vis spectrum. Thus, formation of H_2O_2 was monitored by the formation of tri-iodide in aqueous solution.[10]

$$I \xrightarrow{H_2O_2} I_2 \xrightarrow{H_2O_2} I_3$$

(ii) Titration with $KMnO_4$

The highly oxidizing purple colored MnO_4^- ion can be reduced by H_2O_2 to generate colorless Mn^{2+} ion under an acidic condition, according to the following equation:

$$5H_2O_2 + 2\ MnO_4^- + 6H^+ \longrightarrow 2Mn^{2+} + 5O_2 + 8H_2O$$

(purple) (colourless)

The concentration of H_2O_2 can be calculated according to the following equation:

$$C_{H2O2} = C_{KMnO4} \times V_{KMnO4}/V_{\text{reaction mixture}}$$

In this case, 0.1 mL of a 2μM $KMnO_4$ solution was used to reduce 1 mL of a reaction mixture containing H_2O_2. Accordingly, the concentration of H_2O_2 was estimated.[11]

Transient Absorption Spectroscopy Experiments

A sample was taken in DMSO in a 2 mm quartz cuvette and stirred constantly by a magnetic stirrer during the measurements. For transient absorption spectral measurements, 375 nm was used as the pump wavelength, and sapphire crystal for visible range white light as the probe. Concentrations of the freshly prepared samples were adjusted to 2-4 mOD in a 2mm quartz cuvette. To check charring or any damage to the sample during transient absorption spectral measurements, ground state absorption spectra were taken before and after laser exposure and there was no change in the spectra. Surface Xplorer version 4.5 and Glotaran version 1.5.1.1,2 were used to analyse the transient absorption spectral data.

Calculations of Decay Time

The transient decays were fitted by using equation (1), using a deconvoluting IRF of ~150 fs with the help of Surface Xplorer software and averaged lifetimes were calculated according to equation (2), where ΔA (λ, t) is the observed change in absorbance at time t and wavelength λ, A is amplitude and τ_i is the time constant of i^{th} components.[12]

$$\Delta A\ (\lambda, t) = A_0 + \sum_i A_i e^{-\frac{t}{\tau_i}} \qquad \text{(eqn. 1)}$$

$$< \tau >= \frac{\sum_i A_i \tau_i}{\sum_i A_i} \qquad \text{(eqn. 2)}$$

Global Analyses

Global analyses of the ultrafast decay kinetics were carried out with the help of fitting software Glotaran.[13,14] The global analyses are based on the singular value decomposition (SVD) method and the fitted global decays were used to plot the decay associated spectra (DAS). Independent

single wavelength kinetic fits for a series of such decays along with the global fits were also compared to ascertain the reliability of the global analyses.

Characterization data for organic products

1. *Benzaldehyde* (**1a**). Colorless liquid, **^{1}H NMR** spectrum (400 MHz, $CDCl_3$) δ 10.01 (s, 1H), 7.90 – 7.87 (m, 2H), 7.66 – 7.60 (m, 1H), 7.52 (t, J = 7.5 Hz, 2H). **^{13}C NMR** spectrum (100 MHz, $CDCl_3$): δ 192.58, 136.36, 134.54, 129.79, 129.02.
2. *4-(trifluoromethyl)benzaldehyde* (**1b**). Yellow liquid, **^{1}H NMR** spectrum (400 MHz, $CDCl_3$) δ 10.11 (s), 8.02 (d, J = 7.9 Hz), 7.82 (d, J = 7.8 Hz). **^{13}C NMR** spectrum (100 MHz, $CDCl_3$): δ 191.05, 141.37, 130.62, 125.57, 106.74.
3. *Fluorobenzaldehyde* (**1c**). Yellow liquid, **^{1}H NMR** spectrum (400 MHz, $CDCl_3$): δ 9.97 (s, 1H), 7.95–7.89 (m, 2H), 7.26–7.19 (m, 2H). **^{13}C NMR** spectrum (100 MHz, $CDCl_3$): δ 190.60, 167.78, 132.29, 132.20, 116.45.
4. *Chlorobenzaldehyde* (**1d**). Yellow liquid, **^{1}H NMR** spectrum (400 MHz, $CDCl_3$): δ 9.99 (s, 1H), 7.85–7.81 (m, 2H), 7.55–7.49 (m, 2H). **^{13}C NMR** spectrum (100 MHz, $CDCl_3$): δ 190.94, 141.01, 134.71, 130.94, 129.49.
5. *Bromobenzaldehyde* (**1e**). White solid, **^{1}H NMR** spectrum (400 MHz, $CDCl_3$): δ 9.98 (s, 1H), 7.75 (d, J = 8.5 Hz, 2H), 7.69 (d, J = 8.4 Hz, 2H). **^{13}C NMR** spectrum (100 MHz, $CDCl_3$): δ 191.12, 135.06, 132.46, 131.00, 129.80.
6. *Anisaldehyde* (**1f**). Colorless liquid, **^{1}H NMR** spectrum (400 MHz, $CDCl_3$): δ 9.88 (s, 1H), 7.88–7.80 (m, 2H), 7.04–6.98 (m, 2H), 3.88 (s, 3H). **^{13}C NMR** spectrum (100 MHz, $CDCl_3$): δ 190.94, 164.70, 132.07, 130.01, 114.39, 55.65.
7. *Salicaldehyde* (**1g**). Yellow liquid, **^{1}H NMR** spectrum (400 MHz, $CDCl_3$): δ 11.03 (s, 1H), 9.88 (s, 1H), 7.57–7.49 (m, 2H), 7.04–6.97 (m, 2H). **^{13}C NMR** spectrum (100 MHz, $CDCl_3$): δ 196.67, 161.61, 137.02, 133.77, 119.88, 117.60.
8. *P-toulenealdehyde* (**1h**). Colorless liquid, **^{1}H NMR** spectrum (400 MHz, $CDCl_3$): δ 9.94 (s, 1H), 7.76 (d, J = 8.1 Hz, 2H), 7.31 (d, J = 8.0 Hz, 2H), 2.42 (s, 3H). **^{13}C NMR** spectrum (100 MHz, $CDCl_3$): δ 192.10, 145.60, 134.16, 129.86, 129.72, 21.86.
9. *Cuminaldehyde* (**1i**). Colorless liquid, **^{1}H NMR** spectrum (400 MHz, $CDCl_3$): δ 9.96 (s, 1H), 7.83 – 7.79 (m, 2H), 7.38 (d, J = 8.2 Hz, 2H), 3.02–2.94 (m, 1H), 1.27 (d, J = 6.9 Hz,

6H). **^{13}C NMR** spectrum (100 MHz, $CDCl_3$): δ 192.09, 156.26, 134.69, 130.03, 127.16, 34.48, 23.63.

10. *2-nitrobenzaldehyde* (**1j**). White solid, **^{1}H NMR** spectrum (400 MHz, $CDCl_3$): δ 10.43 (s, 1H), 8.16–8.12 (m, 1H), 7.99 – 7.95 (m, 1H), 7.84–7.75 (m, 2H). **^{13}C NMR** spectrum (100 MHz, $CDCl_3$): δ 188.19, 149.61, 134.11, 133.73, 131.36, 129.65, 124.52.
11. *3-nitrobenzaldehyde* (**1k**). White solid, **^{1}H NMR** spectrum (400 MHz, $CDCl_3$): δ 10.14 (s, 1H), 8.73 (d, J = 3.7 Hz, 1H), 8.53–8.49 (m, 1H), 8.25 (d, J = 7.6 Hz, 1H), 7.78 (t, J = 7.9 Hz, 1H). **^{13}C NMR** spectrum (100 MHz, $CDCl_3$): δ 189.77, 148.79, 137.39, 134.65, 130.41, 128.63, 124.53.
12. *4-nitrobenzaldehyde* (**1l**). White solid, **^{1}H NMR** spectrum (400 MHz, $CDCl_3$): δ 10.17 (s, 1H), 8.41 (d, J = 8.6 Hz, 2H), 8.09 (d, J = 8.7 Hz, 2H). **^{13}C NMR** spectrum (100 MHz, $CDCl_3$): δ 190.31, 151.17, 140.05, 130.51, 124.34.
13. *2,4-dimethylbenzaldehyde* (**1m**). White solid, **^{1}H NMR** spectrum (400 MHz, $CDCl_3$): δ 9.92 (s, 1H), 7.63 (s, 1H), 7.60 (d, J = 7.8 Hz, 1H), 7.28 (d, J = 8.0 Hz, 1H), 2.33 (s, 3H), 2.33 (s, 3H). **^{13}C NMR** spectrum (100 MHz, $CDCl_3$): δ 192.36, 144.37, 137.51, 134.58, 130.58, 130.26, 127.77, 20.27, 19.66.
14. *3,4,5-trimethoxybenzaldehyde* (**1n**). White solid, **^{1}H NMR** spectrum (400 MHz, $CDCl_3$): δ 9.88 (s, 1H), 7.14 (s, 2H), 3.94 (d, J = 2.5 Hz, 9H). **^{13}C NMR** spectrum (100 MHz, $CDCl_3$): δ 191.14, 153.66, 143.59, 131.71, 106.71, 61.03, 56.29.
15. *1,1-biphenyl-4-carbaldehyde* (**1o**). White solid, **^{1}H NMR** spectrum (400 MHz, $CDCl_3$): δ 10.06 (s, 1H), 7.98–7.92 (m, 2H), 7.78–7.73 (m, 2H), 7.64 (d, J = 8.6 Hz, 2H), 7.52 – 7.38 (m, 3H). **^{13}C NMR** spectrum (100 MHz, $CDCl_3$): δ 192.01, 147.22, 139.73, 135.20, 130.31, 129.05, 128.51, 127.72, 127.40.
16. *2-napthaldehdye* (**1p**). White solid, **^{1}H NMR** spectrum (400 MHz, $CDCl_3$): δ 10.16 (s, 1H), 8.34 (s, 1H), 8.02 – 7.89 (m, 4H), 7.68–7.57 (m, 2H). **^{13}C NMR** spectrum (100 MHz, $CDCl_3$): δ 192.35, 136.48, 134.63, 134.12, 132.66, 129.56, 129.16, 129.14, 128.07, 127.13, 122.78.
17. *Benzil* (**1q**). Pale yellow solid, **^{1}H NMR** spectrum (400 MHz, $CDCl_3$): δ 7.98 (d, J = 7.1 Hz, 4H), 7.69–7.64 (m, 2H), 7.52 (t, J = 7.8 Hz, 4H). **^{13}C NMR** spectrum (100 MHz, $CDCl_3$): δ 194.63, 134.94, 132.99, 129.93, 129.06.

18. *Isophthalaldehyde* (**1r**). White solid, **^{1}H NMR** spectrum (400 MHz, $CDCl_3$): δ 10.13 (s, 2H), 8.39 (s, 1H), 8.17 (d, J = 6.0 Hz, 2H), 7.75 (t, J = 7.6 Hz, 1H). **^{13}C NMR** spectrum (100 MHz, $CDCl_3$): δ 191.09, 137.01, 134.67, 131.06, 129.95.
19. *Cinnamaldehyde* (**1s**). Red liquid, **^{1}H NMR** spectrum (400 MHz, $CDCl_3$): δ 9.68 (d, J = 7.7 Hz, 1H), 7.55 (d, J = 7.7 Hz, 2H), 7.46–7.38 (m, 4H), 6.76–6.69 (m, 1H). **^{13}C NMR** spectrum (100 MHz, $CDCl_3$): δ 194.08, 153.15, 133.98, 131.39, 129.15, 128.59, 128.37.
20. *Undecanal* (**1t**). Colorless liquid, **^{1}H NMR** spectrum (400 MHz, $CDCl_3$): δ 9.76 (t, J = 1.9 Hz, 1H), 2.45–2.40 (m, 2H), 1.31–1.26 (m, 14H), 1.70 – 1.57 (m, 2H), 0.88 (t, J = 16 Hz, 3H). **^{13}C NMR** spectrum (100 MHz, $CDCl_3$): δ 203.05, 43.90, 33.89, 31.87, 29.53, 29.35, 29.16, 24.71, 22.66, 22.06, 14.09.
21. *4-Formylmorpholine* (**1u**). Colorless liquid, **^{1}H NMR** spectrum (400 MHz, $CDCl_3$): δ 8.06 (s, 1H), 3.60–3.52 (m, 2H), 3.45–3.39 (m,2H). **^{13}C NMR** spectrum (100 MHz, $CDCl_3$): δ 160.85, 66.30, 45.70.
22. *Camphor* (**1v**). White solid, **^{1}H NMR** spectrum (400 MHz, $CDCl_3$): δ 2.09 (t, J = 4.5 Hz, 1H), 1.85 (d, J = 18.2 Hz, 2H), 1.72–1.65 (m, 2H), 1.38 (s, 2H), 0.96 (s, 3H), 0.91 (s, 3H), 0.84 (s, 3H). **^{13}C NMR** spectrum (100 MHz, $CDCl_3$): δ 57.73, 46.82, 43.32, 27.05, 19.80, 19.15, 9.26. Peak at ca. δ 216 could not be marked since the spectrum was only recorded up to 210 ppm.
23. *2-octanone* (**1w**). Colourless liquid, **^{1}H NMR** spectrum (400 MHz, $CDCl_3$): δ 2.43 (t, J = 7.5 Hz, 2H), 2.14 (s, 3H), 1.62–1.52 (m, 2H), 1.28 (s, 6H), 0.88 (t, J = 6.8 Hz, 3H). **^{13}C NMR** spectrum (100 MHz, $CDCl_3$): δ 209.20, 43.68, 31.52, 29.71, 28.77, 23.73, 22.41, 13.92.
24. *3-pyridinecarboxaldehyde* (**1x**). Yellow liquid, **^{1}H NMR** spectrum (400 MHz, $CDCl_3$): δ 10.15 (s, 1H), 9.11 (s, 1H), 8.87 (d, J = 4.8 Hz, 1H), 8.23 – 8.19 (m,1H), 7.55–7.51 (m, 1H). **^{13}C NMR** spectrum (100 MHz, $CDCl_3$): δ 190.80, 154.67, 151.99, 135.85, 131.40, 124.11.
25. *Furaldehyde* (**1y**). White solid, **^{1}H NMR** spectrum (400 MHz, $CDCl_3$): δ 9.67 (s, 1H), 7.71 (d, J = 0.8 Hz, 1H), 7.28 (d, J = 3.1 Hz, 1H), 6.62 (d, J = 1.9 Hz, 1H). **^{13}C NMR** spectrum (100 MHz, $CDCl_3$): δ 177.94, 152.97, 148.13, 121.12, 112.62.

26. *5-nitro-2-furaldehyde* (**1z**). Red solid, **^{1}H NMR** spectrum (400 MHz, $CDCl_3$): δ 9.84 (s, 1H), 7.42 (d, J = 3.9 Hz, 1H), 7.36 (d, J = 3.8 Hz, 1H). **^{13}C NMR** spectrum (100 MHz, $CDCl_3$): δ 178.37, 150.97, 118.80, 111.78. one peak doubt in spectra, require total 5 peaks.
27. *5-(3-chloro-4-methoxyphenyl)furan-2-carbaldehyde* (**1aa**). White solid, **^{1}H NMR** spectrum (400 MHz, $CDCl_3$): δ 9.54 (s, 1H), 7.76 (s, 1H), 7.65–7.61 (m, 1H), 7.24 (d, J = 3.7 Hz, 1H), 6.91 (d, J = 8.7 Hz, 1H), 6.67 (d, J = 3.7 Hz, 1H), 3.88 (s, 3H). **^{13}C NMR** spectrum (100 MHz, $CDCl_3$): δ 177.02, 158.22, 156.12, 151.88, 127.29, 125.06, 123.31, 122.58, 112.21, 107.04, 56.32.
28. *Progesterone* (**1ab**). White solid, **^{1}H NMR** spectrum (400 MHz, $CDCl_3$): δ 5.74 (s, 1H), 2.54 (t, J = 9.0 Hz, 1H), 2.41 – 2.07 (m, 8H), 2.06–2.01 (m, 1H), 1.73 – 1.41 (m, 9H), 1.19 (s, 7H), 0.67 (s, 3H). **^{13}C NMR** spectrum (100 MHz, $CDCl_3$): δ 209.41, 199.55, 171.03, 123.95, 63.51, 56.03, 53.64, 43.94, 38.67, 38.58, 35.72, 35.55, 33.96, 32.79, 31.89, 31.54, 24.37, 22.83, 21.02, 17.38, 13.35. **ESI-MS**, m/z 315.2338 $[M + H]^+$
29. *Estrone* (**1ac**). White solid, **^{1}H NMR** spectrum (400 MHz, $CDCl_3$): δ 9.09 (s, 1H), 7.04 (d, J = 8.5 Hz, 1H), 6.54 – 6.44 (m, 1H), 6.45 (d, J = 2.5 Hz, 1H), 2.74 (d, J = 4.9 Hz, 2H), 2.47–2.39 (m, 1H), 2.30 (s, 1H), 2.11 – 2.01 (m, 4H), 1.74 (d, J = 11.0 Hz, 1H), 1.56–1.27 (m, 6H), 0.82 (s, 3H). **^{13}C NMR** spectrum (100 MHz, $CDCl_3$): δ 160.22, 142.22, 135.02, 131.15, 120.14, 117.97, 54.84, 52.52, 48.68, 43.20, 40.56, 36.56, 35.84, 34.30, 31.36, 30.78, 26.35, 18.73. **ESI-MS**, m/z 271.1710 $[M + H]^+$
30. *Stanolone* (**1ad**). White solid, **^{1}H NMR** spectrum (400 MHz, $CDCl_3$): δ 7.27 (s, 1H), 3.65 (t, J = 8.6 Hz, 1H), 2.33 – 2.07 (m, 8H), 1.85 – 1.79 (m, 1H), 1.65 (s, 7H), 1.39–1.24 (m, 5H), 1.02 (s, 4H), 0.76 (s, 3H). **^{13}C NMR** spectrum (100 MHz, $CDCl_3$): δ 212.14, 81.86, 53.92, 50.83, 46.75, 44.70, 43.00, 38.17, 36.65, 35.76, 35.45, 31.26, 30.95, 30.52, 28.81, 23.40, 21.04, 11.51, 11.15. **ESI-MS**, m/z 291.2336 $[M + H]^+$
31. *(methylsulfinyl)benzene* (**2a**). White solid, **^{1}H NMR** spectrum (400 MHz, $CDCl_3$): δ 7.69–7.62 (m, 2H), 7.58–7.46 (m, 3H), 2.73 (s, 3H). **^{13}C NMR** spectrum (100 MHz, $CDCl_3$): δ 145.58, 131.02, 129.34, 123.45, 43.89.
32. *Sulfinyldibenzene* (**2b**). White solid, **^{1}H NMR** spectrum (400 MHz, $CDCl_3$): δ 7.70–7.61 (m, 4H), 7.50–7.39 (m, 6H). **^{13}C NMR** spectrum (100 MHz, $CDCl_3$): δ 145.61, 131.07, 129.34, 124.80.

33. *1-nitro-4-(phenylsulfinyl)benzene* (**2c**). White solid, **^{1}H NMR** spectrum (400 MHz, $CDCl_3$): δ 8.31 (d, J = 8.8 Hz, 2H), 7.85 (d, J = 8.7 Hz, 2H), 7.72–7.65 (m, 2H), 7.55 – 7.46 (m, 3H). **^{13}C NMR** spectrum (100 MHz, $CDCl_3$): δ 152.95, 149.26, 144.39, 132.04, 129.83, 125.30, 124.90, 124.45.
34. *1-methyl-4-(phenylsulfinyl)benzene* (**2d**). White solid, **^{1}H NMR** spectrum (400 MHz, $CDCl_3$): δ 7.68–7.57 (m, 2H), 7.53 (d, J = 8.2 Hz, 2H), 7.47–7.37 (m, 3H), 7.25 (d, J = 8.2 Hz, 2H), 2.35 (s, 3H). **^{13}C NMR** spectrum (100 MHz, $CDCl_3$): δ 145.72, 142.38, 141.69, 130.92, 130.06, 129.29, 125.00, 124.69, 21.42.
35. *(sulfinylbis(methylene))dibenzene* (**2e**). White solid, **^{1}H NMR** spectrum (400 MHz, $CDCl_3$): δ 7.42–7.22 (m, 10H), 3.85 (s, 4H). **^{13}C NMR** spectrum (100 MHz, $CDCl_3$): δ 130.17, 129.02, 128.40, 127.54, 57.23.
36. *Diethyl-4,4'-(sulfinylbis(methylene))dibenzoate* (**2f**). White solid, **^{1}H NMR** spectrum (400 MHz, $CDCl_3$): δ 8.09 (d, J = 8.2 Hz, 4H), 7.38 (d, J = 8.2 Hz, 4H), 4.38 (q, J = 7.1 Hz, 4H), 4.21 (s, 4H), 1.40 (t, J = 7.1 Hz, 6H). **^{13}C NMR** spectrum (100 MHz, $CDCl_3$): δ 166.09, 134.82, 130.88, 130.16, 130.14, 61.20, 57.15, 14.32.
37. *Tetrahydrothiophene-1-oxide* (**2g**). White solid, **^{1}H NMR** spectrum (400 MHz, $CDCl_3$): δ 3.03–2.82 (m, 4H), 2.56 – 2.37 (m, 1H), 2.10 – 2.01 (m, 2H). **^{13}C NMR** spectrum (100 MHz, $CDCl_3$): δ 54.19, 25.62.
38. *1-(butylsulfinyl)butane* (**2h**). White solid, **^{1}H NMR** spectrum (400 MHz, $CDCl_3$): δ 2.84–2.60 (m, 4H), 1.81–1.71 (m, 4H), 1.56–1.44 (m, 4H), 0.97 (t, J = 7.3 Hz, 6H). **^{13}C NMR** spectrum (100 MHz, $CDCl_3$): δ 51.73, 24.55, 21.97, 13.61.
39. *1-(octylsulfinyl)octane* (**2i**). White solid, **^{1}H NMR** spectrum (400 MHz, $CDCl_3$): δ 2.74–2.57 (m, 4H), 1.83 – 1.71 (m, 4H), 1.52–1.39 (m, 4H), 1.37–1.26 (m, 16H), 0.88 (t, J = 6.9 Hz, 6H). **^{13}C NMR** spectrum (100 MHz, $CDCl_3$): δ 52.43, 31.73, 29.16, 29.02, 28.88, 22.60, 14.06.
40. *1-(decylsulfinyl)decane* (**2j**). White solid, **^{1}H NMR** spectrum (400 MHz, $CDCl_3$): δ 2.70–2.59 (m, 4H), 1.82 – 1.70 (m, 4H), 1.53–1.38 (m, 4H), 1.36–1.24 (m, 24H), 0.88 (t, J = 6.9 Hz, 6H). **^{13}C NMR** spectrum (100 MHz, $CDCl_3$): δ 52.37, 31.86, 29.49, 29.37, 29.27, 29.21, 28.88, 22.67, 22.61, 14.11.
41. *1-chloro-2-(ethylsulfinyl)ethane* (**2k**). White solid, **^{1}H NMR** spectrum (400 MHz, $CDCl_3$): δ 4.04–3.88 (m, 2H), 3.28–3.18 (m, 1H), 3.09 – 3.04 (m, 1H), 2.94–2.83 (m, 2H),

1.38 (t, J = 7.5 Hz, 3H). **^{13}C NMR** spectrum (100 MHz, $CDCl_3$): δ 53.66, 45.58, 36.93, 6.80. **ESI-MS**, m/z 141.0143 $[M + H]^+$

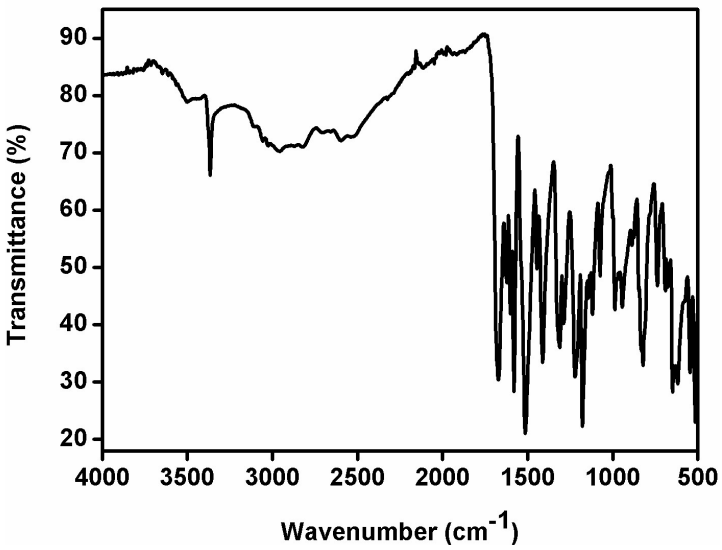

Fig. S1 FTIR spectrum of ligand **L**.

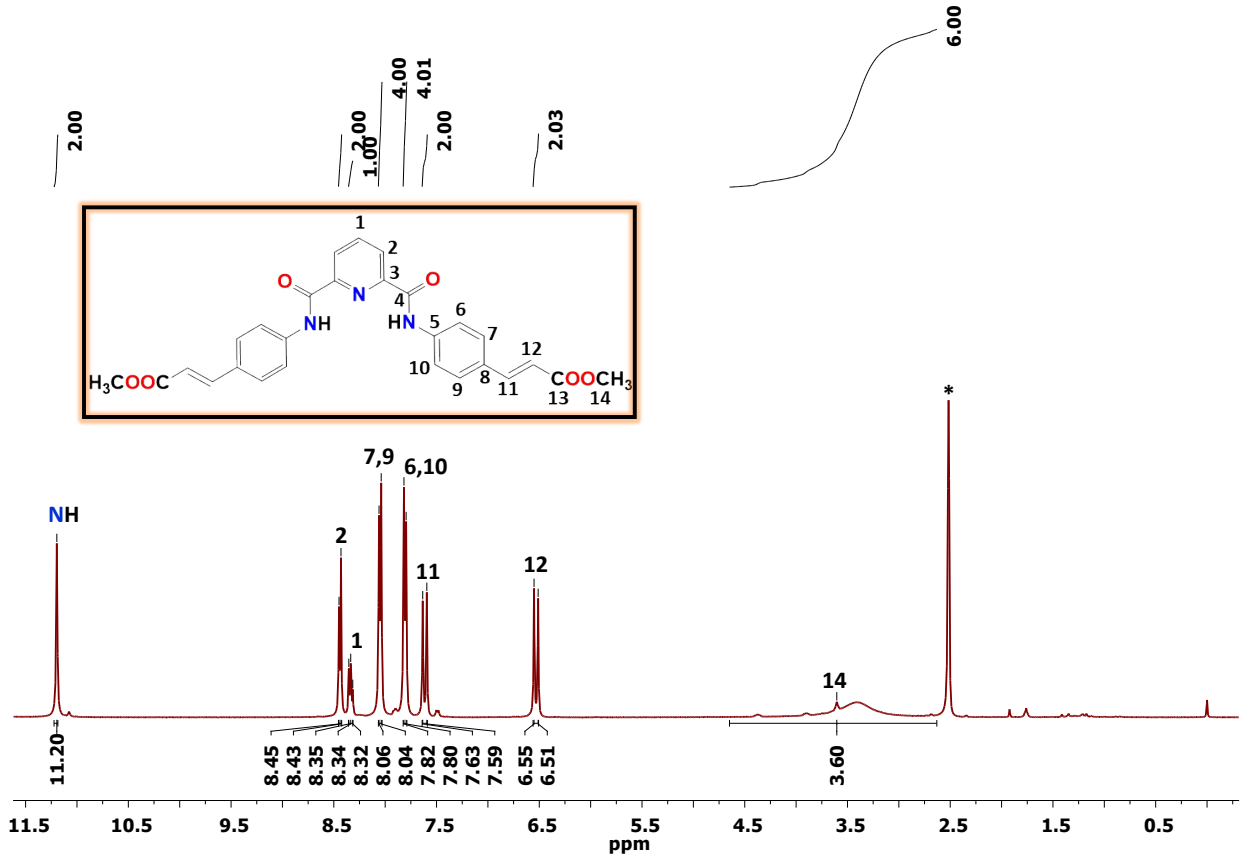

Fig. S2 ^{1}H NMR spectrum of ligand **L** in DMSO-d_6 solvent where * represents the residual solvent and/or adventitious water peaks.

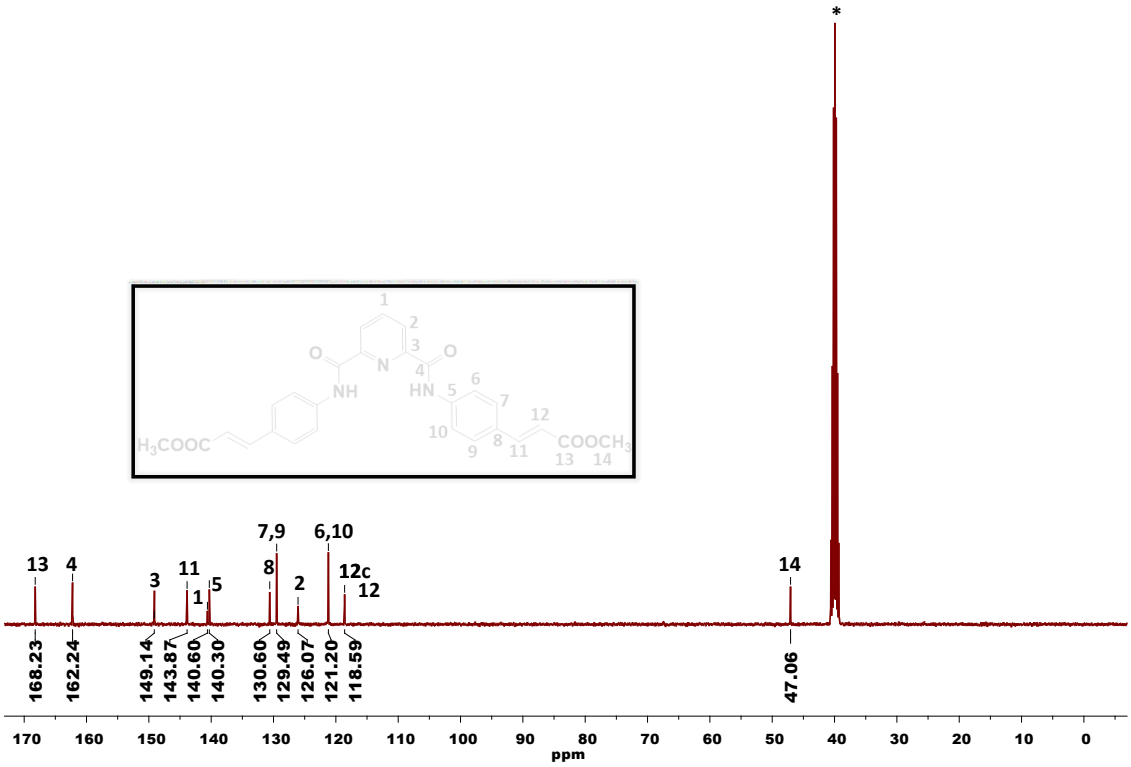

Fig. S3 ^{13}C NMR spectrum of ligand **L** in DMSO-d_6 solvent where * represents the residual solvent peak.

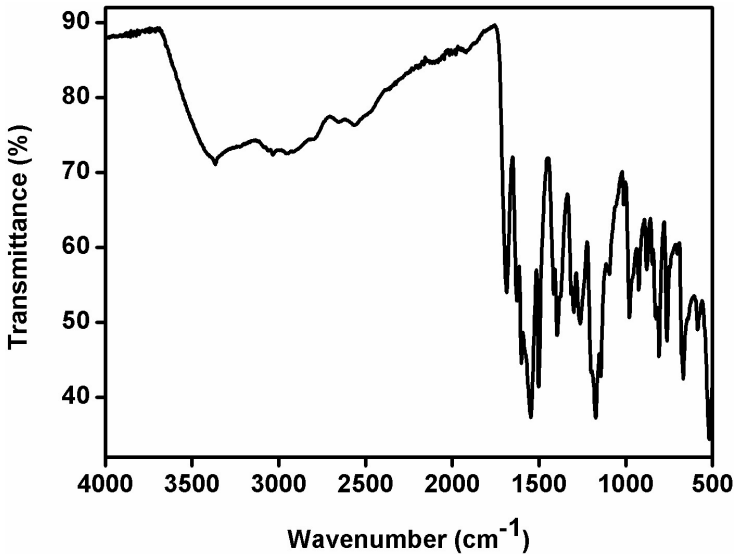

Fig. S4 FTIR spectrum of $\mathbf{1^P}$ bearing protected carboxylic acid groups.

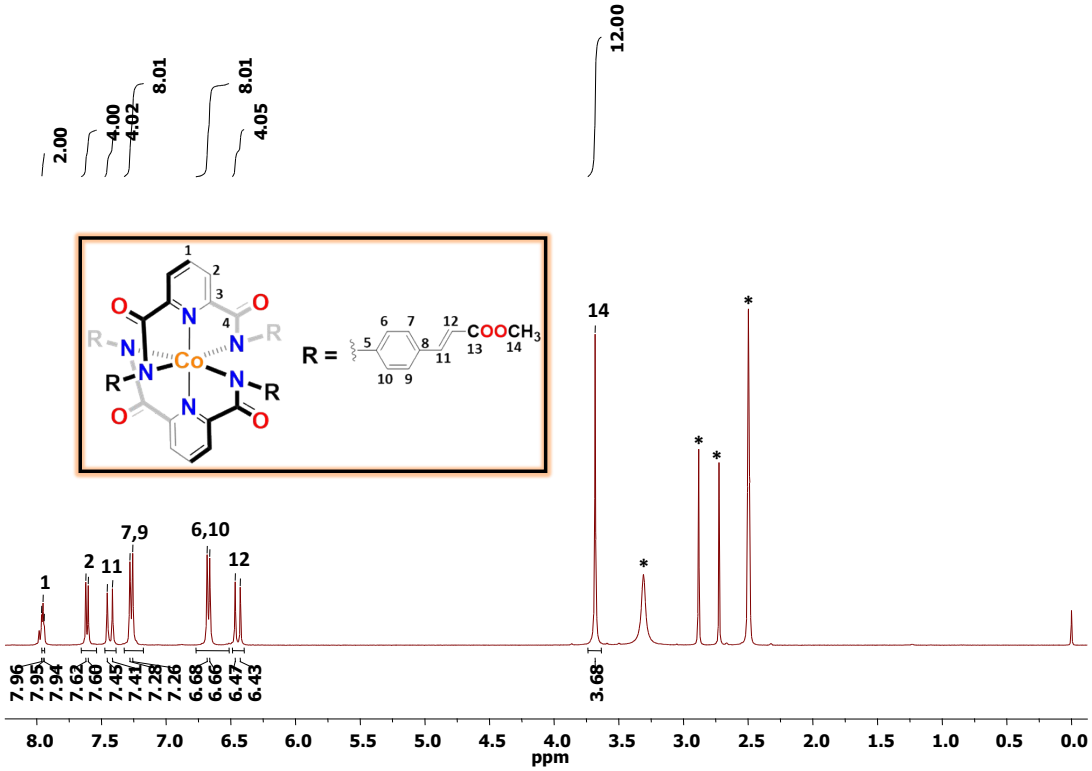

Fig. S5 ^{1}H NMR spectrum of $\mathbf{1^{P}}$ bearing protected carboxylic acid groups in DMSO-d_6 solvent where * represents the residual solvents and/or adventitious water peaks.

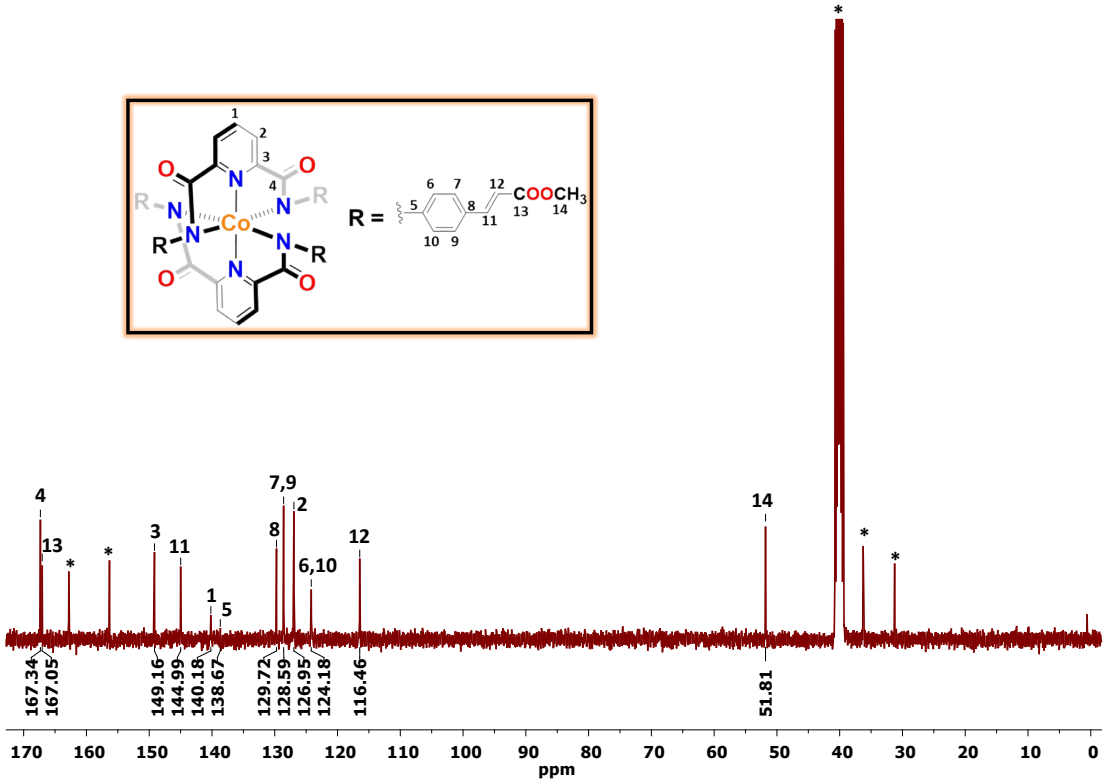

Fig. S6 ^{13}C NMR spectrum of $\mathbf{1^{P}}$ bearing protected carboxylic acid groups in DMSO-d_6 solvent where * represents the residual solvent peak.

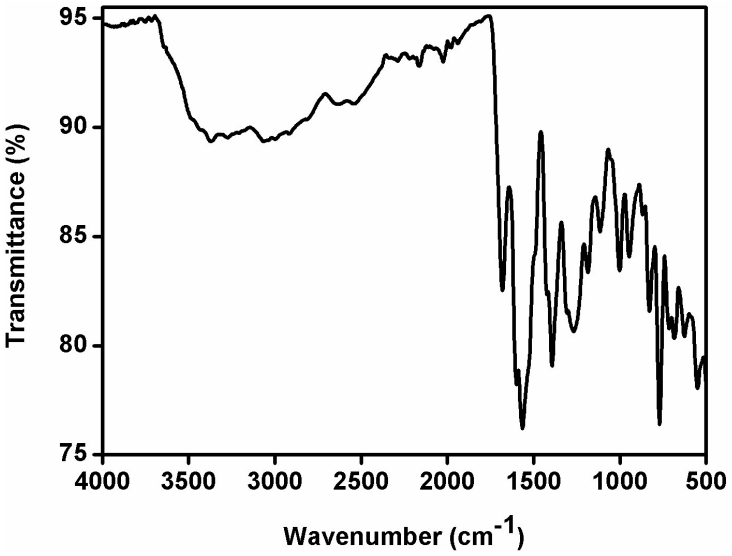

Fig. S7 FTIR spectrum of metalloligand **1**.

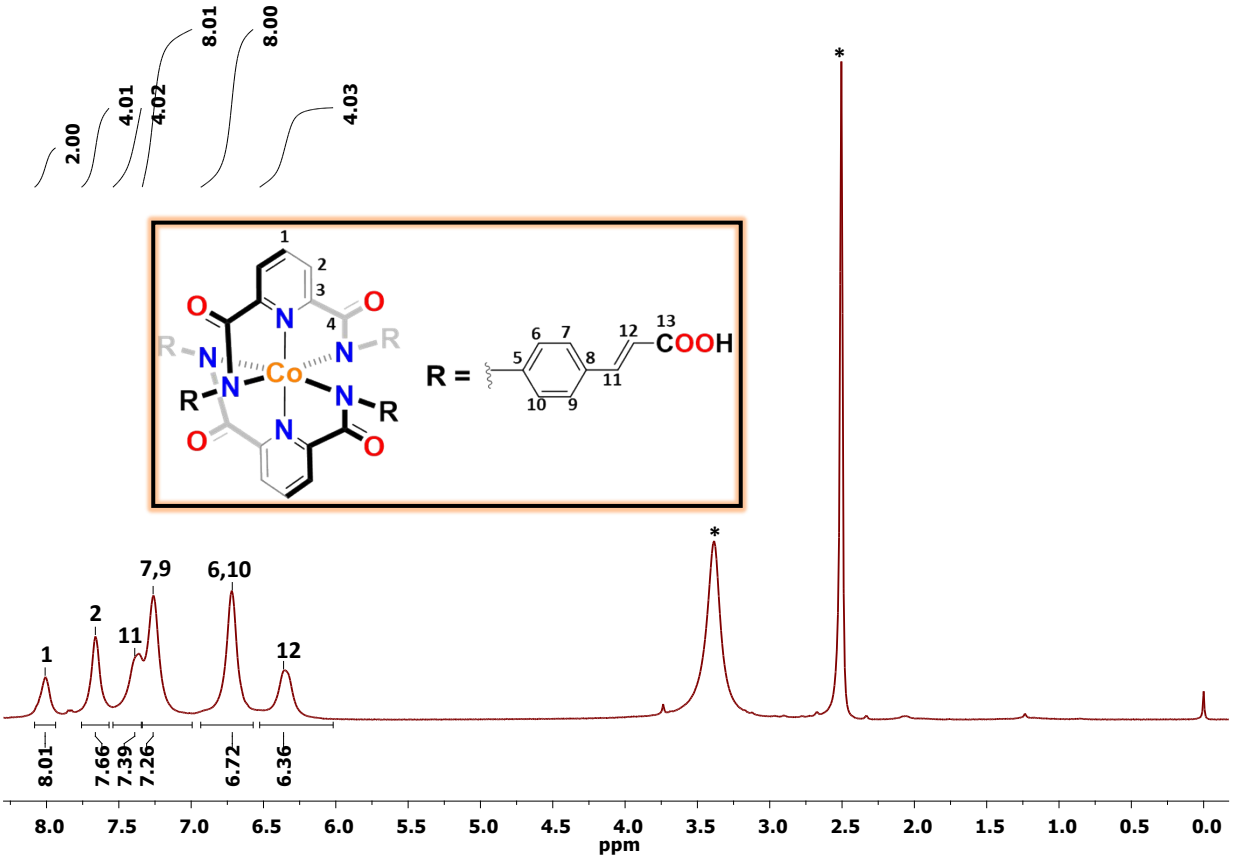

Fig. S8 ^{1}H NMR spectrum of metalloligand **1** in DMSO-d_6 solvent where * represents the residual solvent and/or adventitious water peaks.

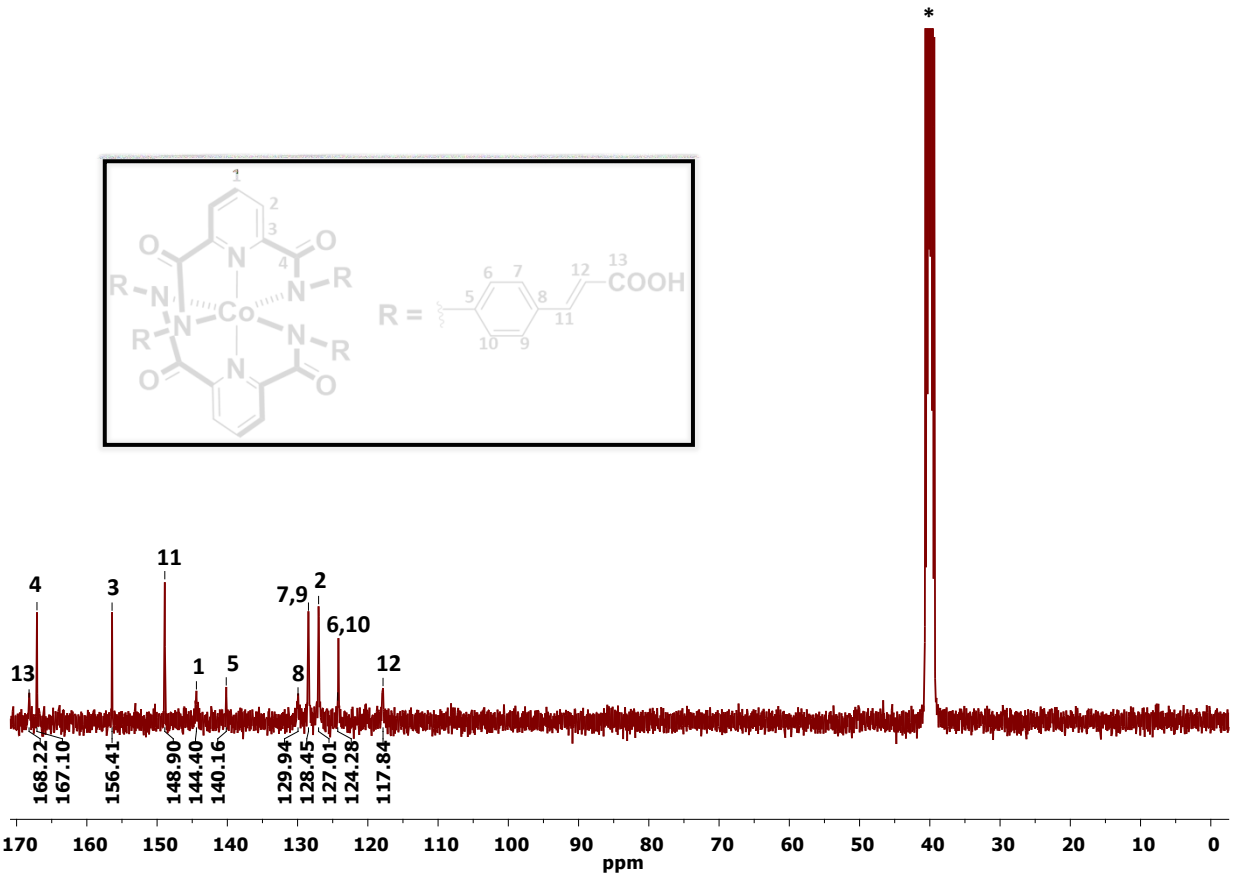

Fig. S9 ^{13}C NMR spectrum of metalloligand **1** in DMSO-d_6 solvent where * represents the residual solvent peak.

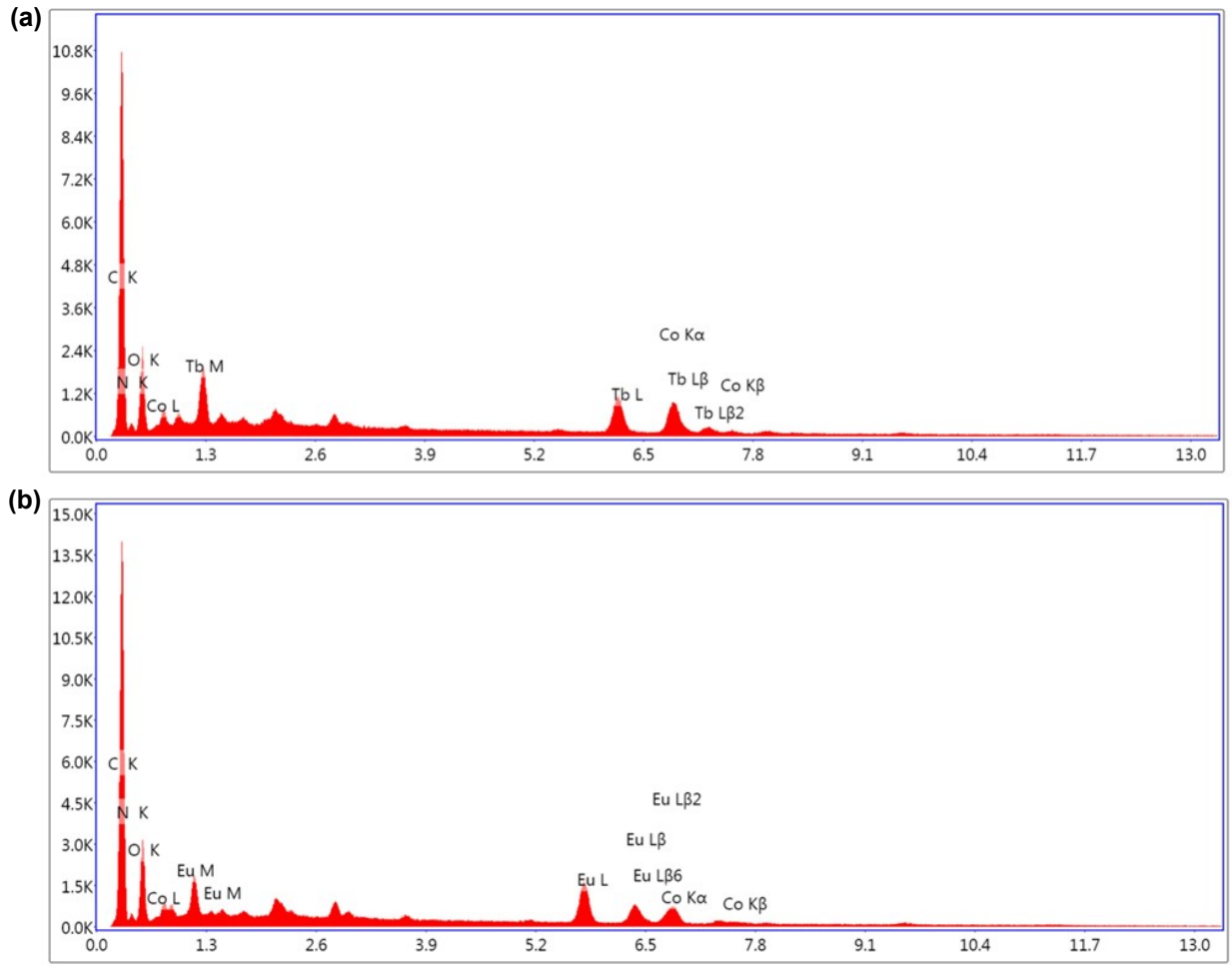

Fig. S10 EDX spectrum of Ln-MOFs (a) **1-Tb** and (b) **1-Eu**.

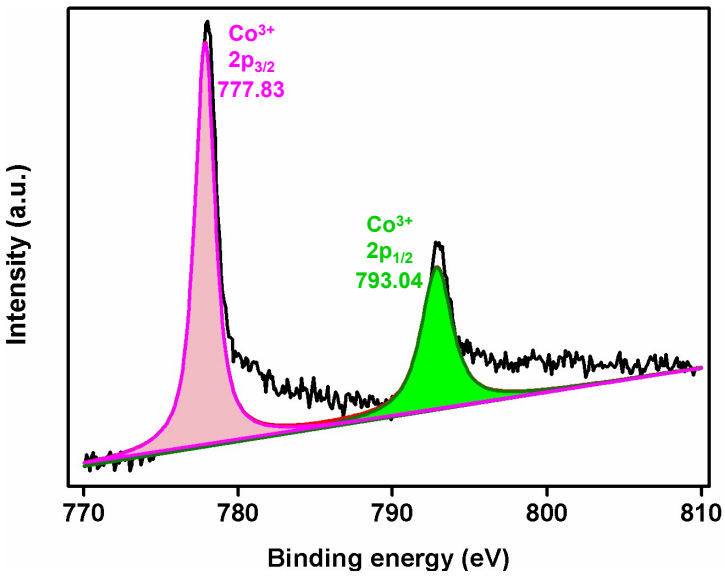

Fig. S11 Core level XPS spectrum for Co 2p in **1**.

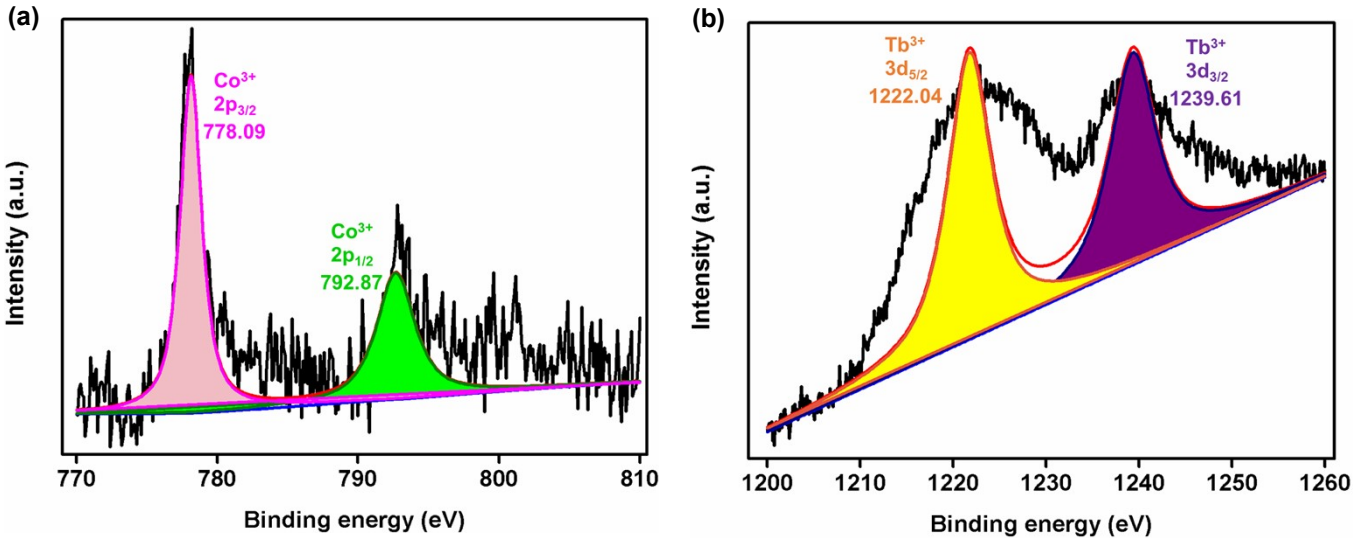

Fig. S12 Core level XPS spectra for (a) Co 2p and (b) Tb 3d in **1-Tb**.

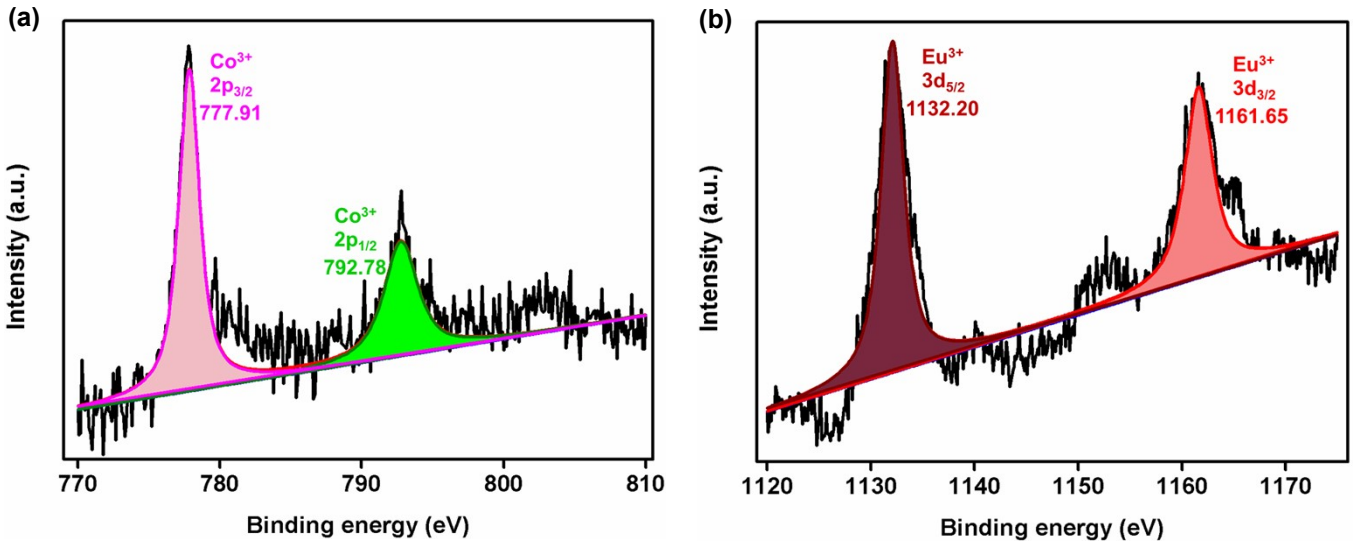

Fig. S13 Core level XPS spectra for (a) Co 2p and (b) Eu 3d in **1-Eu**.

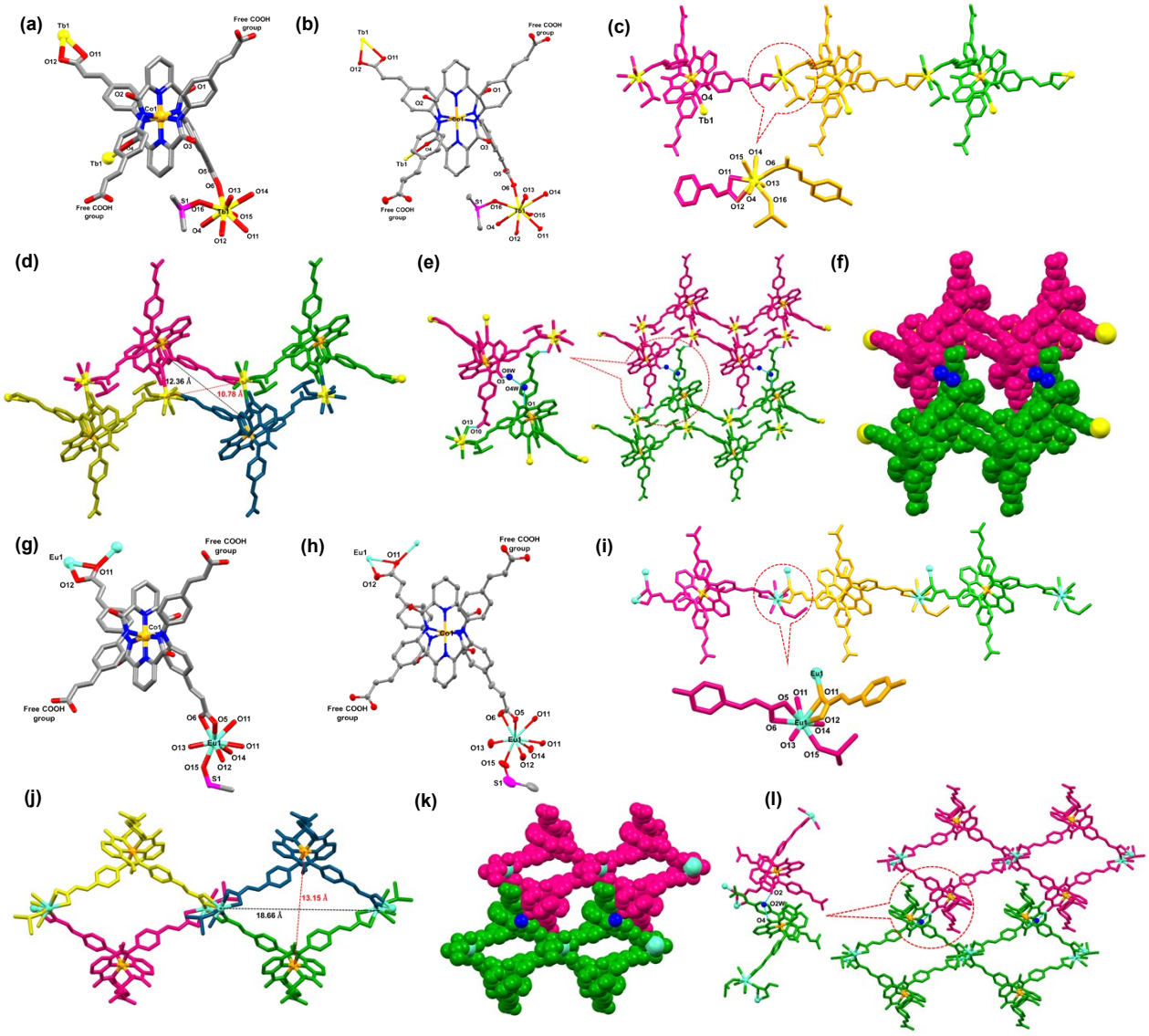

Fig. S14 (a) Stick representation of the crystal structure of **1-Tb**. Color code: Orange, Co; yellow, Tb; pink, S; blue, N; red, O; gray, C. Hydrogen atoms and solvent molecules have been omitted for clarity. (b) Thermal ellipsoidal plot of the crystal structure of **1-Tb**. Color code: Orange, Co; yellow, Tb; pink, S; blue, N; red, O; gray, C. Hydrogen atoms and solvent molecules have been omitted for clarity. (c) Crystal structure of **1-Tb** displaying arrangements of metalloligands (shown in pink, golden and green colors) and Tb^{3+} ions generating a 1D chain when viewed along *b* axis. (d) Crystal structure of **1-Tb** displaying arrangements of metalloligands (shown in pink, green, olive and dark blue colors) and Tb^{3+} ions generating the double 1D chains when viewed along *a* axis. (e) A view of 2D network created due to H-bonding interactions between O_{amide} and lattice water molecules (shown as blue balls) connecting various double 1D chains (shown in pink and green colors). (f) Spacefill diagram of **1-Tb** when viewed along *a* axis. (g) Stick representation of the crystal structure of **1-Eu**. Color code: Orange, Co; cyan, Eu; pink, S; blue, N; red, O; gray, C. Hydrogen atoms and solvent molecules have been omitted for clarity. (h) Thermal ellipsoidal plot of the crystal structure of **1-Eu**. Color code: Orange, Co; cyan, Eu; pink, S; blue, N; red, O; gray,

C. Hydrogen atoms and solvent molecules have been omitted for clarity. (i) Crystal structure of **1-Eu** displaying arrangements of metalloligands (shown in pink, golden and green colors) and Eu^{3+} ions generating a 1D chain when viewed along *b* axis. (j) Crystal structure of **1-Eu** displaying arrangements of metalloligands (shown in pink, green, olive and dark blue colors) and Eu^{3+} ions generating the dimeric chains when viewed along *a* axis. (k) A view of 2D network created due to H-bonding interactions between O_{amide} and lattice water molecules (shown as blue balls) connecting various dimeric chains (shown in pink and green colors). (l) Spacefill diagram of **1-Eu** when viewed along *a* axis.

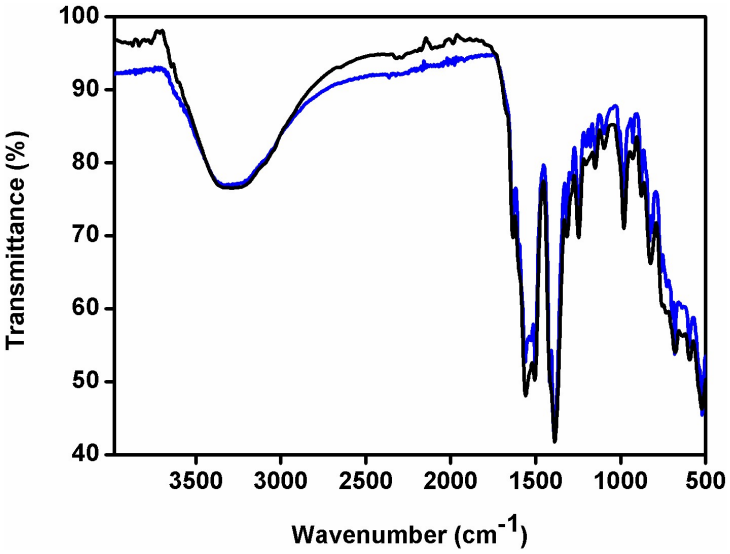

Fig. S15 FTIR spectra of **1-Tb** (black trace) and **1-Eu** (blue trace).

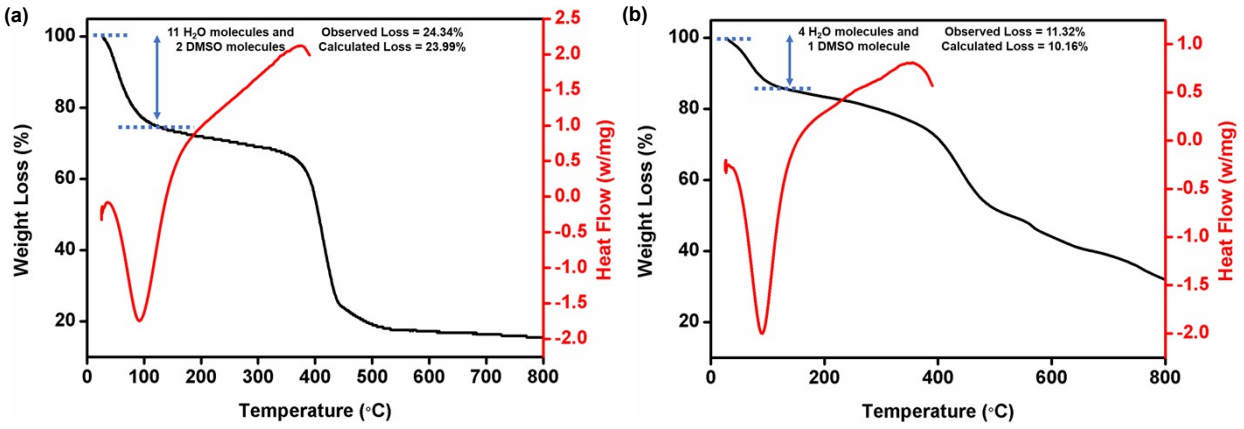

Fig. S16 (a) Thermal Gravimetric Analysis (TGA, black trace) and Differential Scanning Calorimetric (DSC, red trace) plots for (a) **1-Tb** and (b) **1-Eu.**

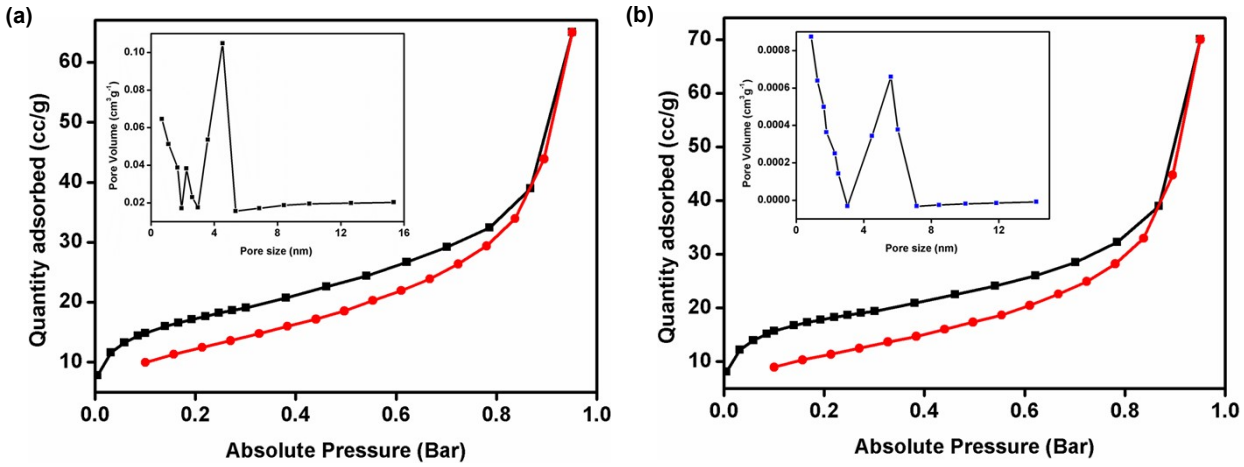

Fig. S17 (a) N_2 gas sorption isotherms measured at 77 K for (a) **1-Tb** and (b) **1-Eu**. Black and red traces respectively denote sorption and desorption plots. Insets show the pore size distribution graph.

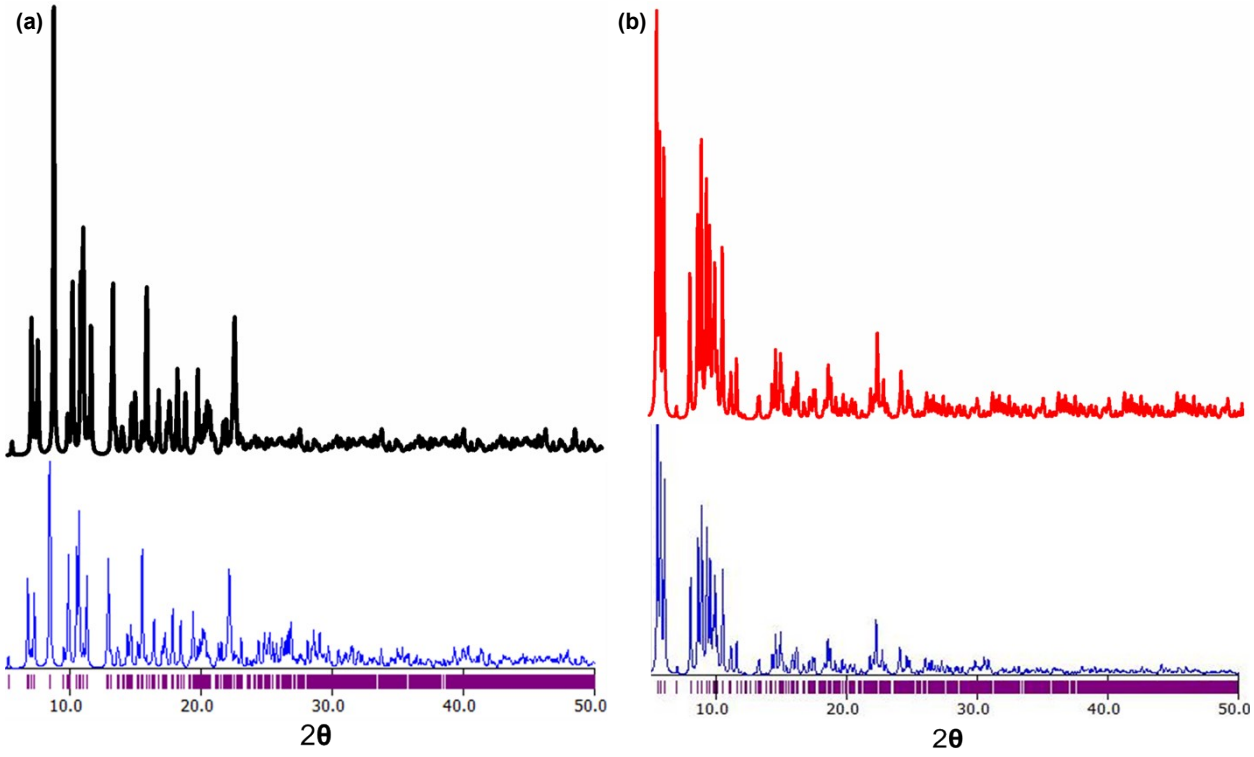

Fig. S18 (a) Powder X-ray diffraction patterns for as-synthesized **1-Tb** (upper) and the one simulated from Mercury 3.0 using the single crystal diffraction data (lower). (b) Powder X-ray diffraction patterns for as-synthesized **1-Eu** (upper) and the one simulated from Mercury 3.0 using the single crystal diffraction data (lower).

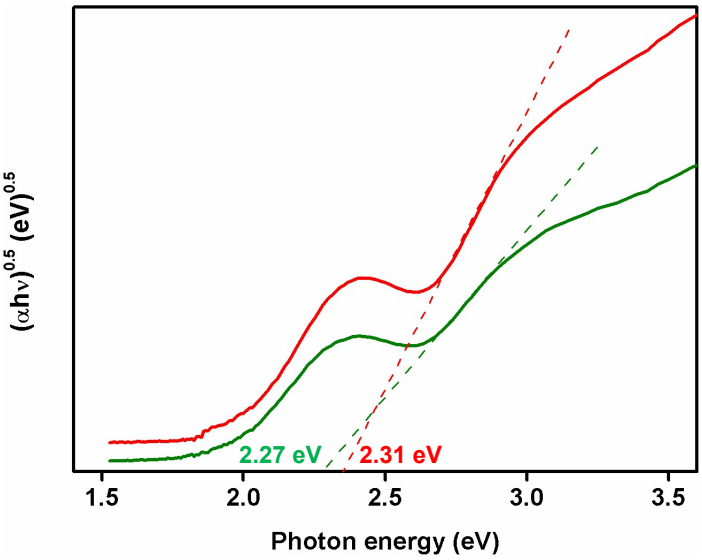

Fig. S19 Tauc plots for **1-Tb** (green trace) and **1-Eu** (red trace) with n = 1 (indirect band gap model).

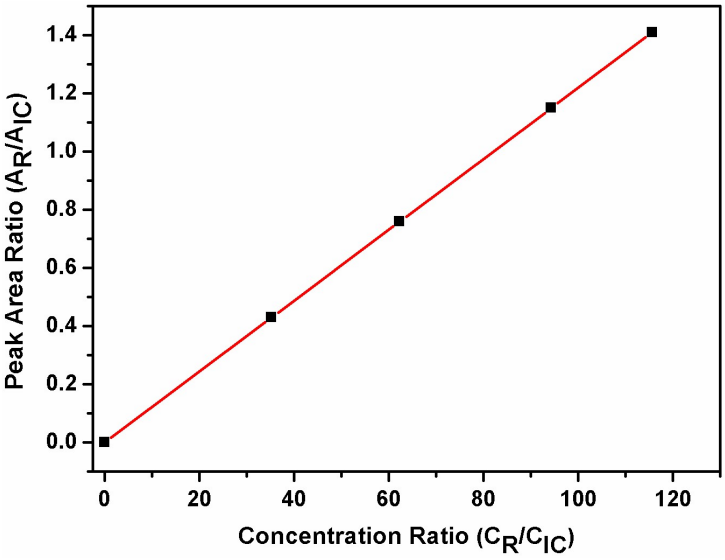

Fig. S20 Calibration plot for the gas chromatographic studies using benzyl alcohol as the substrate and phenol as the internal standard, where 'R' represents reactant (benzyl alcohol) while 'IC' refers to internal used (phenol).

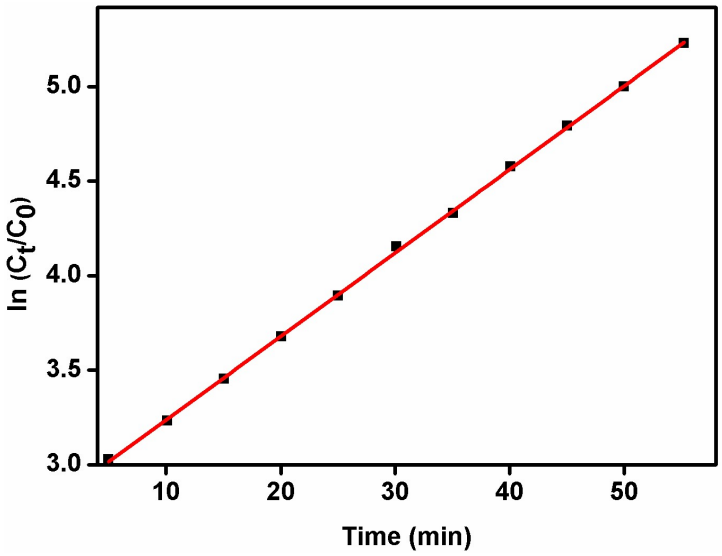

Fig. S21 Plot of ln(C_t/C_o) versus time representing first-order kinetics for the generation of 5-hydroxy-1,4-napthalenedione upon photo-oxidation of 1,5-dihydroxynapthalene in the presence of **1-Tb** as a photocatalyst.

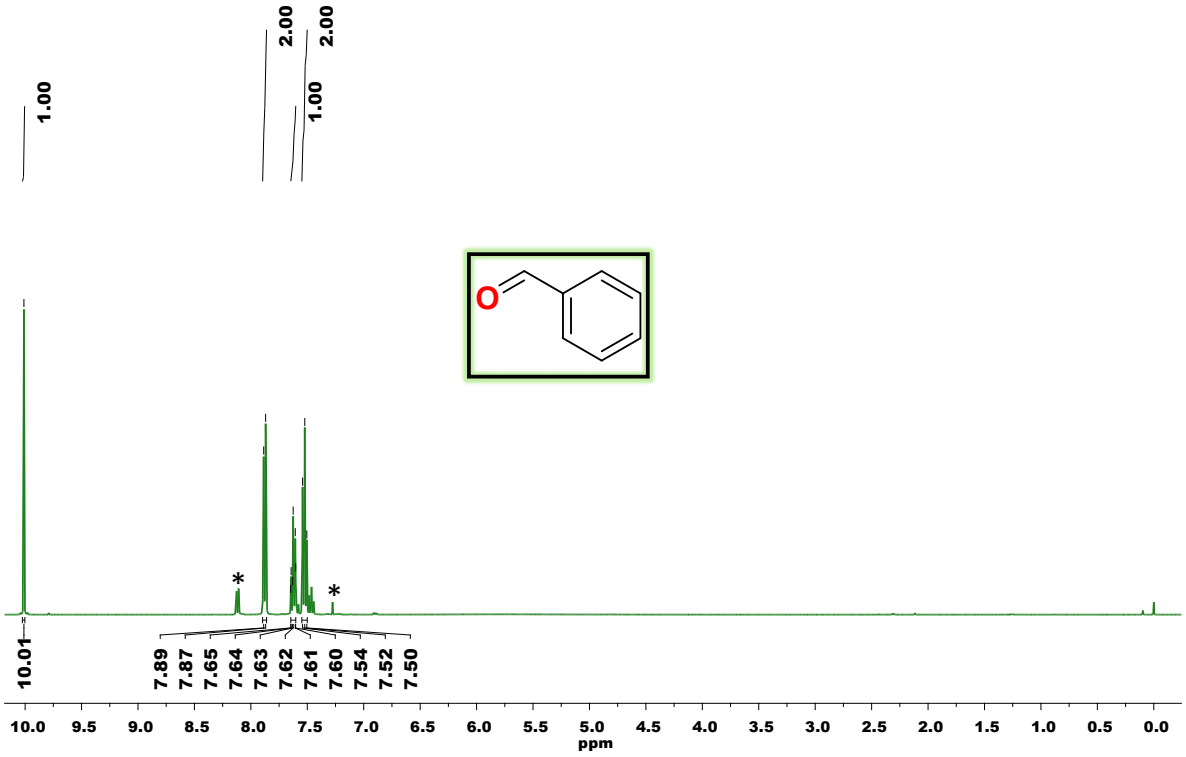

Fig. S22 ^{1}H NMR spectrum of benzaldehyde in $CDCl_3$ solvent where * represents the residual solvent and/or adventitious water peaks.

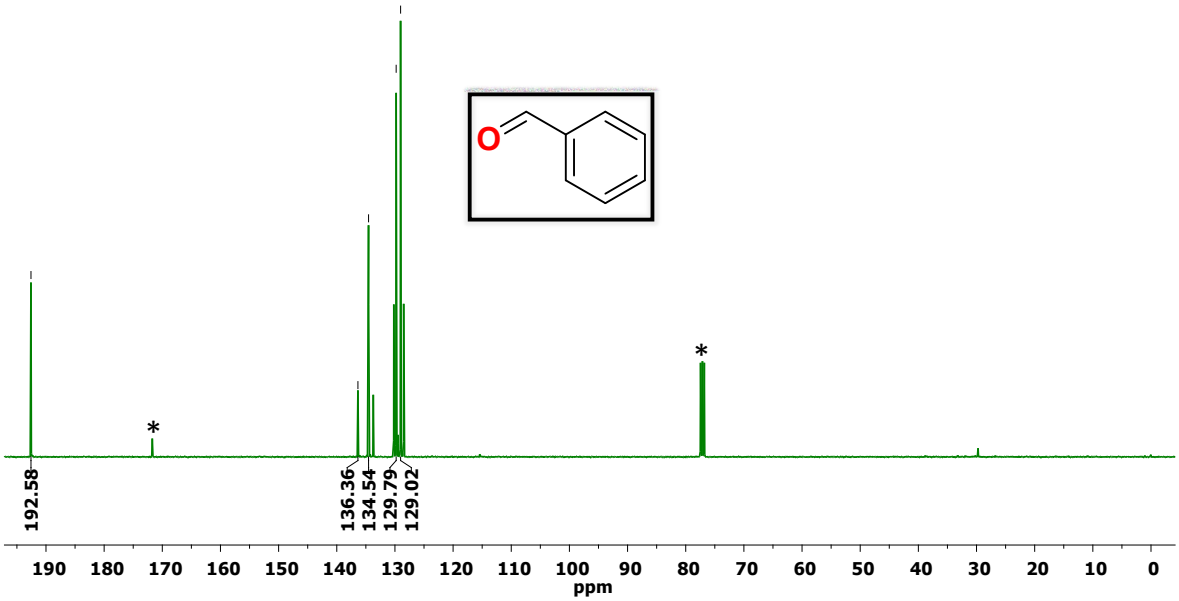

Fig. S23 ^{13}C NMR spectrum of benzaldehyde in $CDCl_3$ solvent where * represents the residual solvent and/or adventitious water peaks.

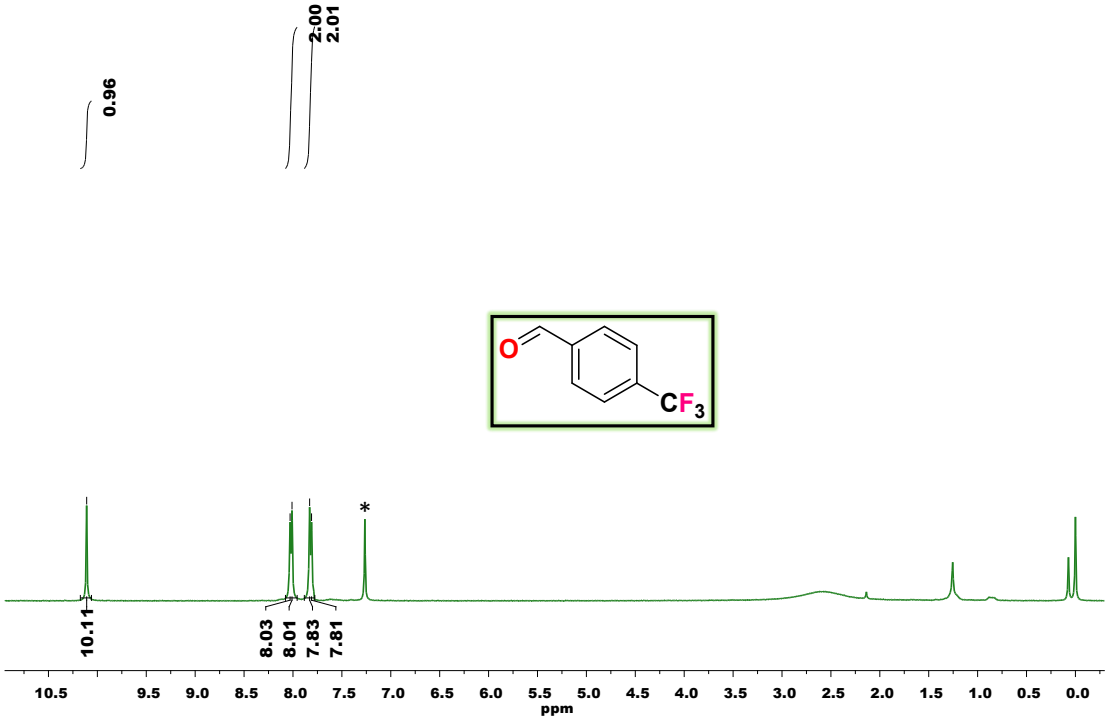

Fig. S24 ^{1}H NMR spectrum of 4-(trifluoromethyl)benzaldehyde in $CDCl_3$ solvent where * represents the residual solvent and/or adventitious water peaks.

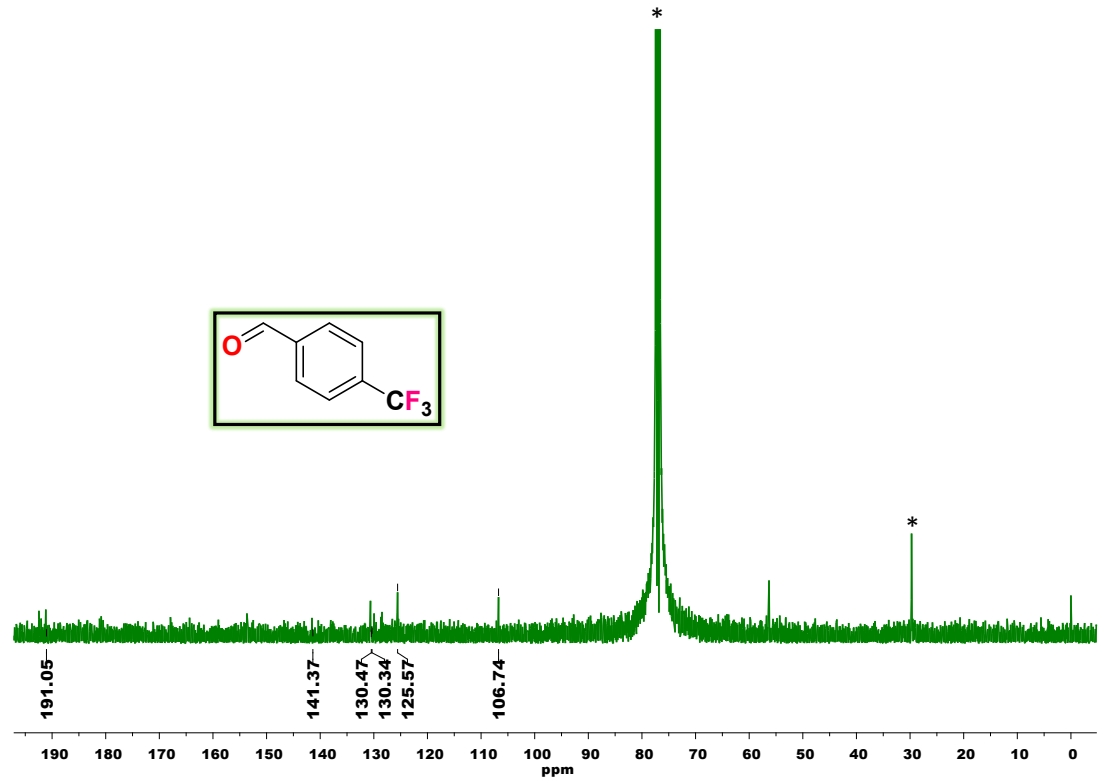

Fig. S25 ^{13}C NMR spectrum of 4-(trifluoromethyl)benzaldehyde in $CDCl_3$ solvent where * represents the residual solvent and/or adventitious water peaks.

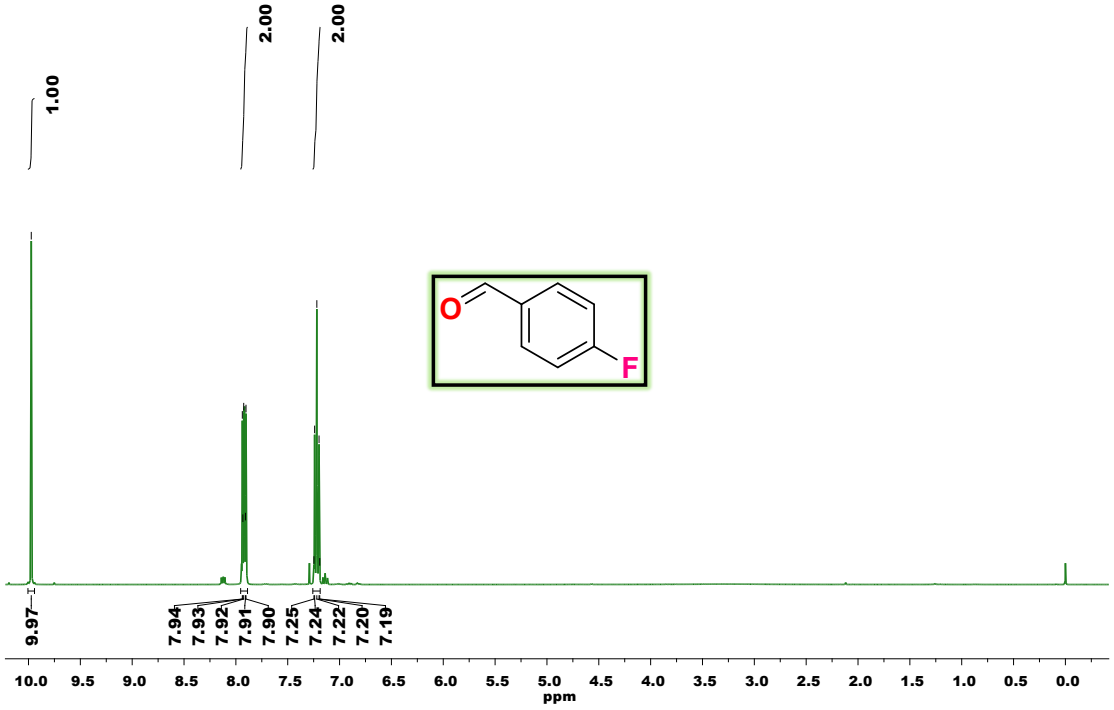

Fig. S26 ^{1}H NMR spectrum of fluorobenzaldehyde in $CDCl_3$ solvent where * represents the residual solvent and/or adventitious water peaks.

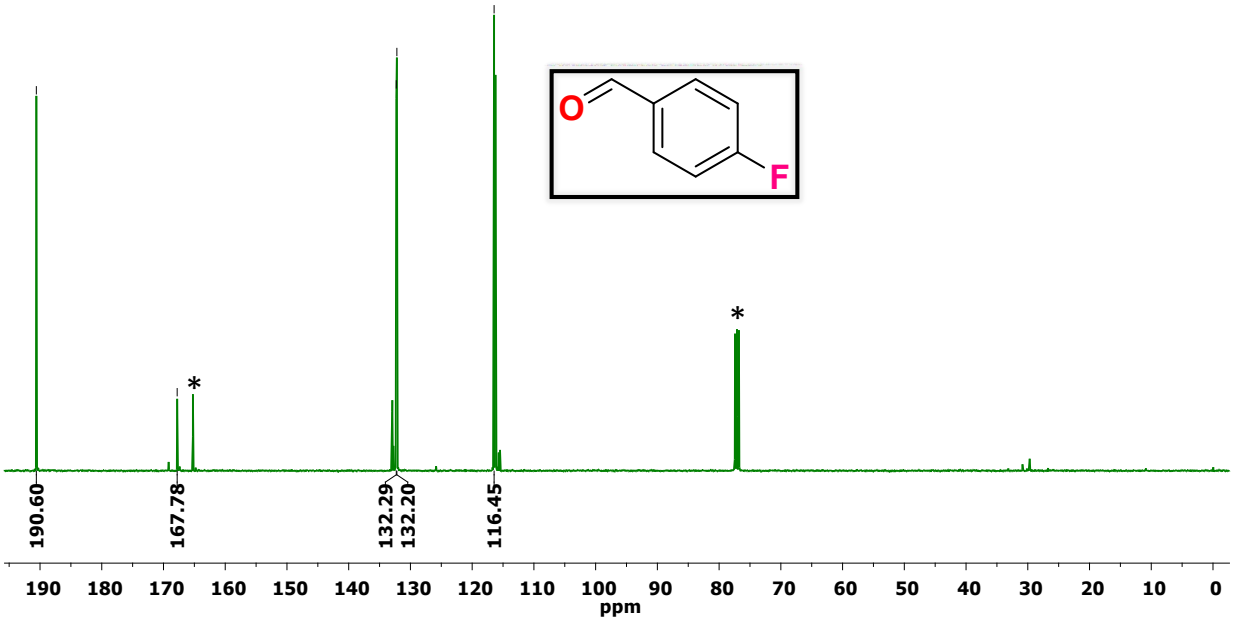

Fig. S27 ^{13}C NMR spectrum of fluorobenzaldehyde in $CDCl_3$ solvent where * represents the residual solvent and/or adventitious water peaks.

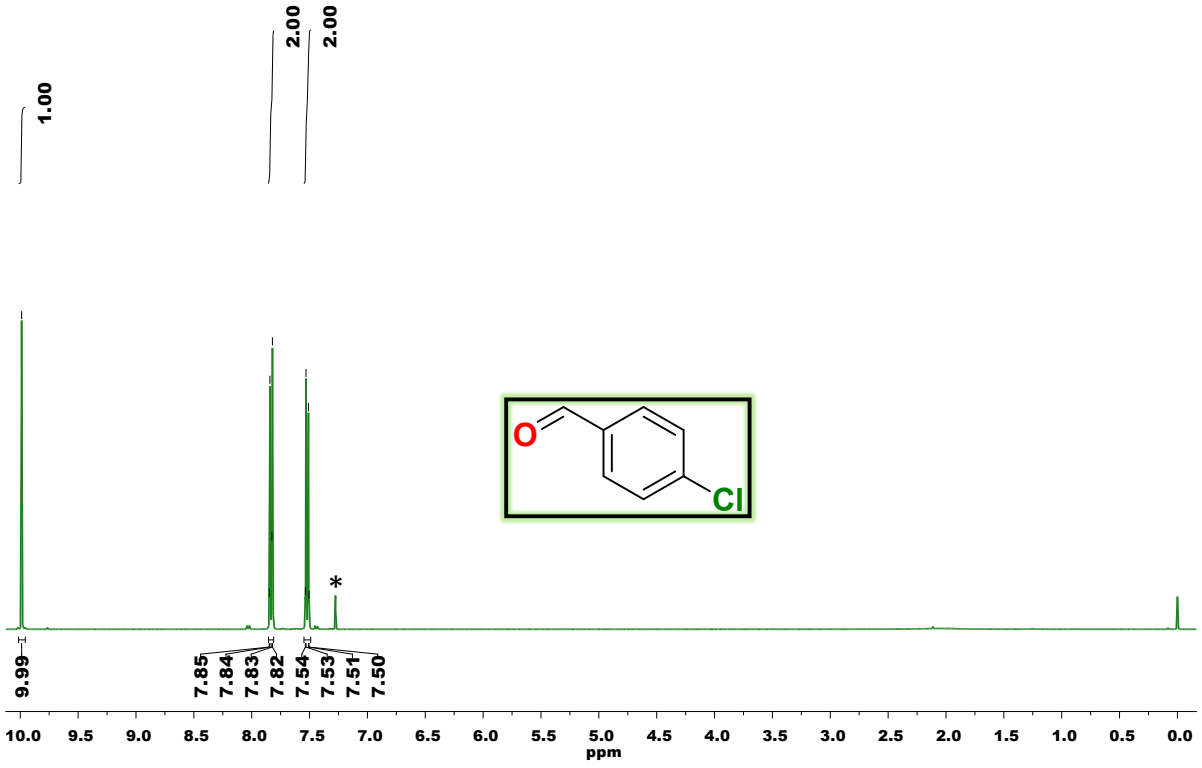

Fig. S28 ^{1}H NMR spectrum of chllorobenzaldehyde in $CDCl_3$ solvent where * represents the residual solvent and/or adventitious water peaks.

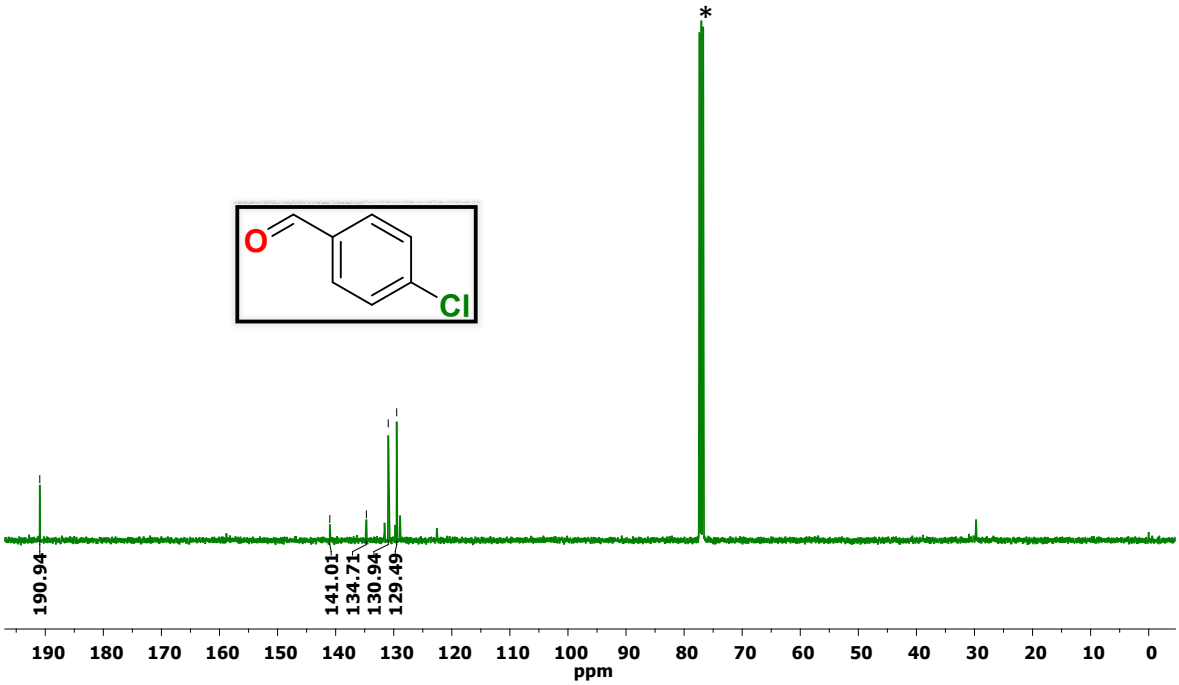

Fig. S29 ^{13}C NMR spectrum of chlorobenzaldehyde in $CDCl_3$ solvent where * represents the residual solvent and/or adventitious water peaks.

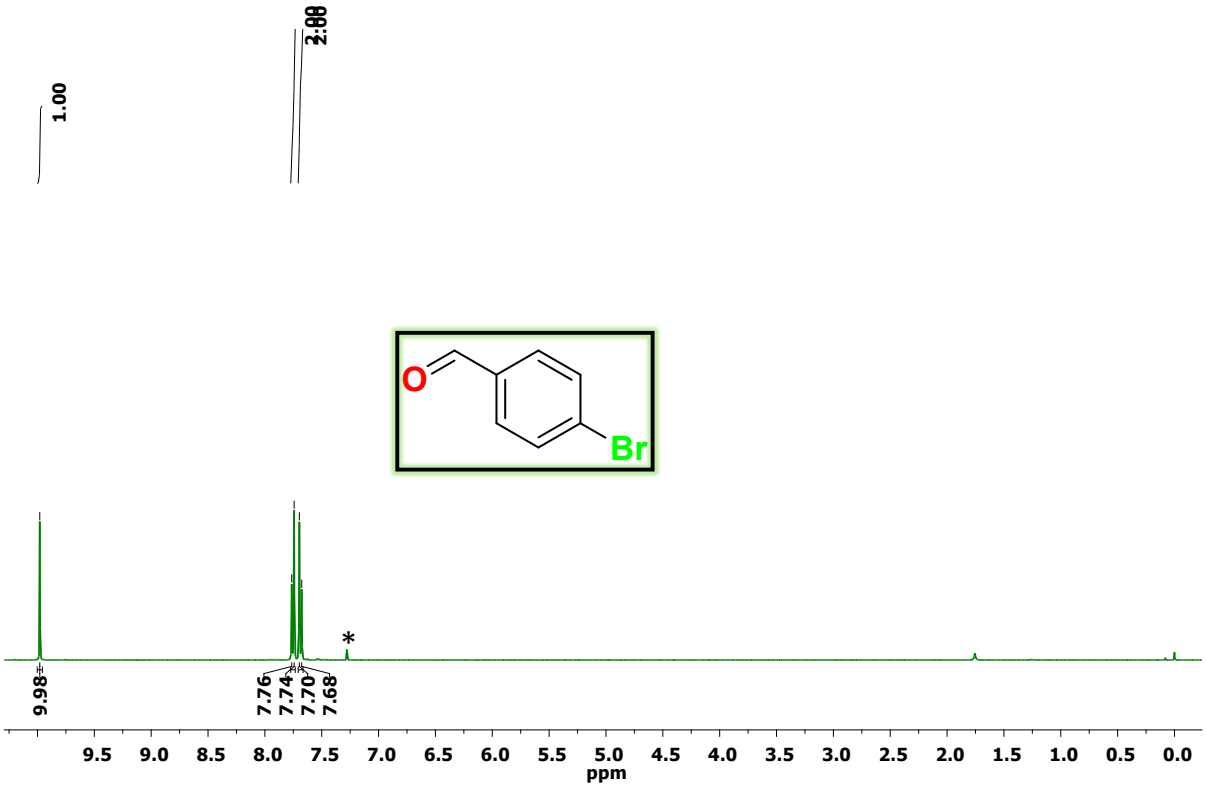

Fig. S30 ^{1}H NMR spectrum of bromobenzaldehyde in $CDCl_3$ solvent where * represents the residual solvent and/or adventitious water peaks.

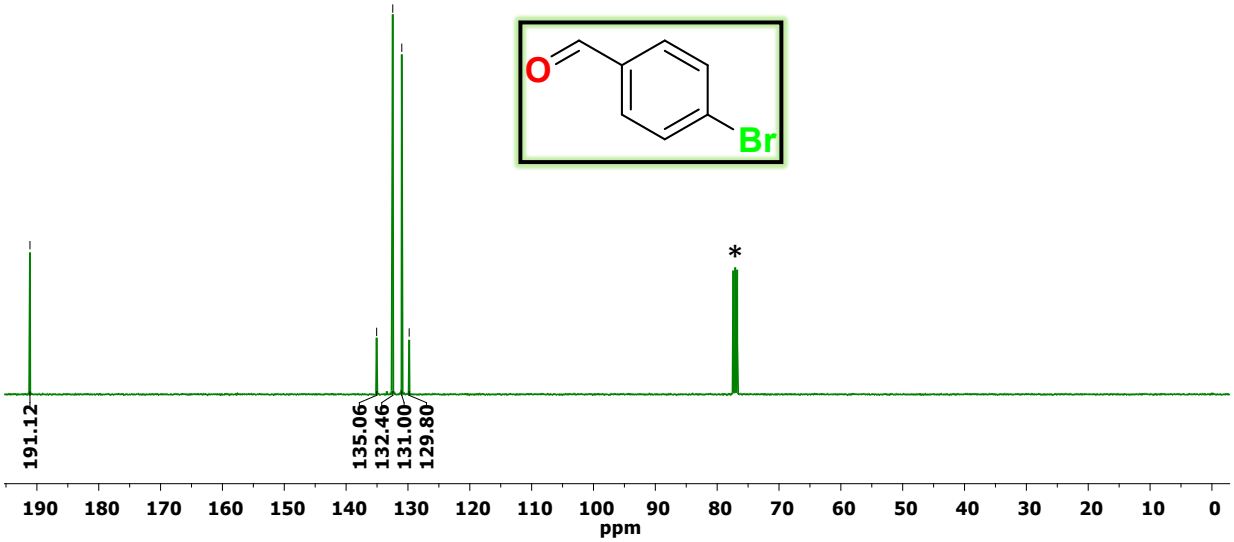

Fig. S31 ^{13}C NMR spectrum of bromobenzaldehyde in $CDCl_3$ solvent where * represents the residual solvent and/or adventitious water peaks.

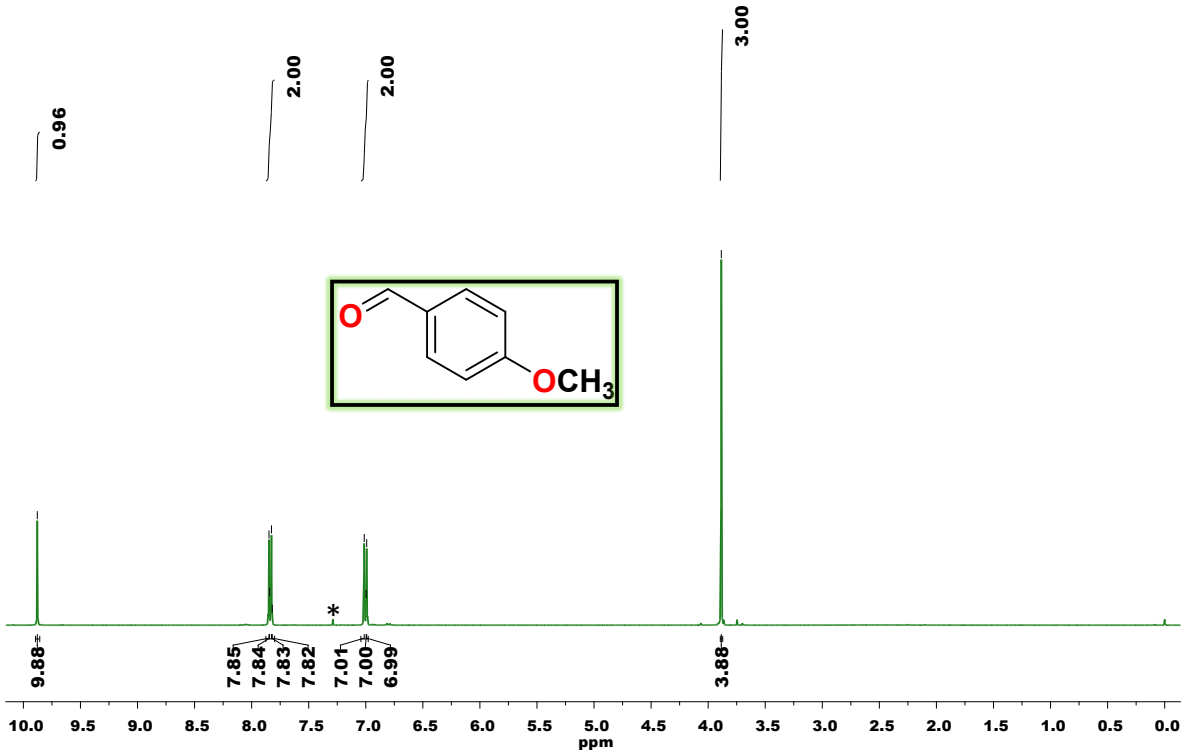

Fig. S32 ^{1}H NMR spectrum of anisaldehyde in $CDCl_3$ solvent where * represents the residual solvent and/or adventitious water peaks.

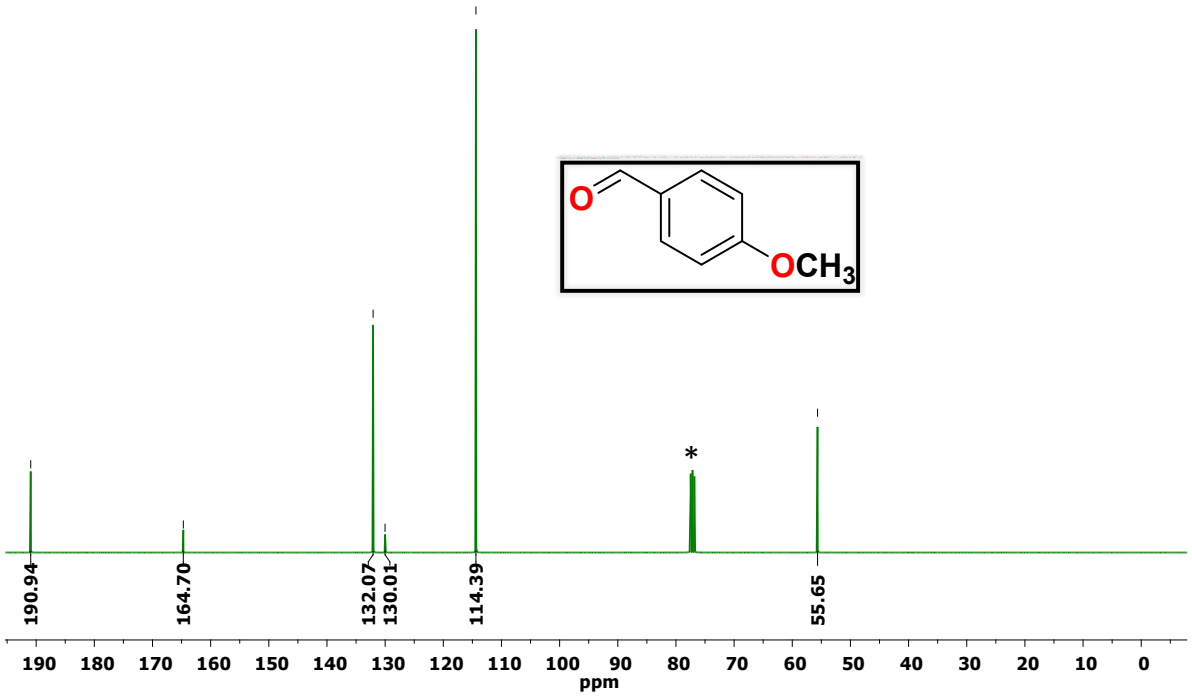

Fig. S33 ^{13}C NMR spectrum of anisaldehyde in $CDCl_3$ solvent where * represents the residual solvent and/or adventitious water peaks.

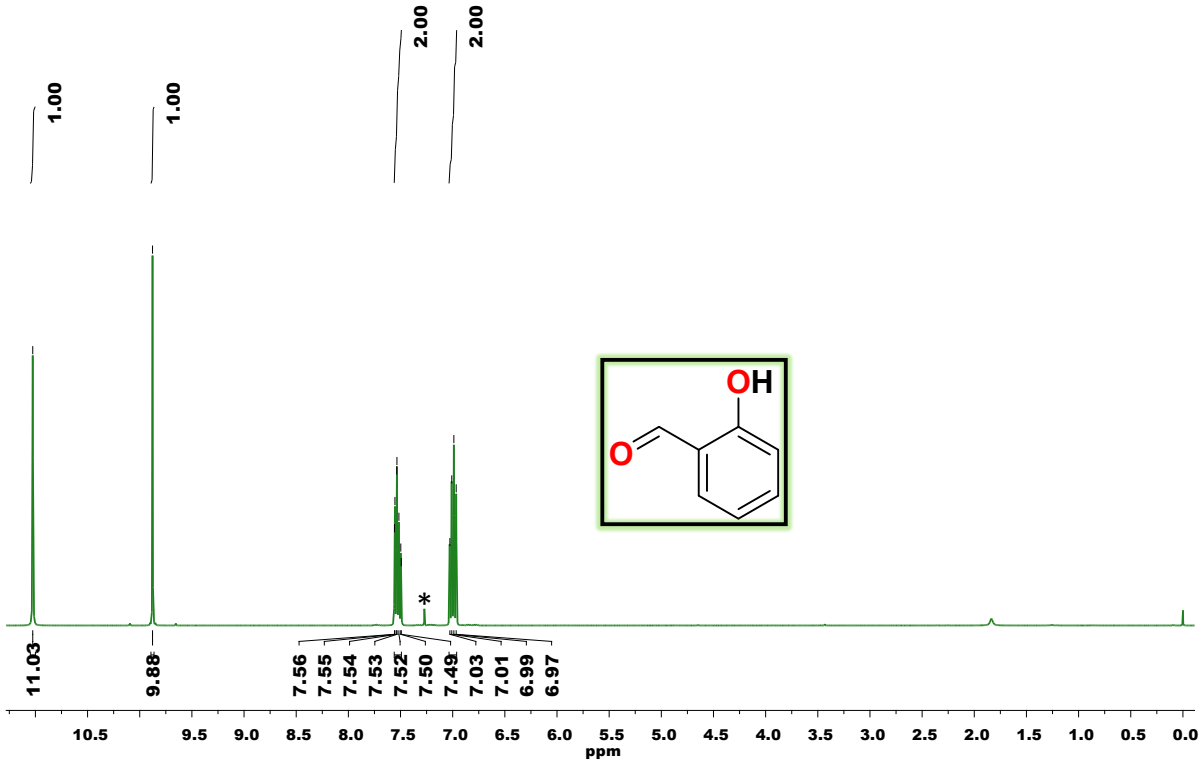

Fig. S34 ^{1}H NMR spectrum of salicaldehyde in $CDCl_3$ solvent where * represents the residual solvent and/or adventitious water peaks.

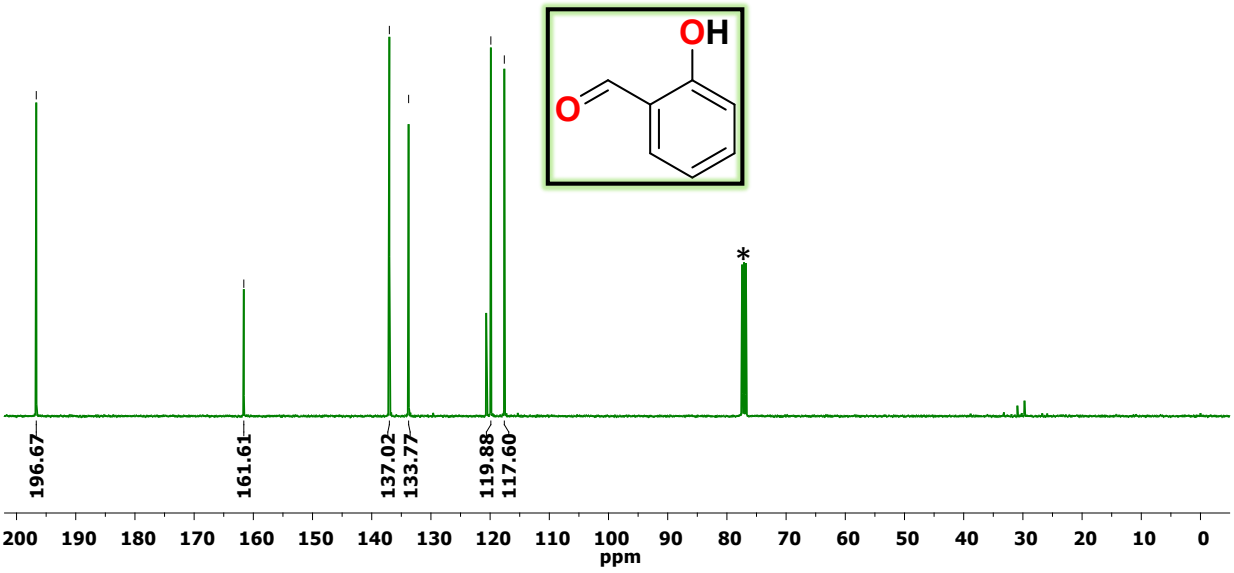

Fig. S35 ^{13}C NMR spectrum of salicaldehyde in $CDCl_3$ solvent where * represents the residual solvent and/or adventitious water peaks.

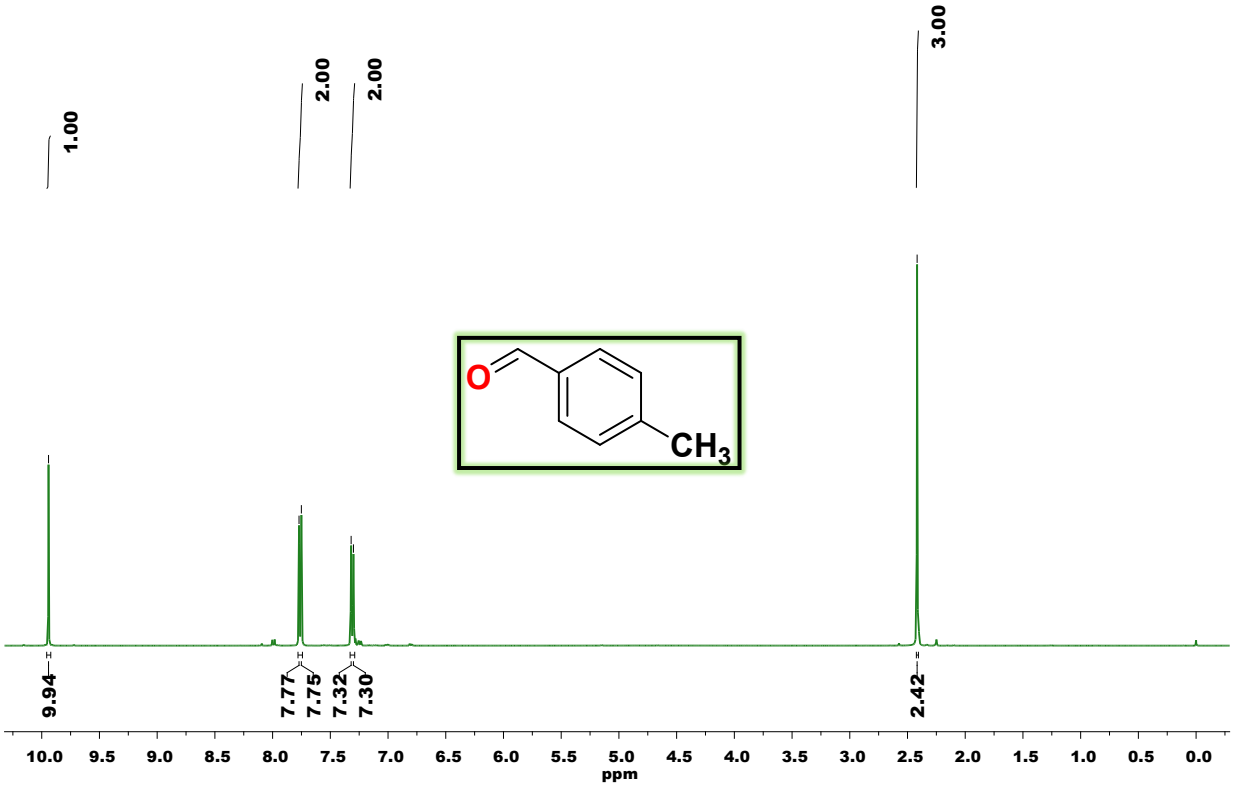

Fig. S36 ^{1}H NMR spectrum of *p*-toulenealdehyde in $CDCl_3$ solvent where * represents the residual solvent and/or adventitious water peaks.

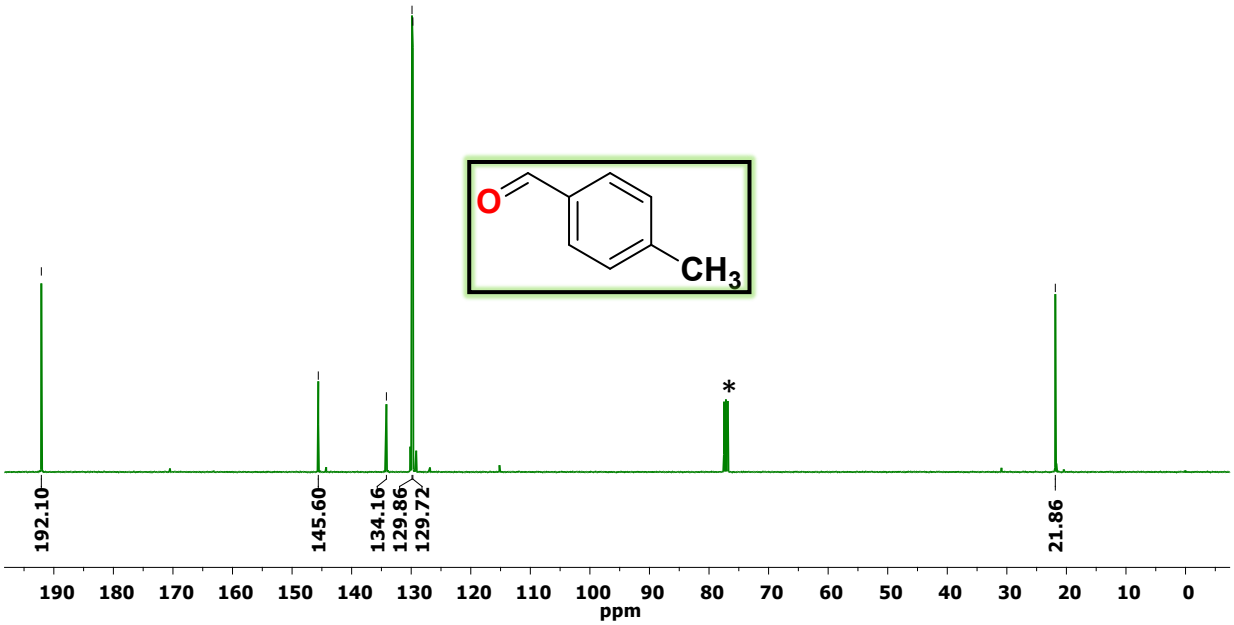

Fig. S37 ^{13}C NMR spectrum of *p*-toulenealdehyde in $CDCl_3$ solvent where * represents the residual solvent and/or adventitious water peaks.

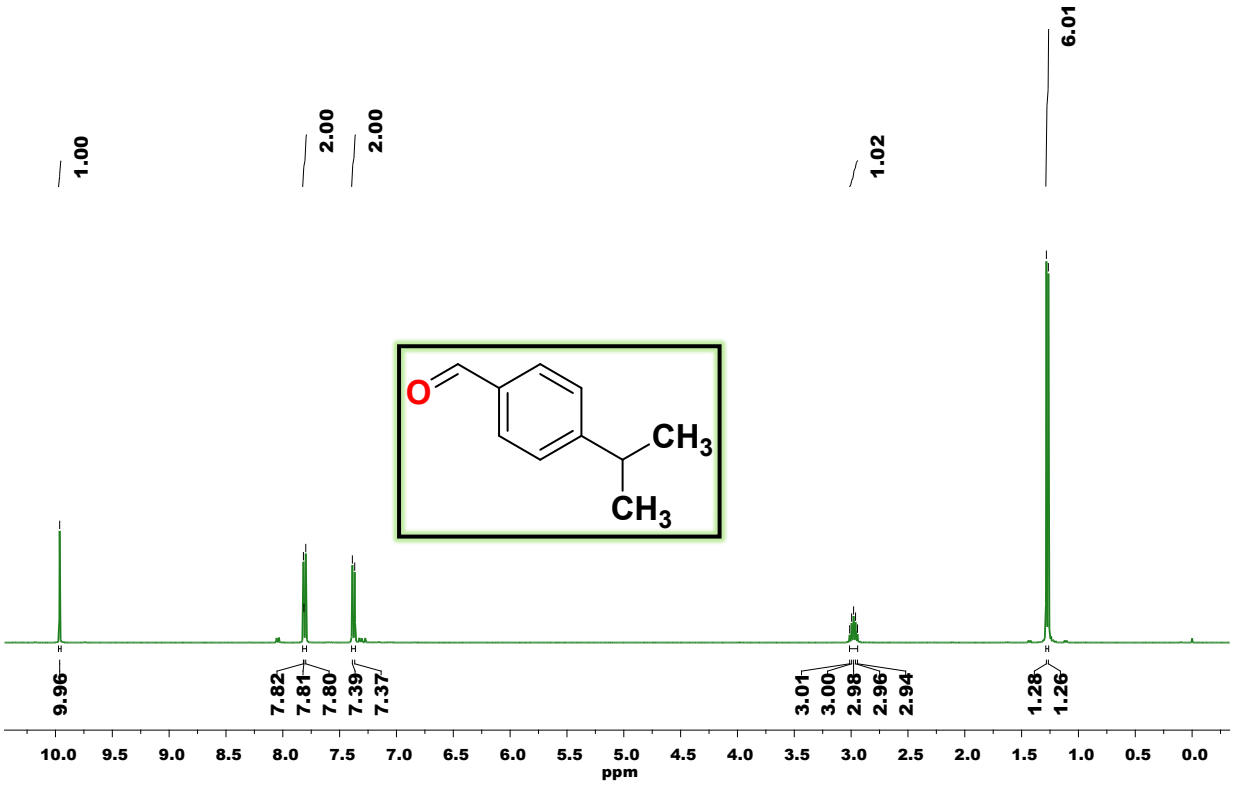

Fig. S38 ^{1}H NMR spectrum of cuminaldehyde in $CDCl_3$ solvent where * represents the residual solvent and/or adventitious water peaks.

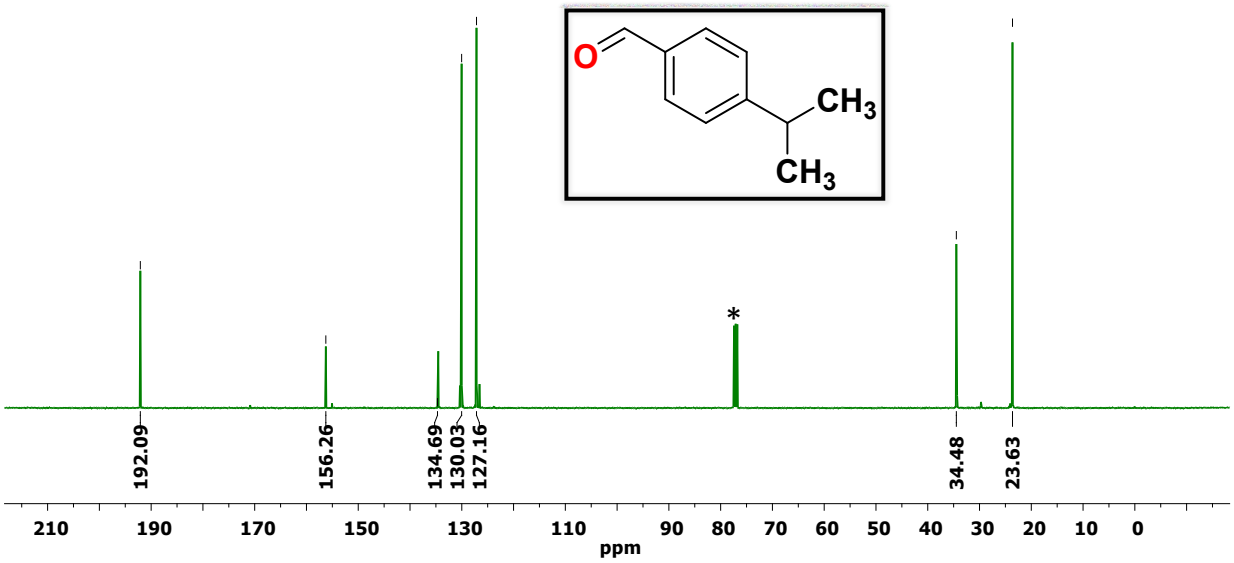

Fig. S39 ^{13}C NMR spectrum of cuminaldehyde in $CDCl_3$ solvent where * represents the residual solvent and/or adventitious water peaks.

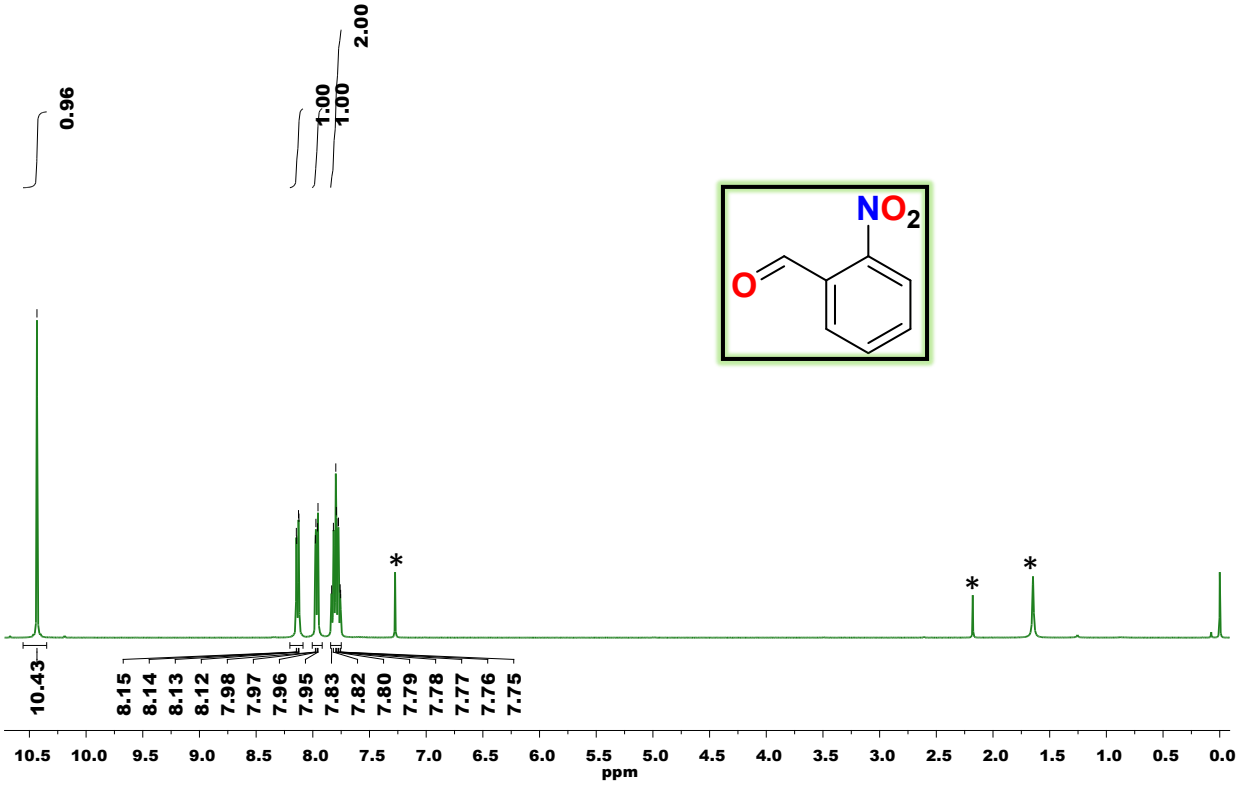

Fig. S40 ^{1}H NMR spectrum of 2-nitrobenzaldehyde in $CDCl_3$ solvent where * represents the residual solvent and/or adventitious water peaks.

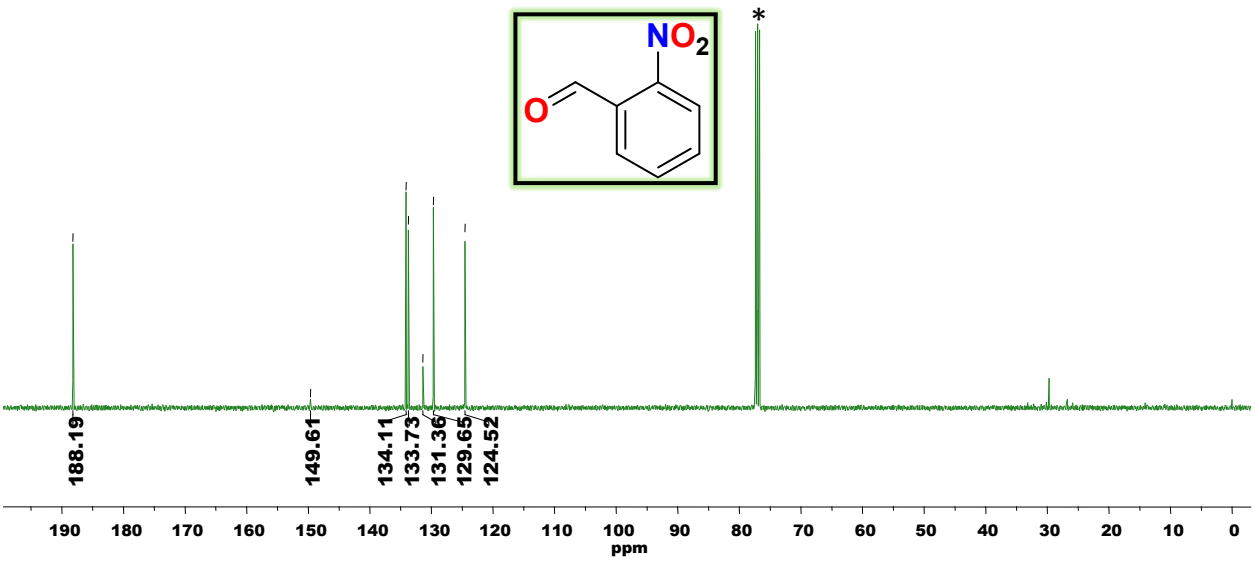

Fig. S41 ^{13}C NMR spectrum of 2-nitrobenzaldehyde in $CDCl_3$ solvent where * represents the residual solvent and/or adventitious water peaks.

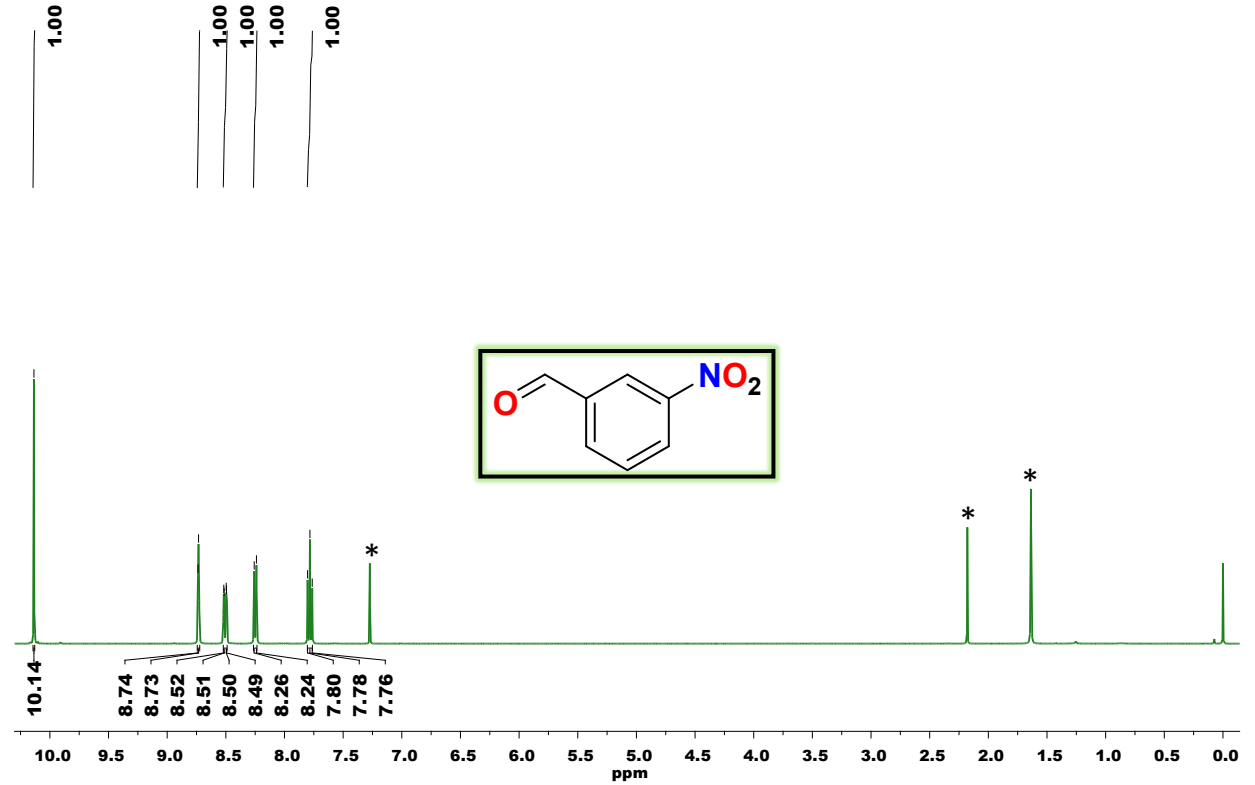

Fig. S42 ^{1}H NMR spectrum of 3-nitrobenzaldehyde in $CDCl_3$ solvent where * represents the residual solvent and/or adventitious water peaks.

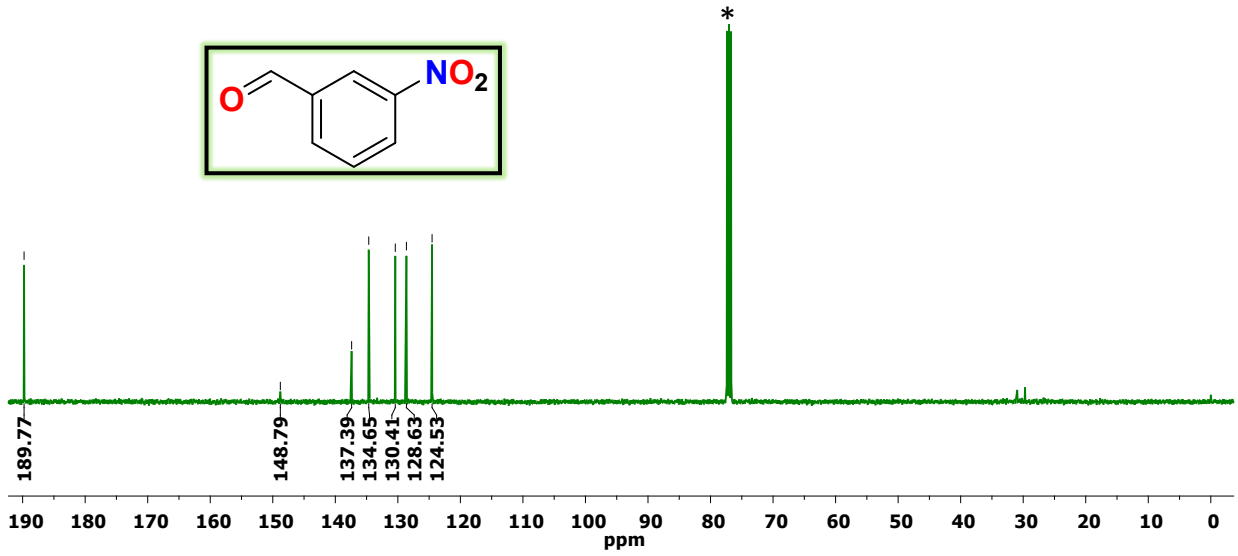

Fig. S43 ^{13}C NMR spectrum of 3-nitrobenzaldehyde in $CDCl_3$ solvent where * represents the residual solvent and/or adventitious water peaks.

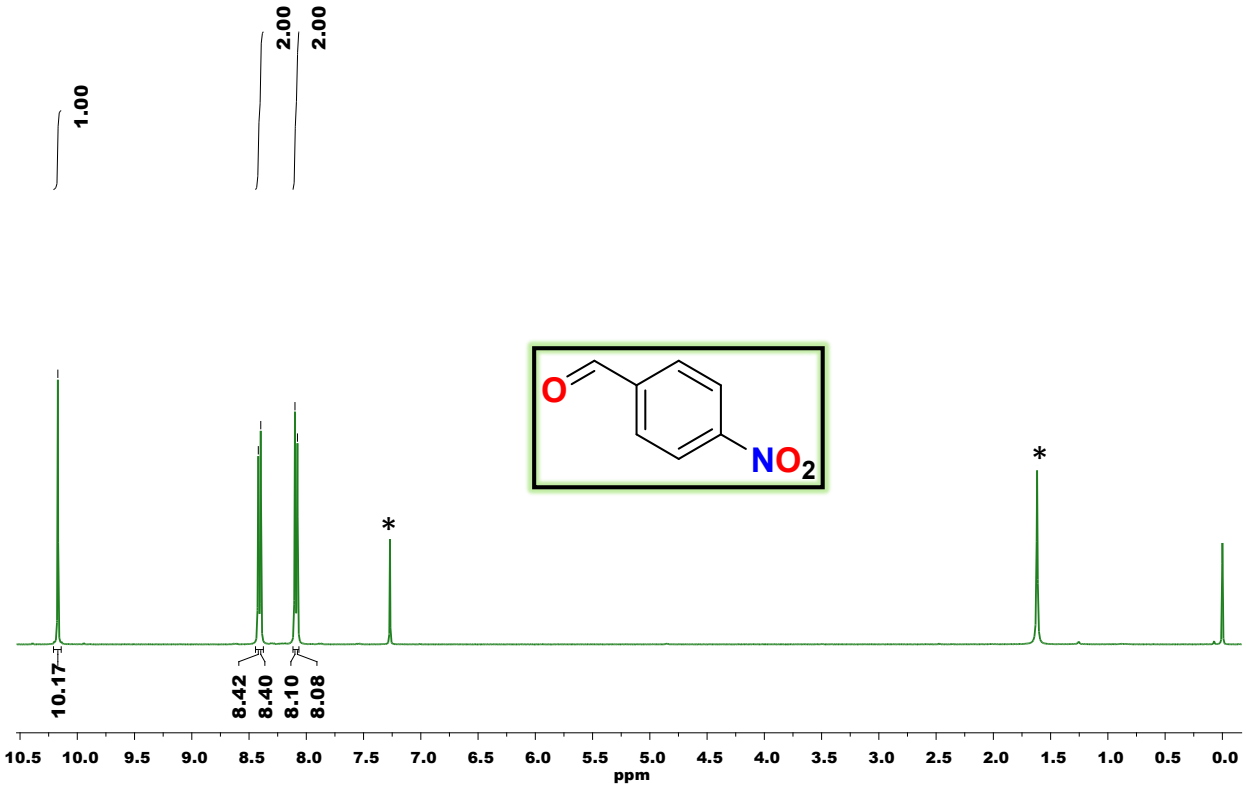

Fig. S44 ^{1}H NMR spectrum of 4-nitrobenzaldehyde in $CDCl_3$ solvent where * represents the residual solvent and/or adventitious water peaks.

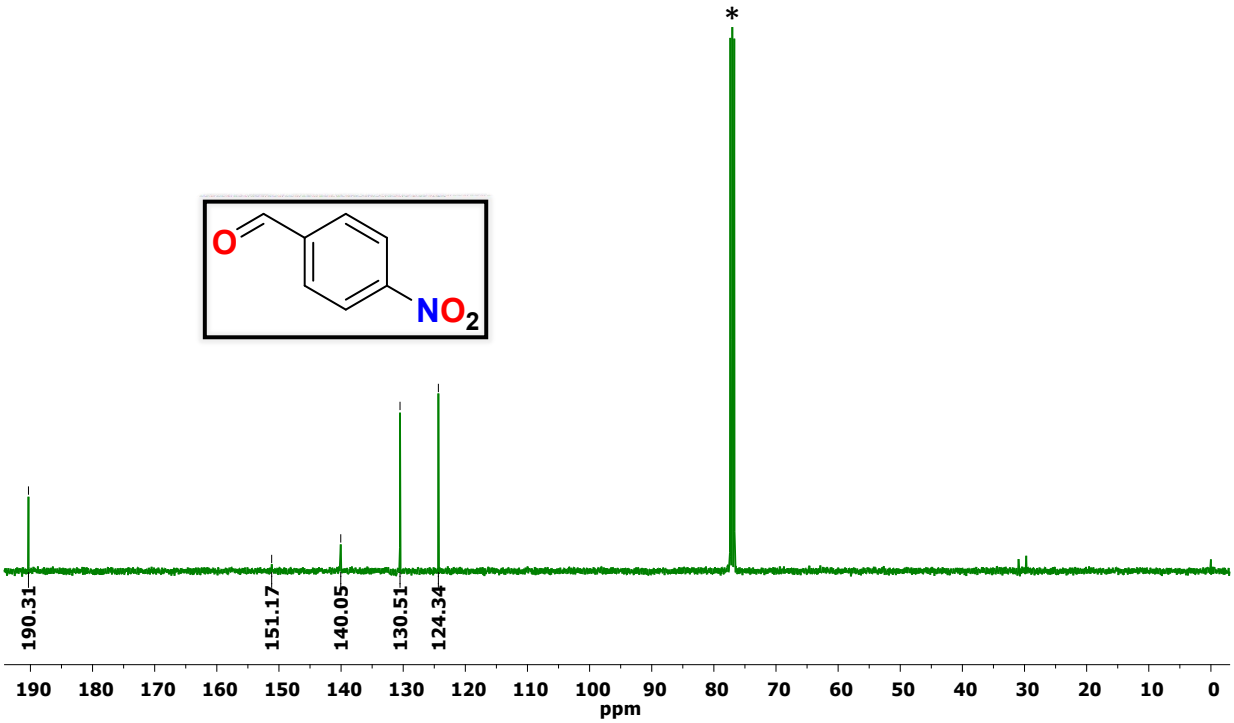

Fig. S45 ^{13}C NMR spectrum of 4-nitrobenzaldehyde in $CDCl_3$ solvent where * represents the residual solvent and/or adventitious water peaks.

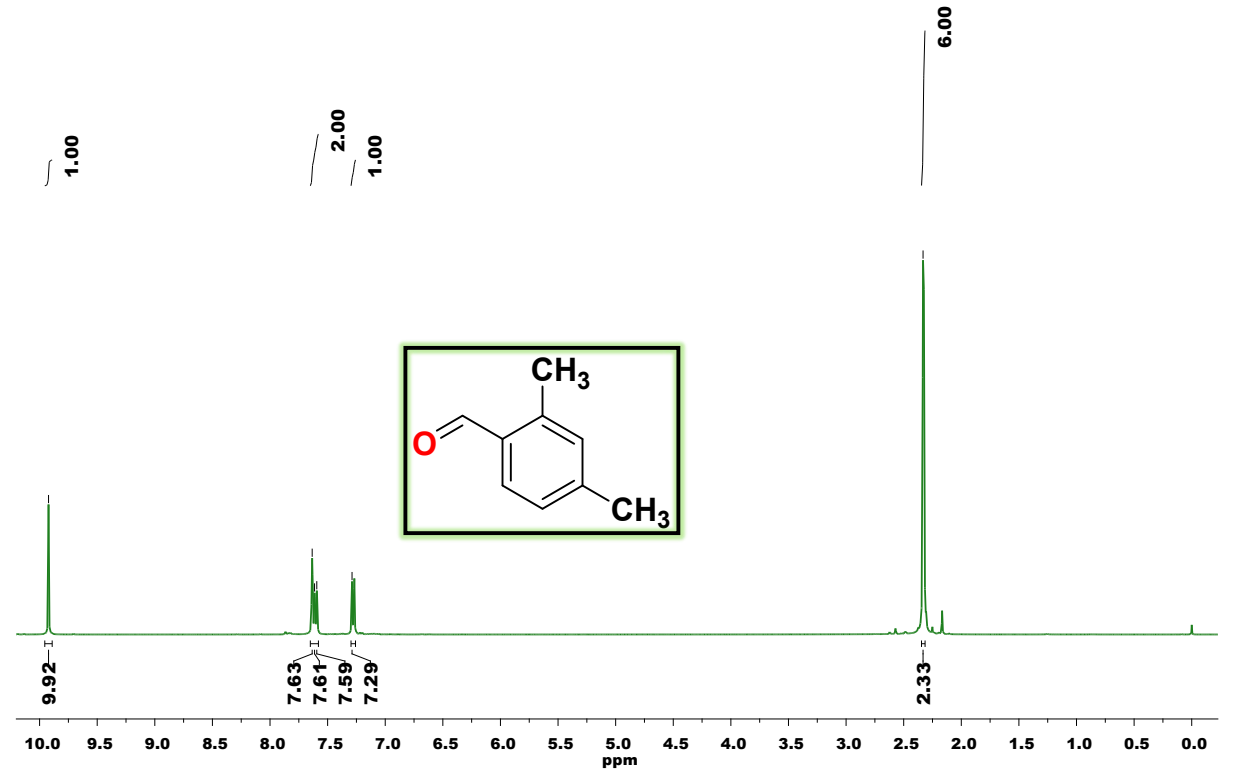

Fig. S46 ^{1}H NMR spectrum of 2,4-dimethylbenzaldehyde in $CDCl_3$ solvent where * represents the residual solvent and/or adventitious water peaks.

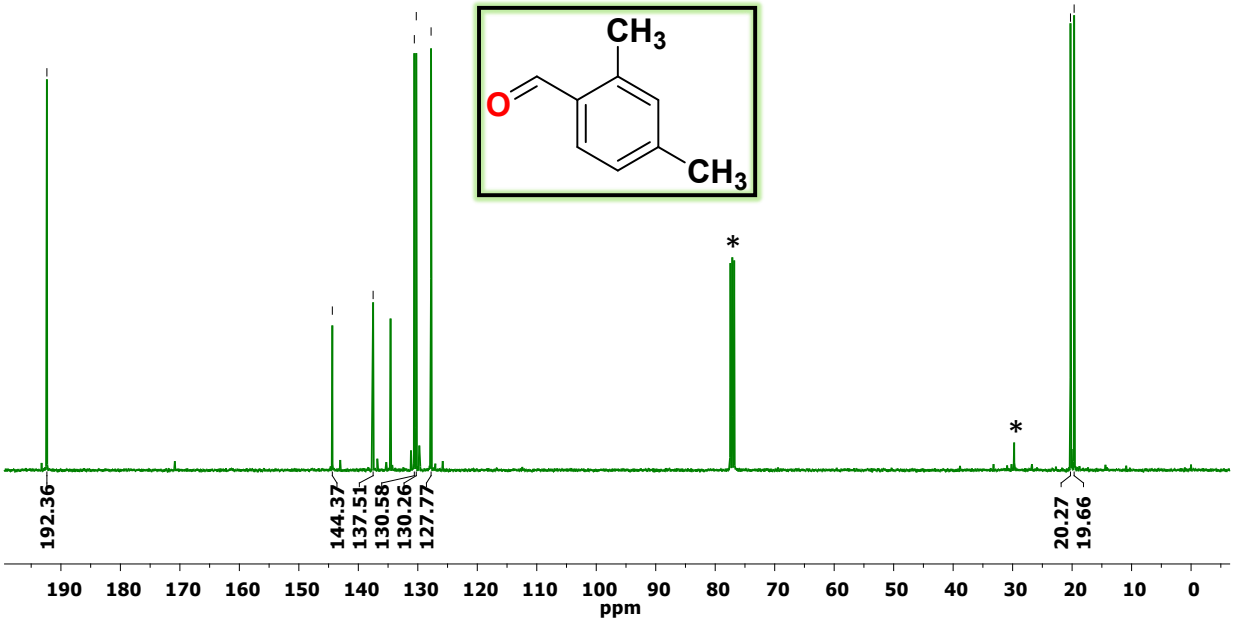

Fig. S47 ^{13}C NMR spectrum of 2,4-dimethylbenzaldehyde in $CDCl_3$ solvent where * represents the residual solvent and/or adventitious water peaks.

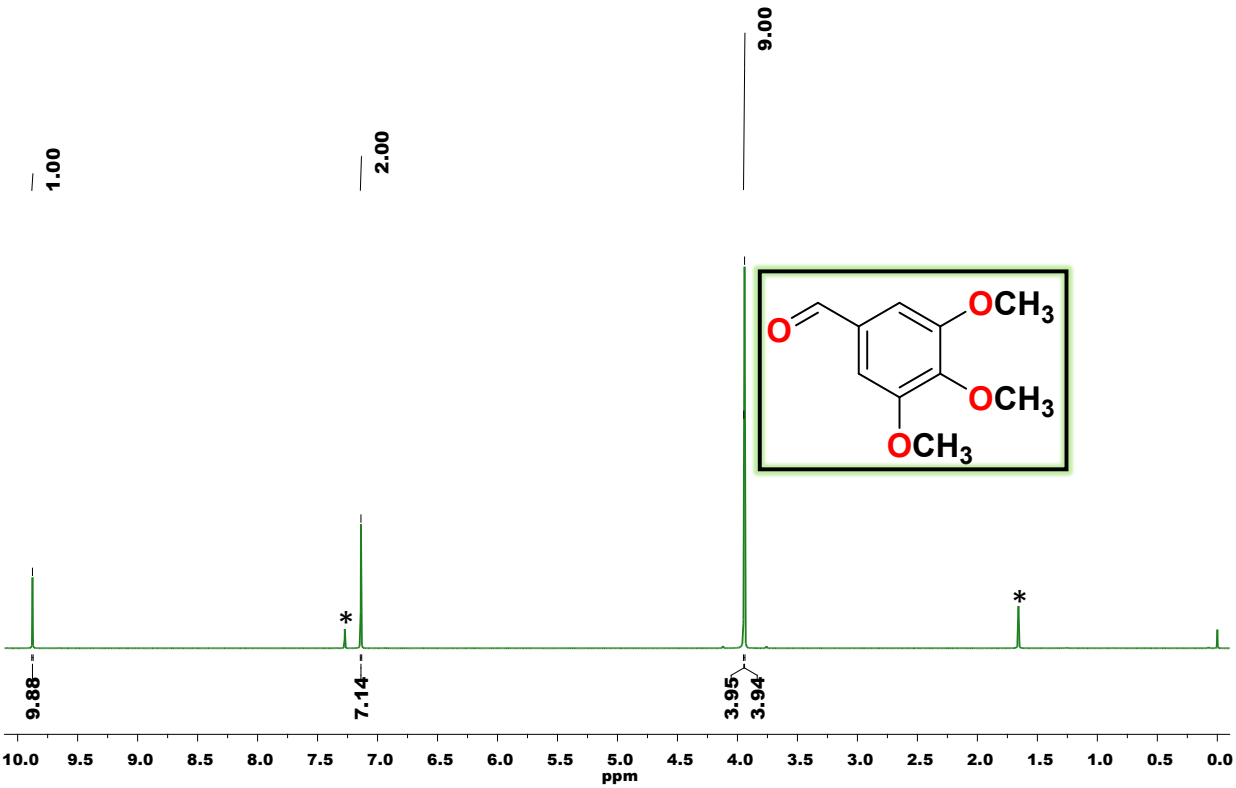

Fig. S48 ^{1}H NMR spectrum of 3,4,5-trimethoxybenzaldehyde in $CDCl_3$ solvent where * represents the residual solvent and/or adventitious water peaks.

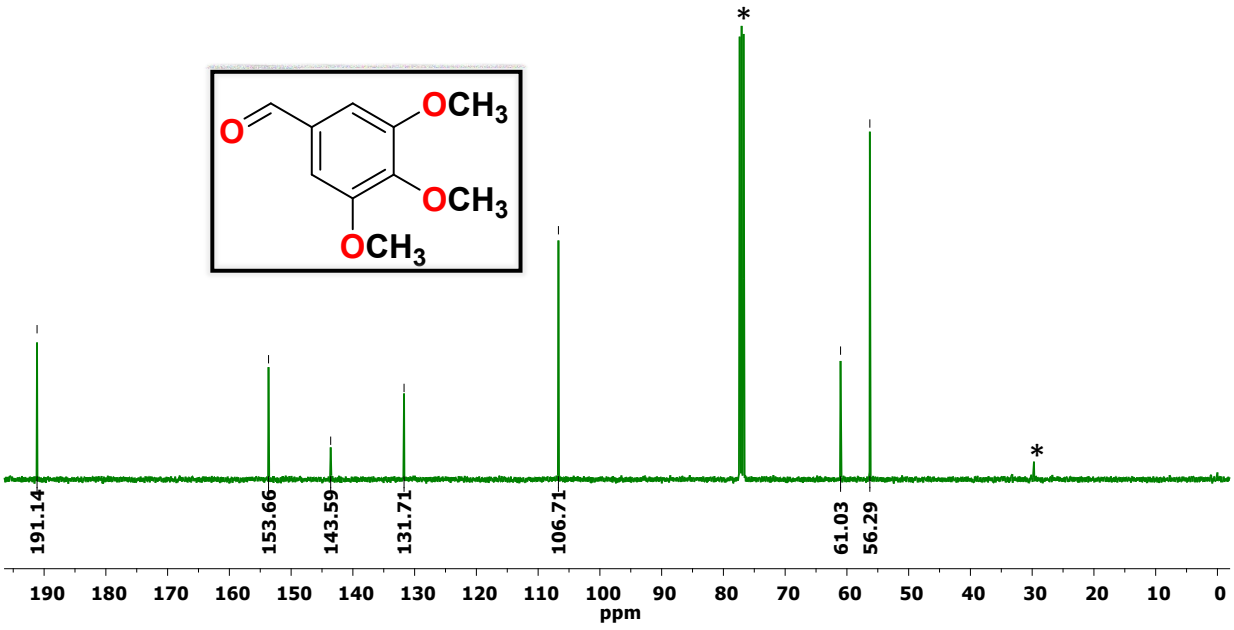

Fig. S49 ^{13}C NMR spectrum of 3,4,5-trimethoxybenzaldehyde in $CDCl_3$ solvent where * represents the residual solvent and/or adventitious water peaks.

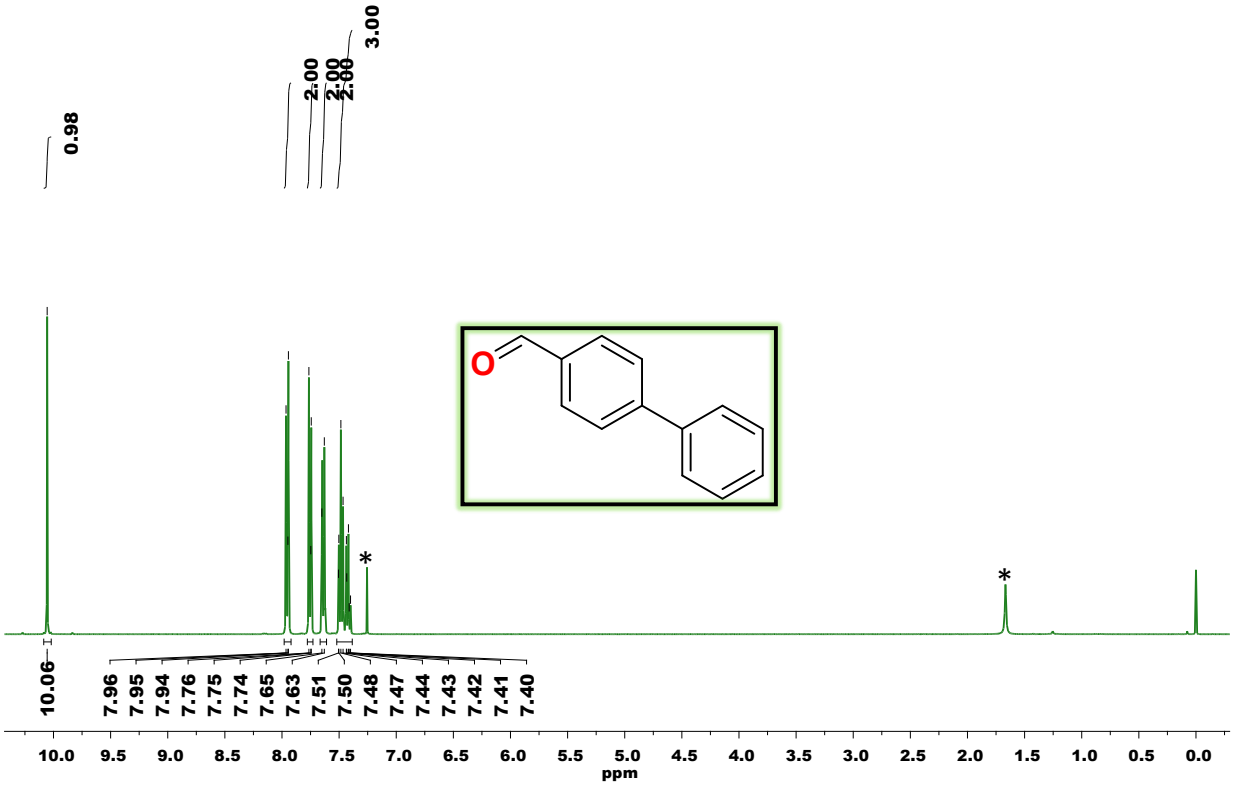

Fig. S50 ^{1}H NMR spectrum of 1,1-biphenyl-4-carbaldehyde in $CDCl_3$ solvent where * represents the residual solvent and/or adventitious water peaks.

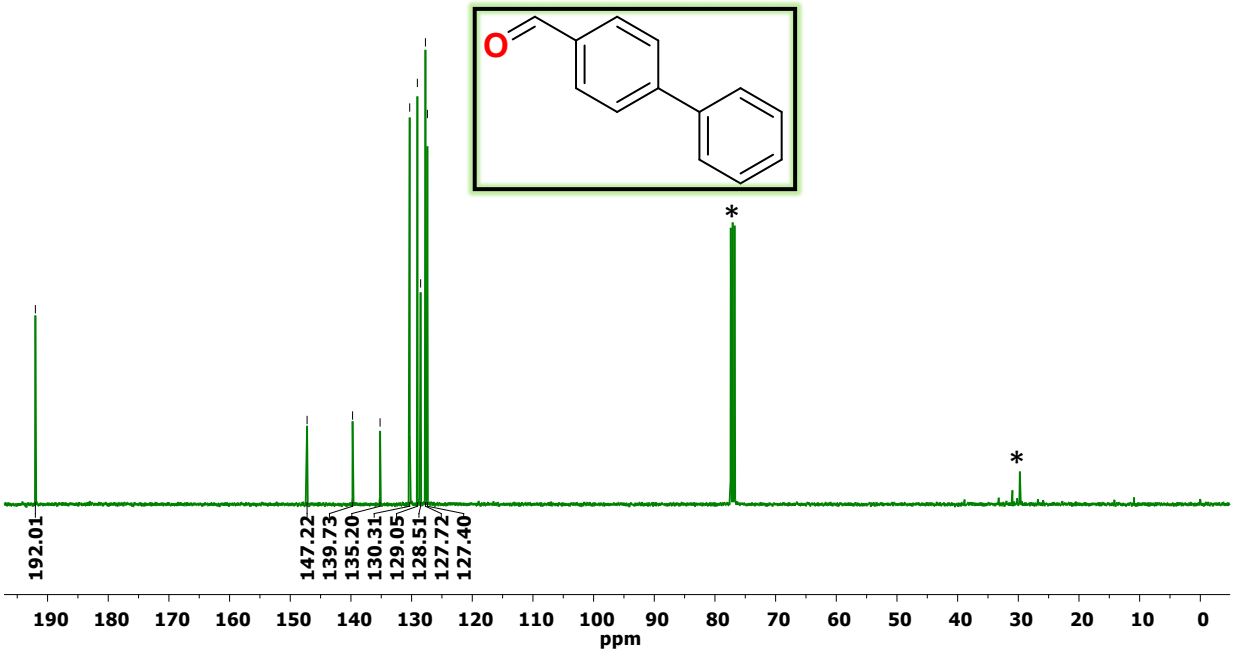

Fig. S51 ^{13}C NMR spectrum of 1,1-biphenyl-4-carbaldehyde in $CDCl_3$ solvent where * represents the residual solvent and/or adventitious water peaks.

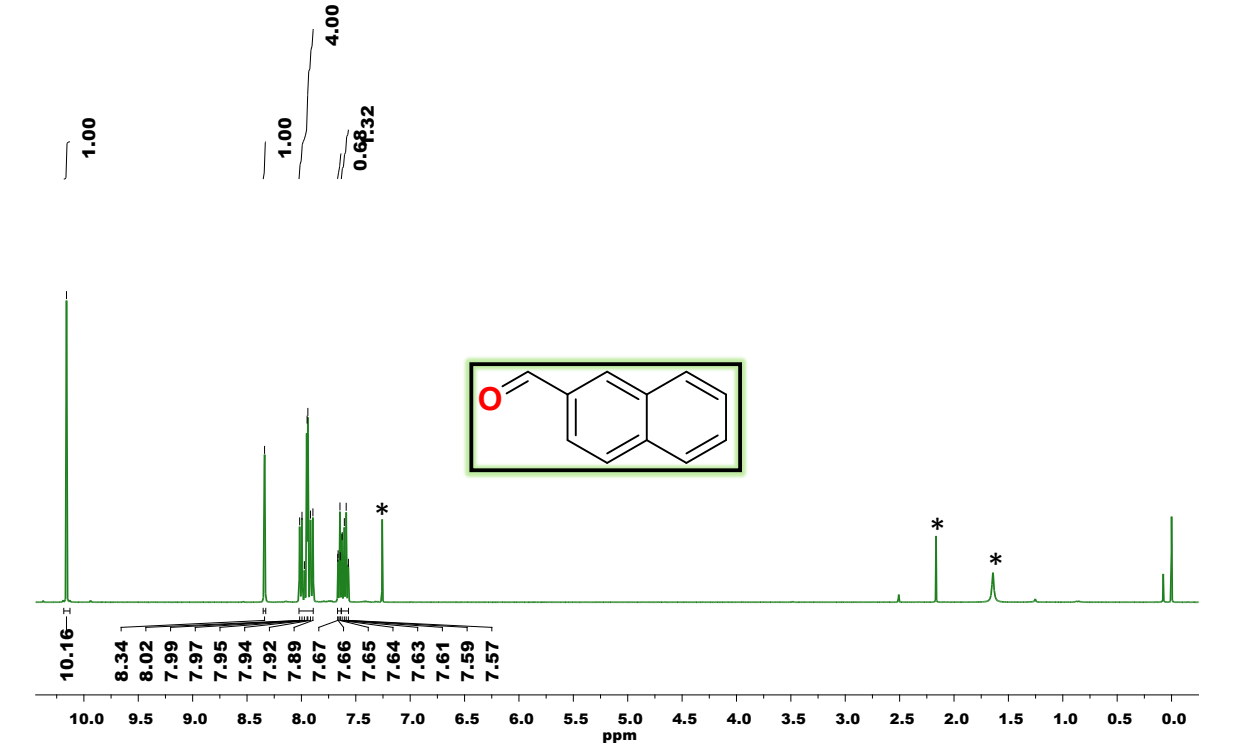

Fig. S52 ^{1}H NMR spectrum of 2-napthaldehyde in $CDCl_3$ solvent where * represents the residual solvent and/or adventitious water peaks.

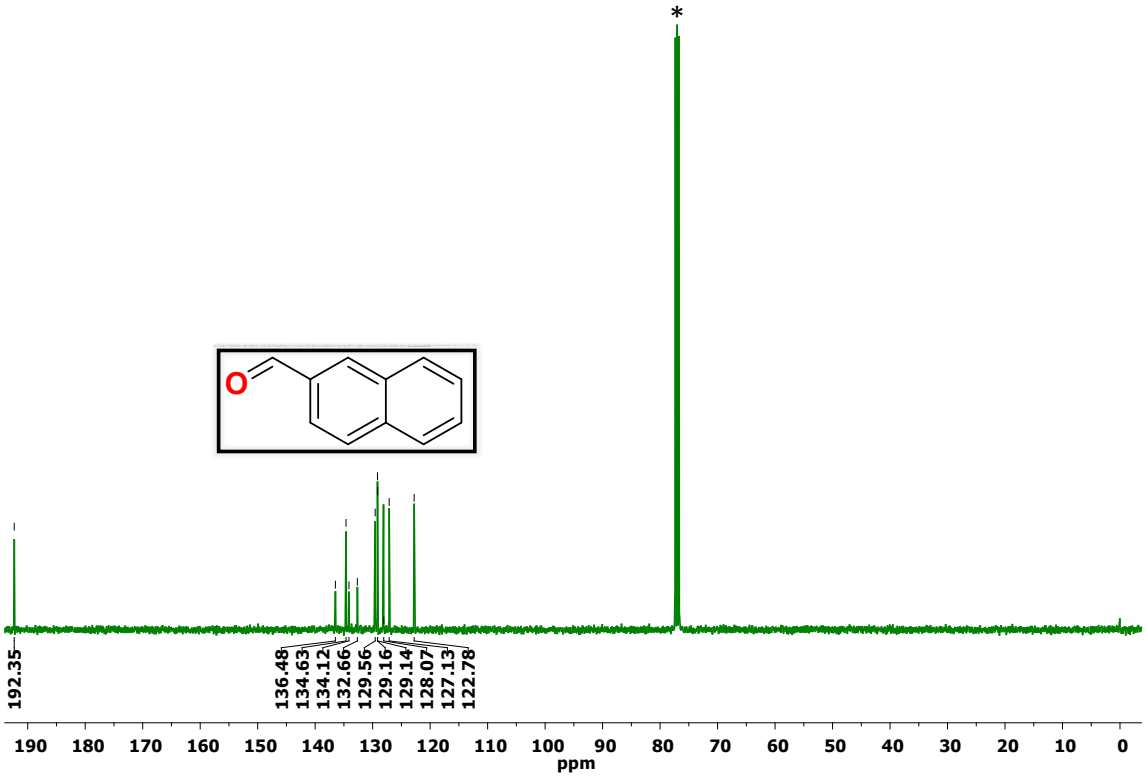

Fig. S53 ^{13}C NMR spectrum of 2-napthaldehyde in $CDCl_3$ solvent where * represents the residual solvent and/or adventitious water peaks.

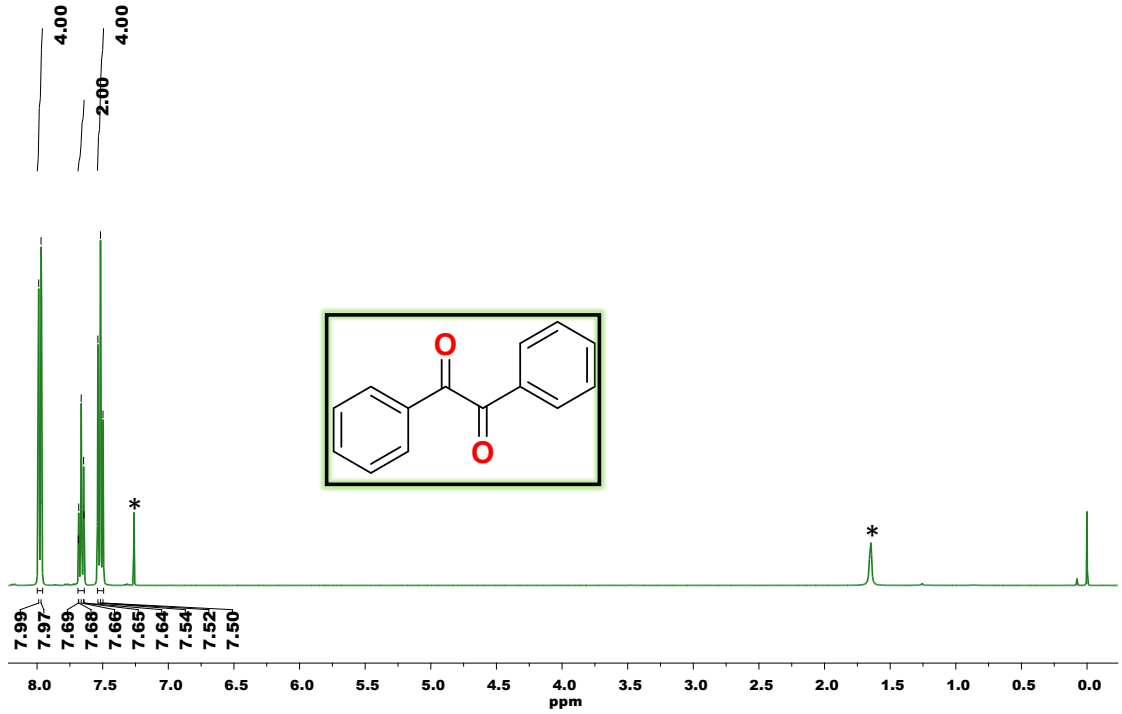

Fig. S54 ^{1}H NMR spectrum of benzil in $CDCl_3$ solvent where * represents the residual solvent and/or adventitious water peaks.

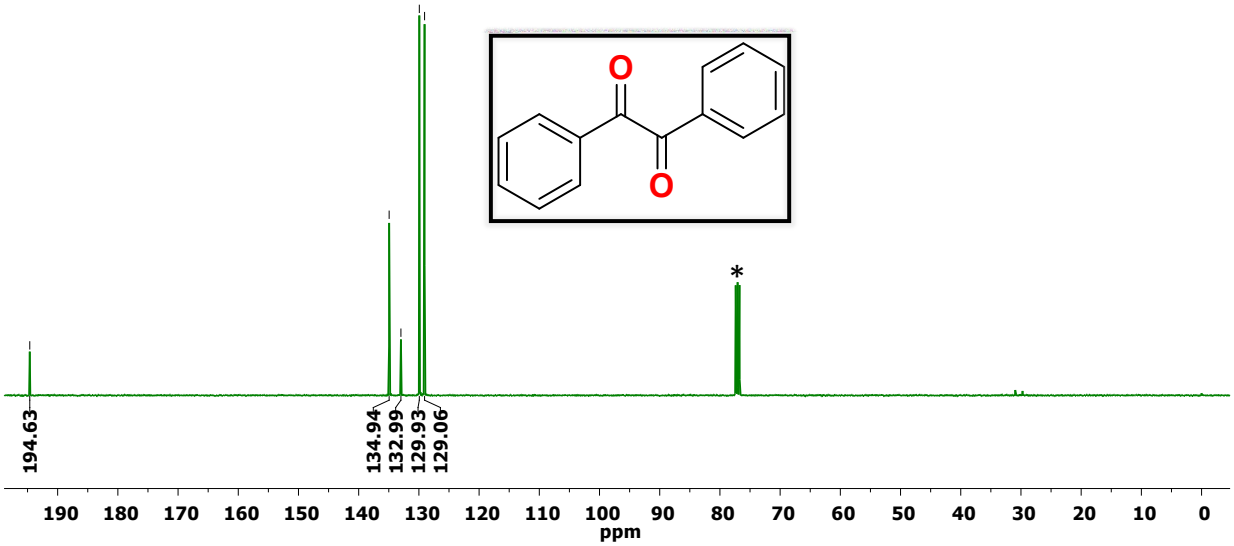

Fig. S55 ^{13}C NMR spectrum of benzil in $CDCl_3$ solvent where * represents the residual solvent and/or adventitious water peaks.

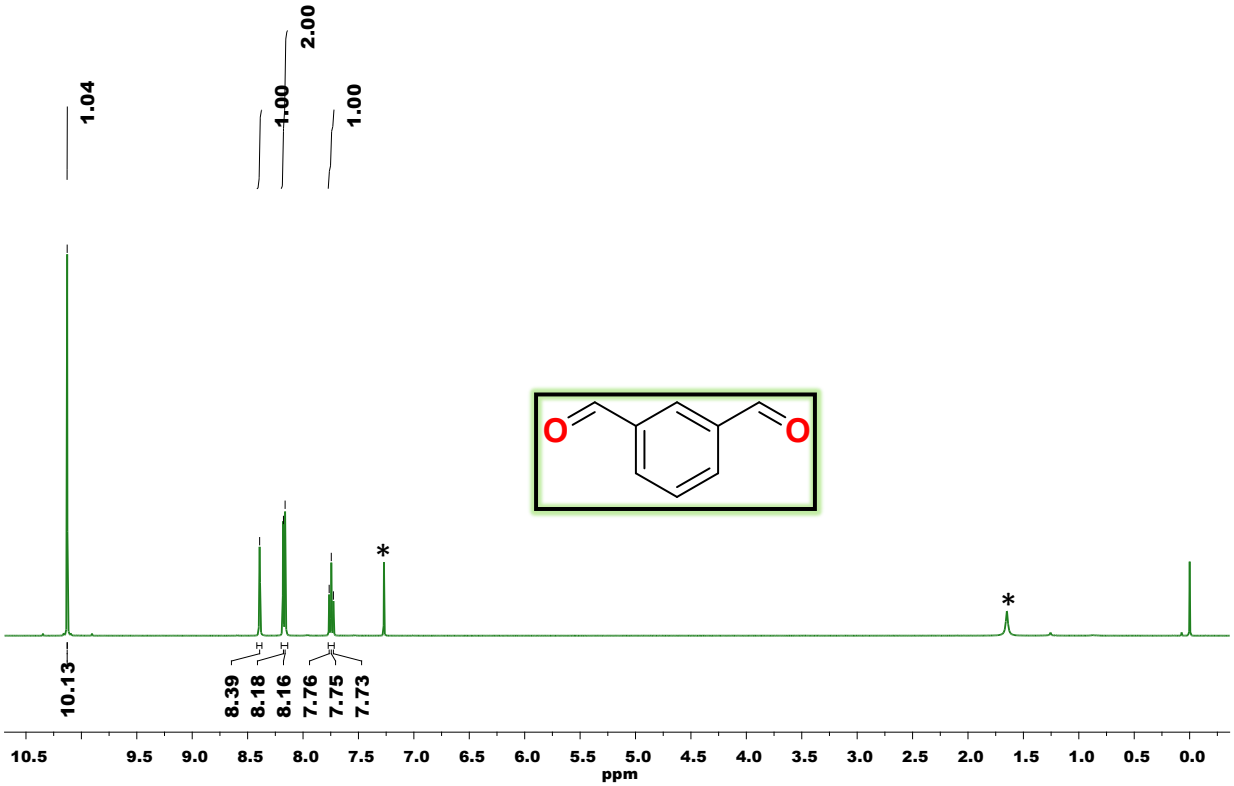

Fig. S56 ^{1}H NMR spectrum of isophthalaldehyde in $CDCl_3$ solvent where * represents the residual solvent and/or adventitious water peaks.

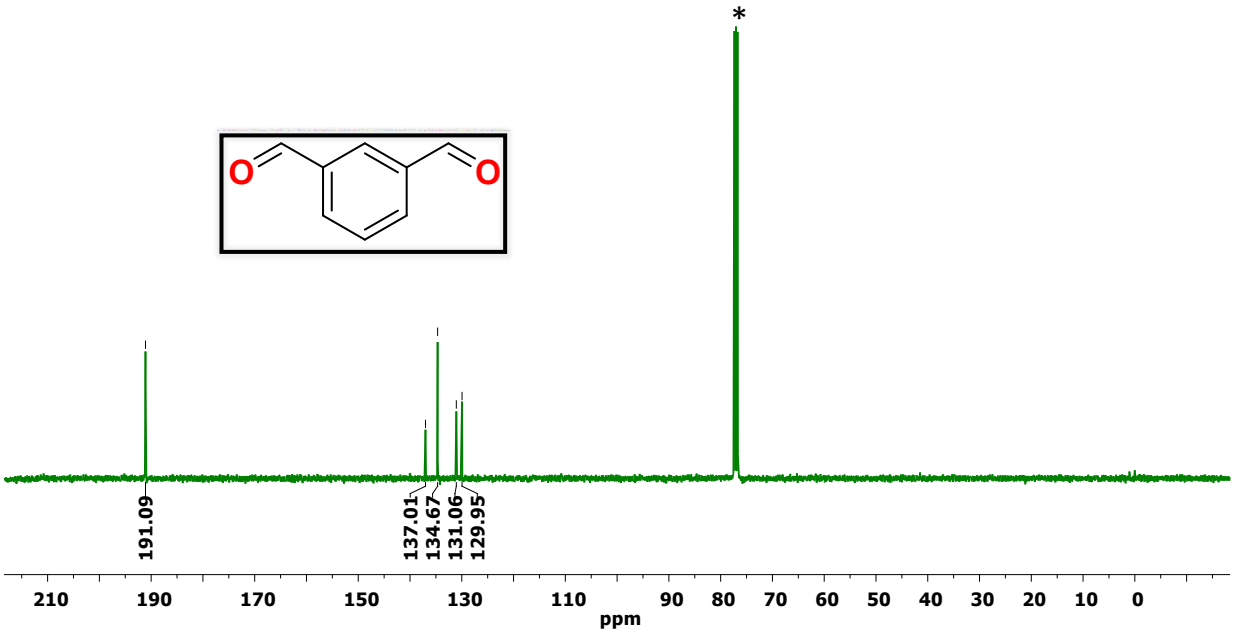

Fig. S57 ^{13}C NMR spectrum of isophthalaldehyde in $CDCl_3$ solvent where * represents the residual solvent and/or adventitious water peaks.

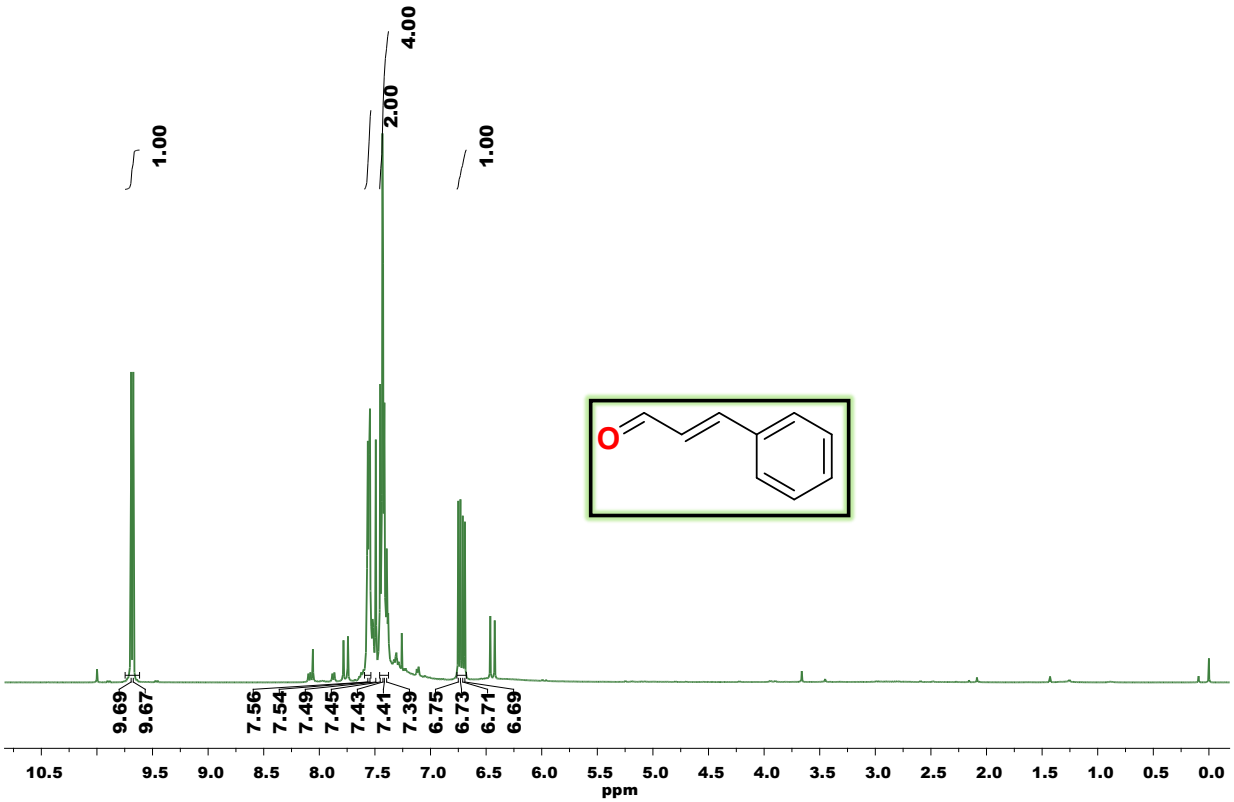

Fig. S58 ^{1}H NMR spectrum of cinnamaldehyde in $CDCl_3$ solvent where * represents the residual solvent and/or adventitious water peaks.

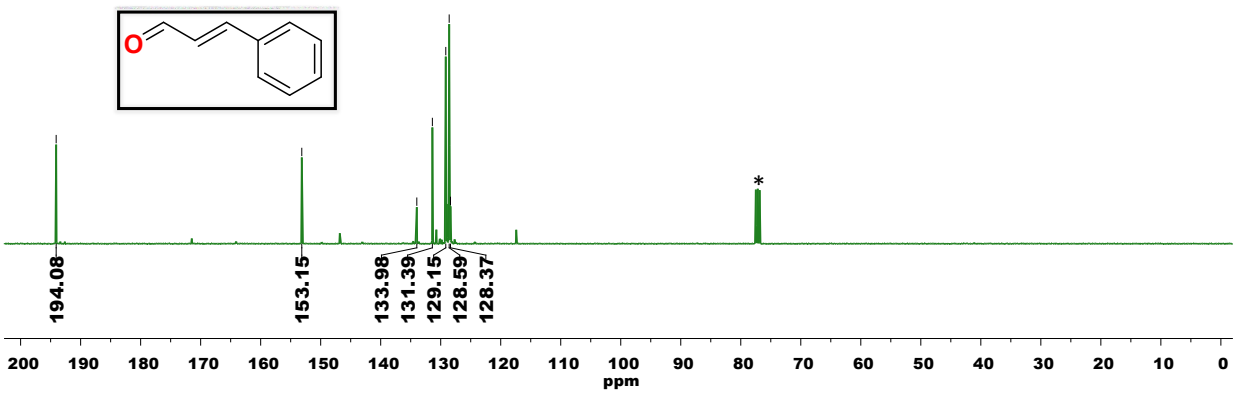

Fig. S59 ^{13}C NMR spectrum of cinnamaldehyde in $CDCl_3$ solvent where * represents the residual solvent and/or adventitious water peaks.

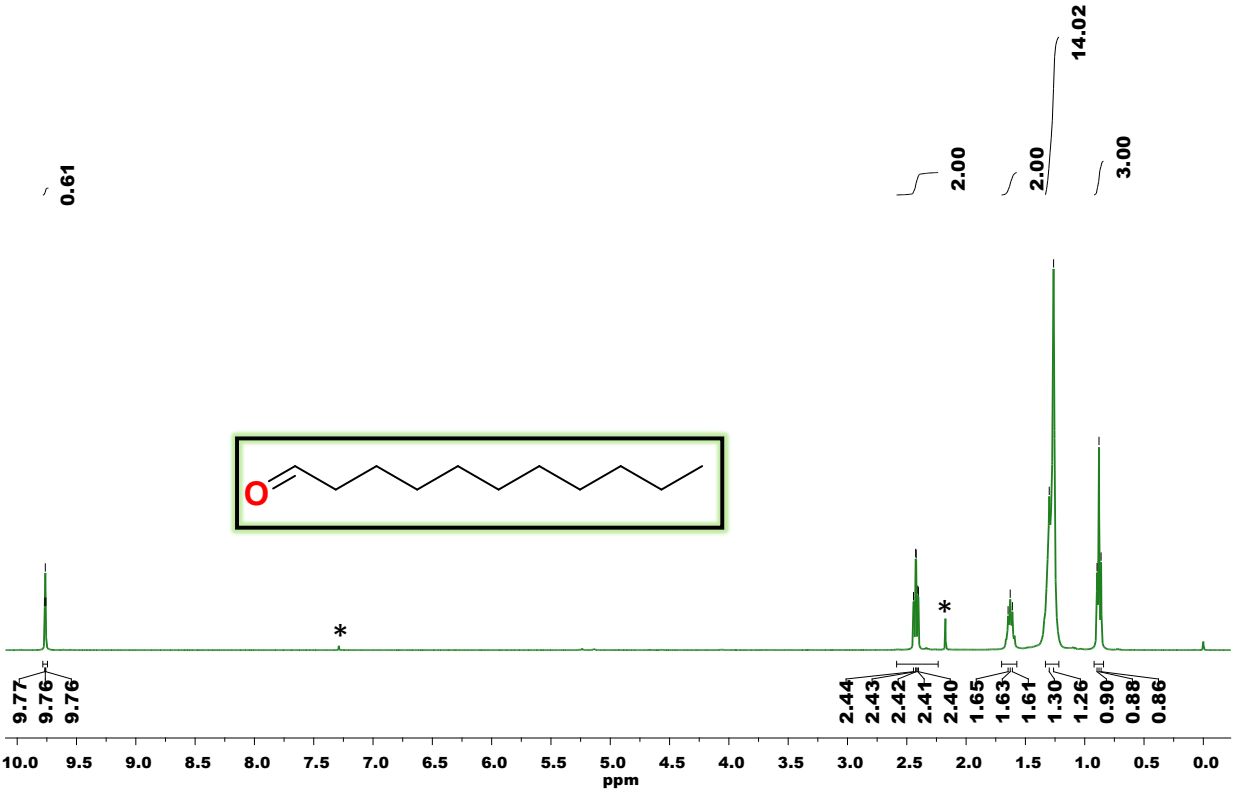

Fig. S60 ^{1}H NMR spectrum of undecanal in $CDCl_3$ solvent where * represents the residual solvent and/or adventitious water peaks.

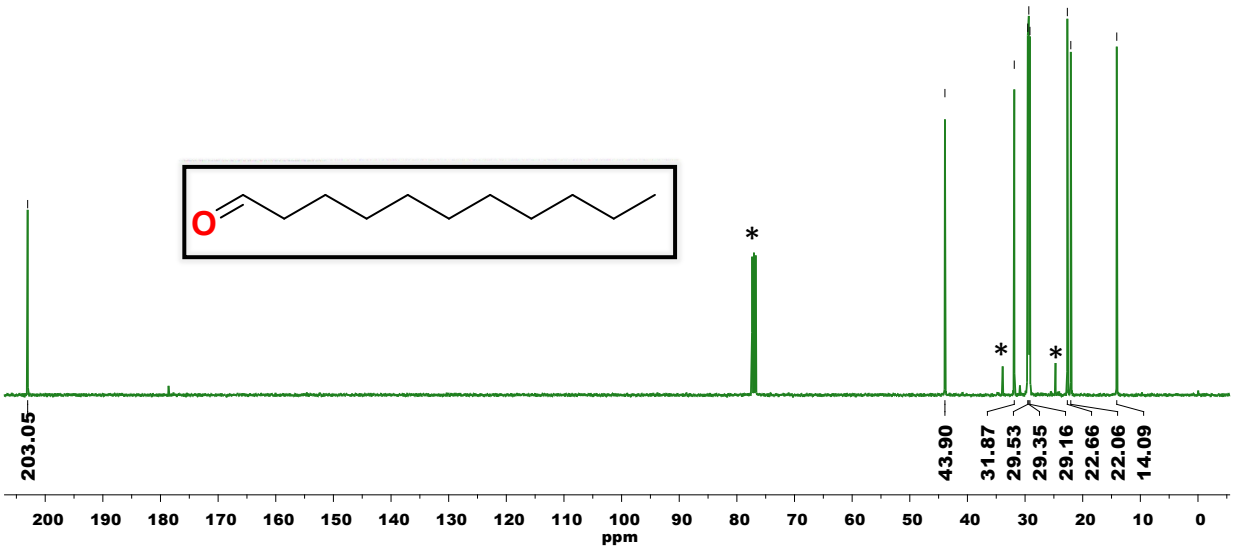

Fig. S61 ^{13}C NMR spectrum of undecanal in $CDCl_3$ solvent where * represents the residual solvent and/or adventitious water peaks.

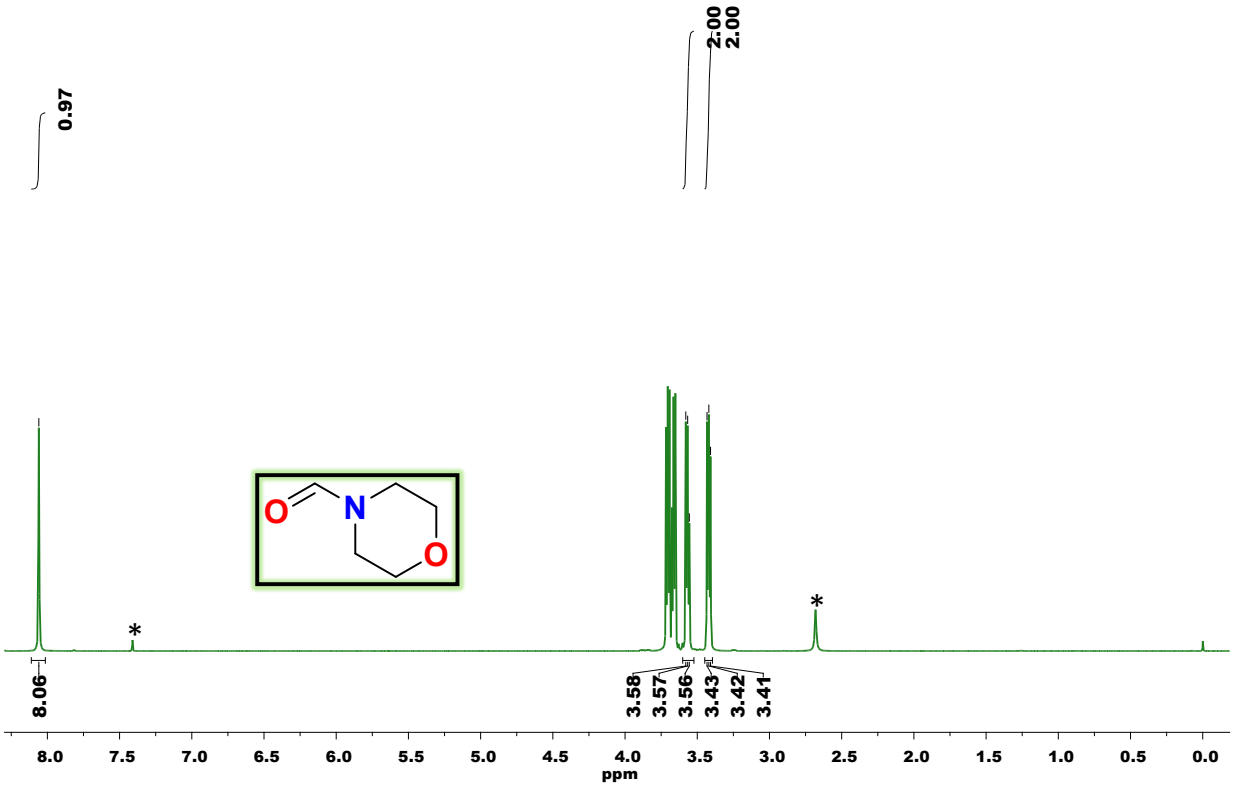

Fig. S62 ^{1}H NMR spectrum of 4-formylmorpholine in $CDCl_3$ solvent where * represents the residual solvent and/or adventitious water peaks.

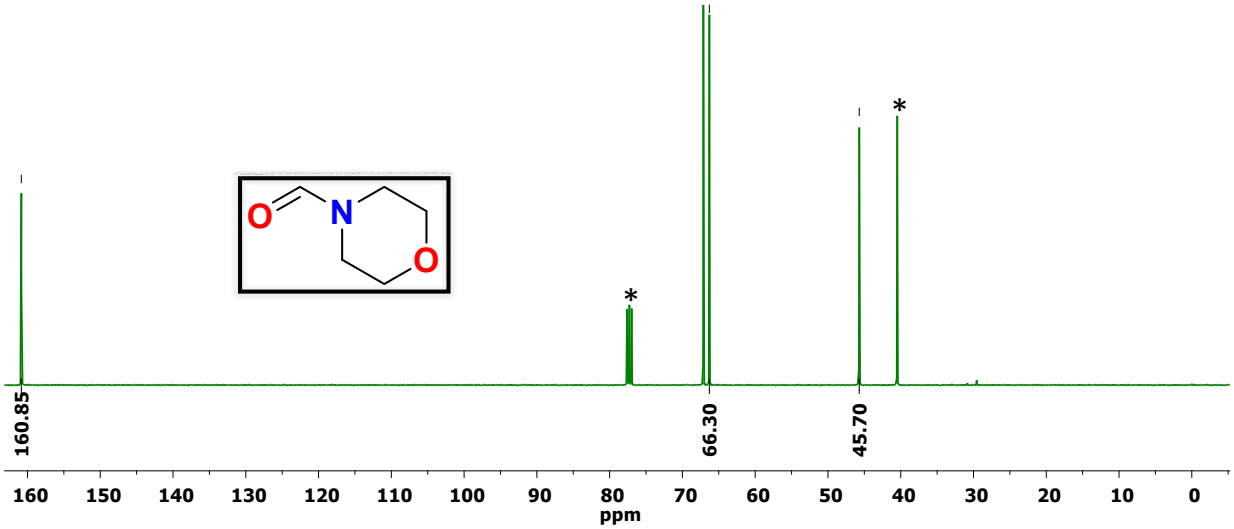

Fig. S63 ^{13}C NMR spectrum of 4-formylmorpholine in $CDCl_3$ solvent where * represents the residual solvent and/or adventitious water peaks.

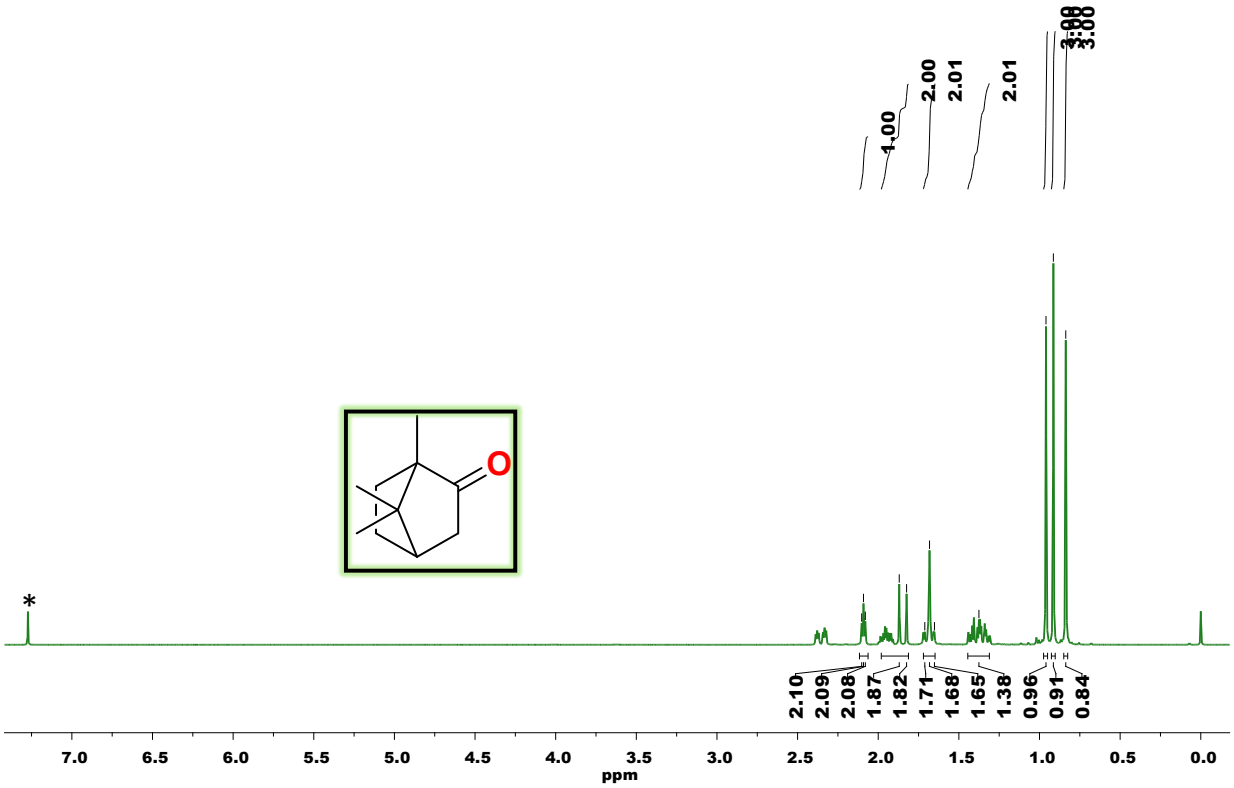

Fig. S64 ^{1}H NMR spectrum of camphor in $CDCl_3$ solvent where * represents the residual solvent and/or adventitious water peaks.

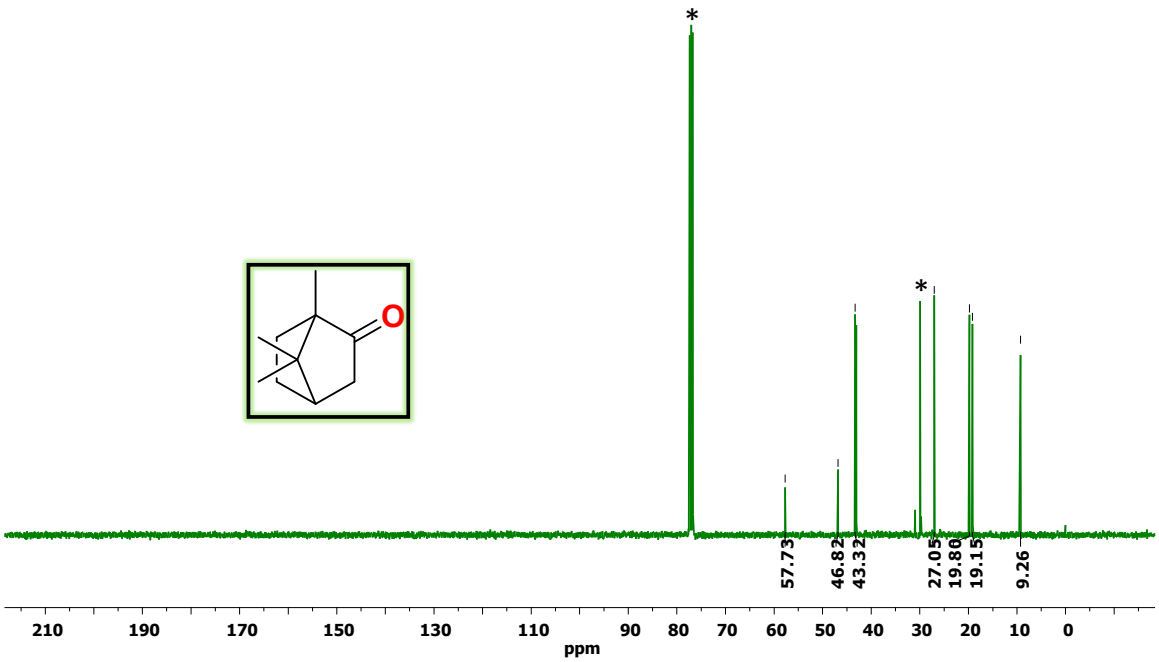

Fig. S65 ^{13}C NMR spectrum of camphor in $CDCl_3$ solvent where * represents the residual solvent and/or adventitious water peaks.

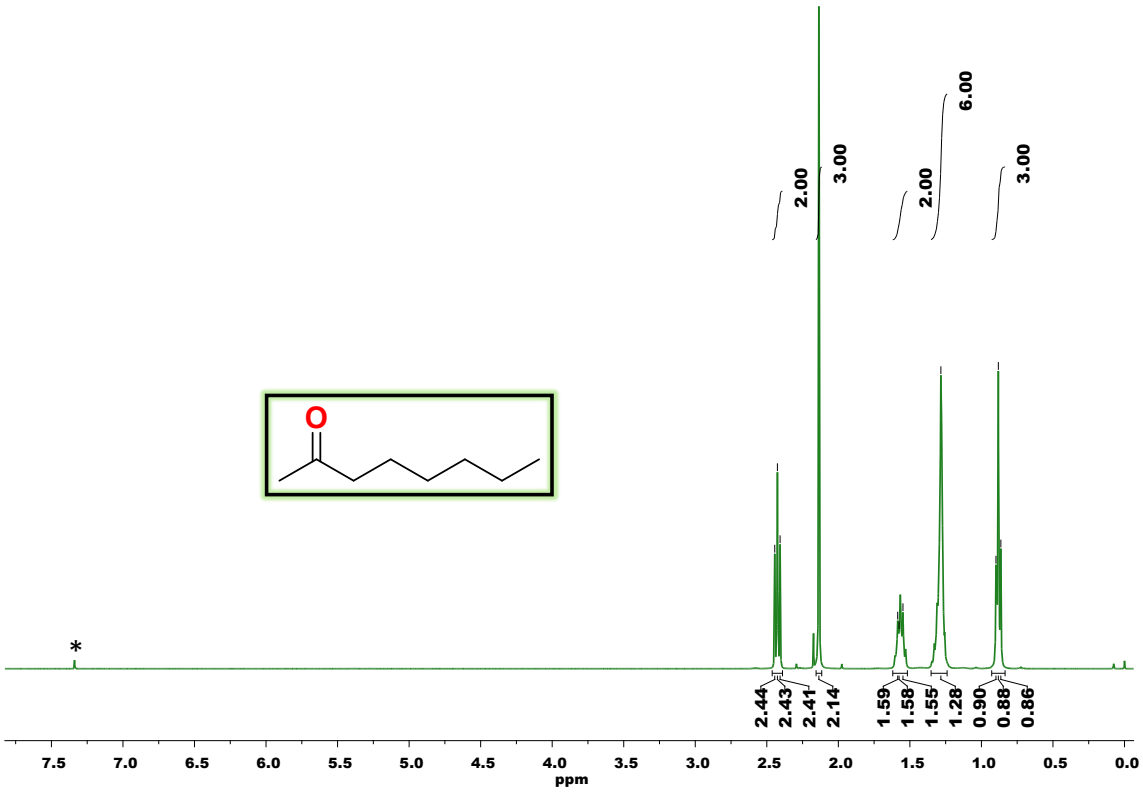

Fig. S66 ^{1}H NMR spectrum of 2-octanone in $CDCl_3$ solvent where * represents the residual solvent and/or adventitious water peaks.

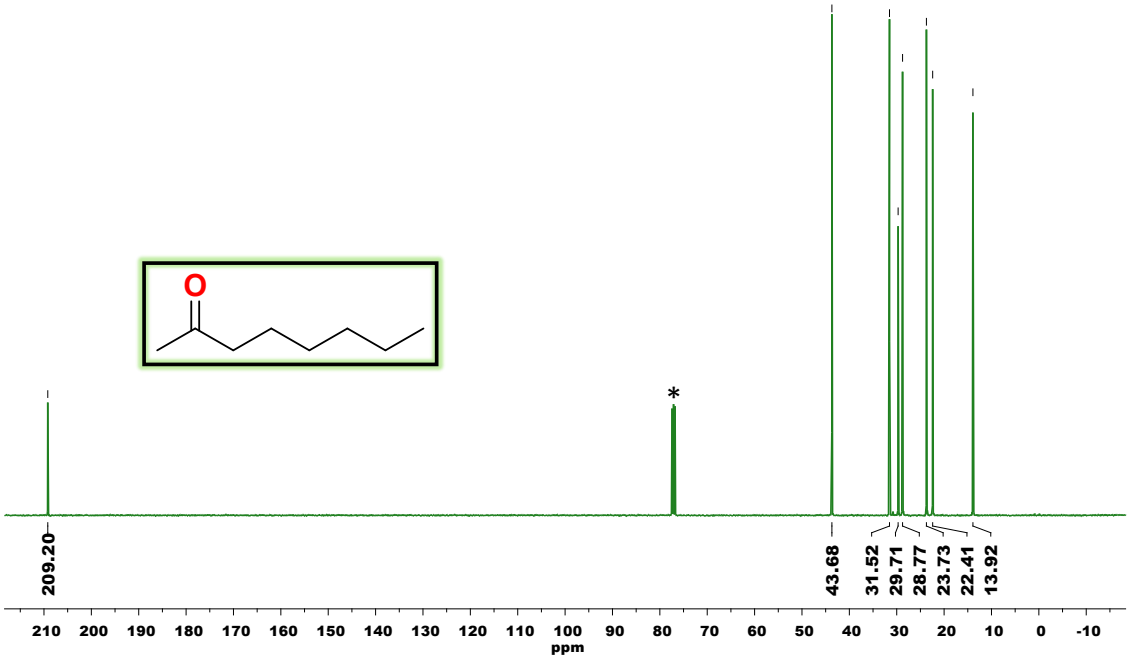

Fig. S67 ^{13}C NMR spectrum of 2-octanone in $CDCl_3$ solvent where * represents the residual solvent and/or adventitious water peaks.

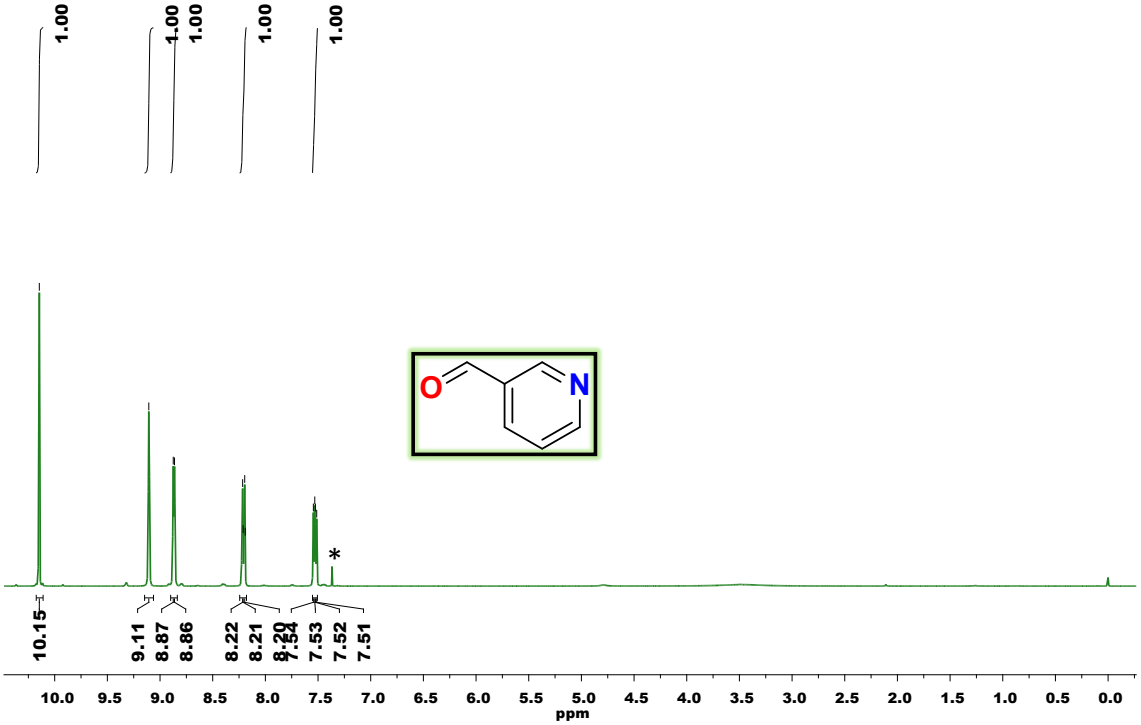

Fig. S68 ^{1}H NMR spectrum of 3-pyridinecarboxaldehyde in $CDCl_3$ solvent where * represents the residual solvent and/or adventitious water peaks.

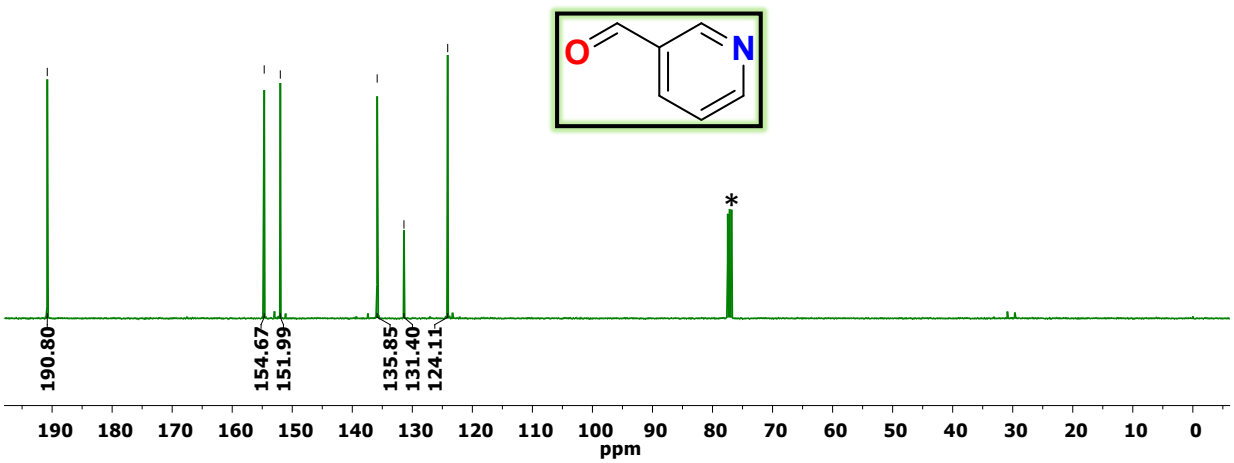

Fig. S69 ^{13}C NMR spectrum of 3-pyridinecarboxaldehyde in $CDCl_3$ solvent where * represents the residual solvent and/or adventitious water peaks.

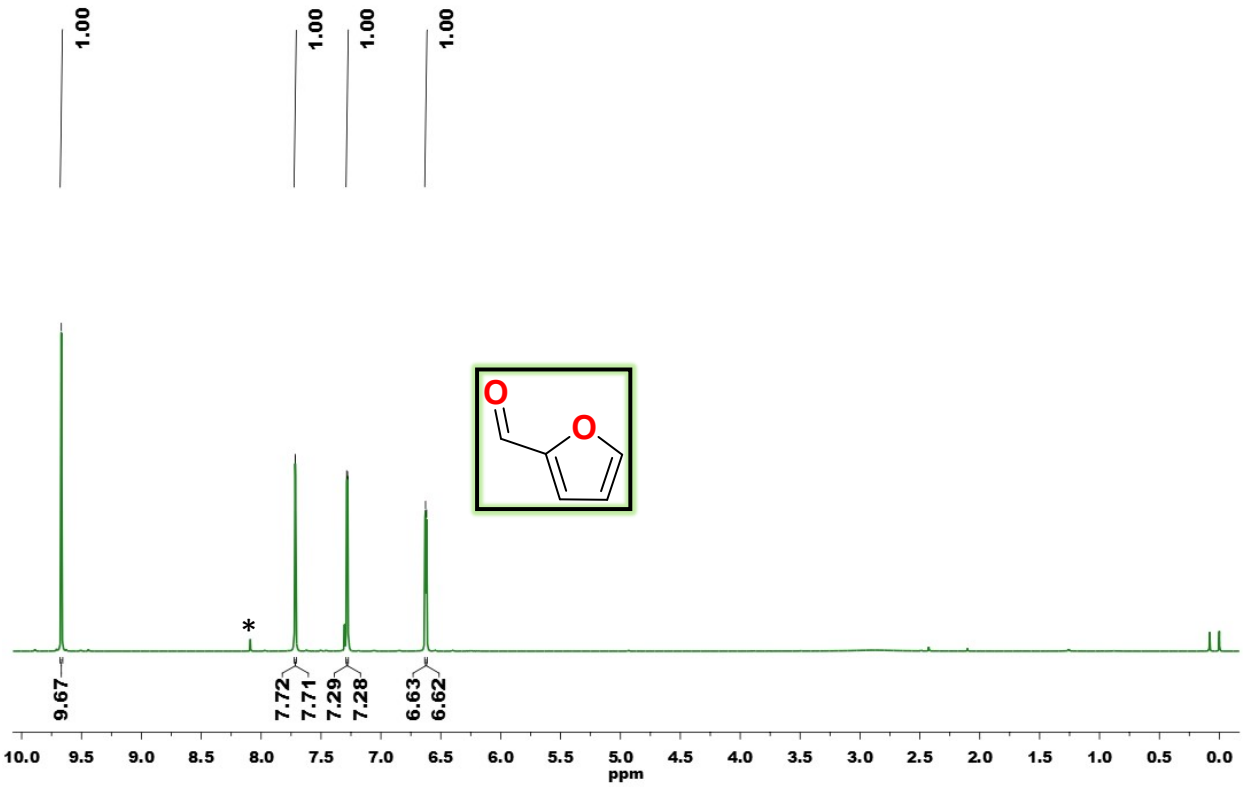

Fig. S70 ^{1}H NMR spectrum of furaldehyde in $CDCl_3$ solvent where * represents the residual solvent and/or adventitious water peaks.

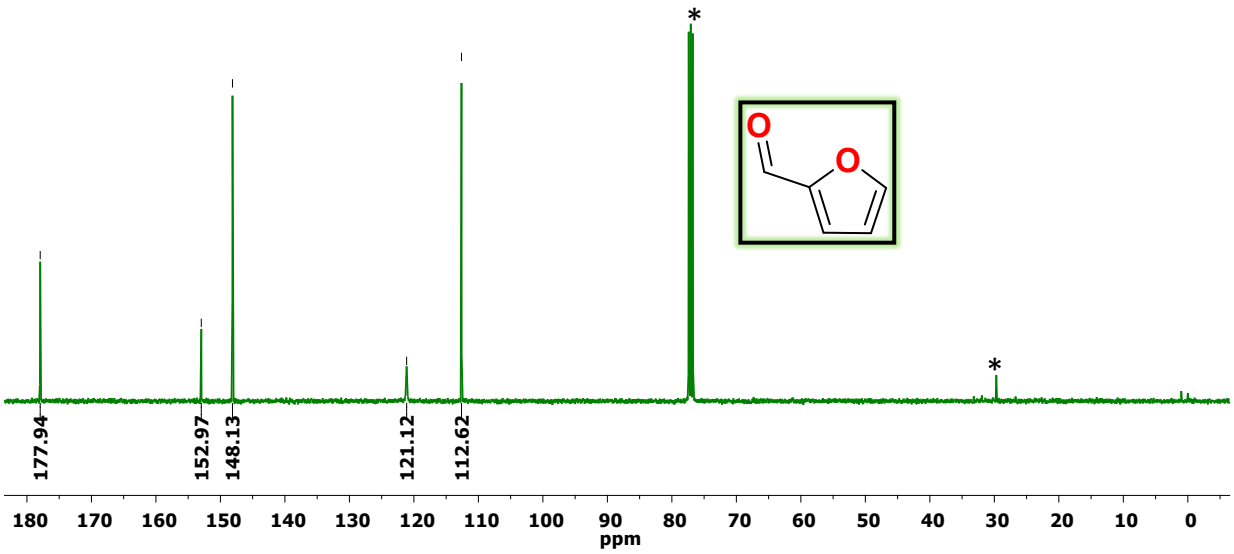

Fig. S71 ^{13}C NMR spectrum of furaldehyde in $CDCl_3$ solvent where * represents the residual solvent and/or adventitious water peaks.

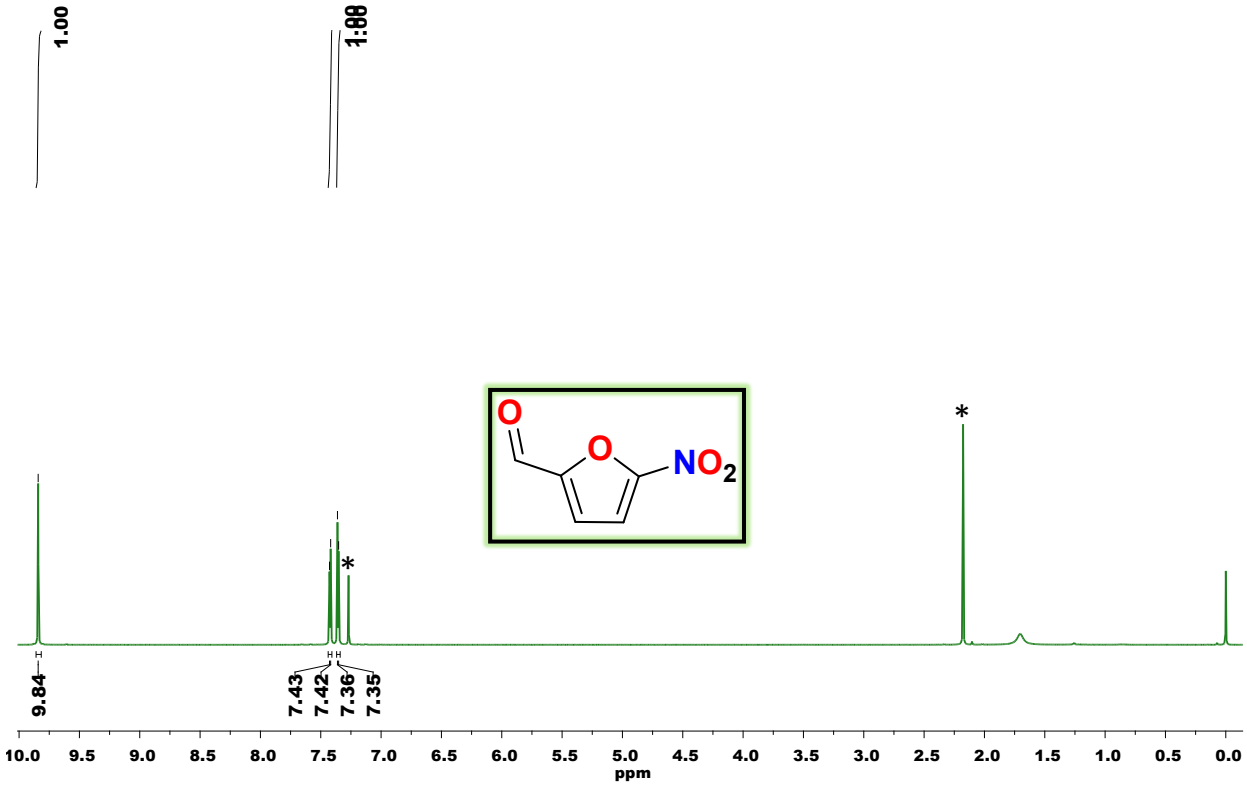

Fig. S72 ^{1}H NMR spectrum of 5-nitro-2-furaldehyde in $CDCl_3$ solvent where * represents the residual solvent and/or adventitious water peaks.

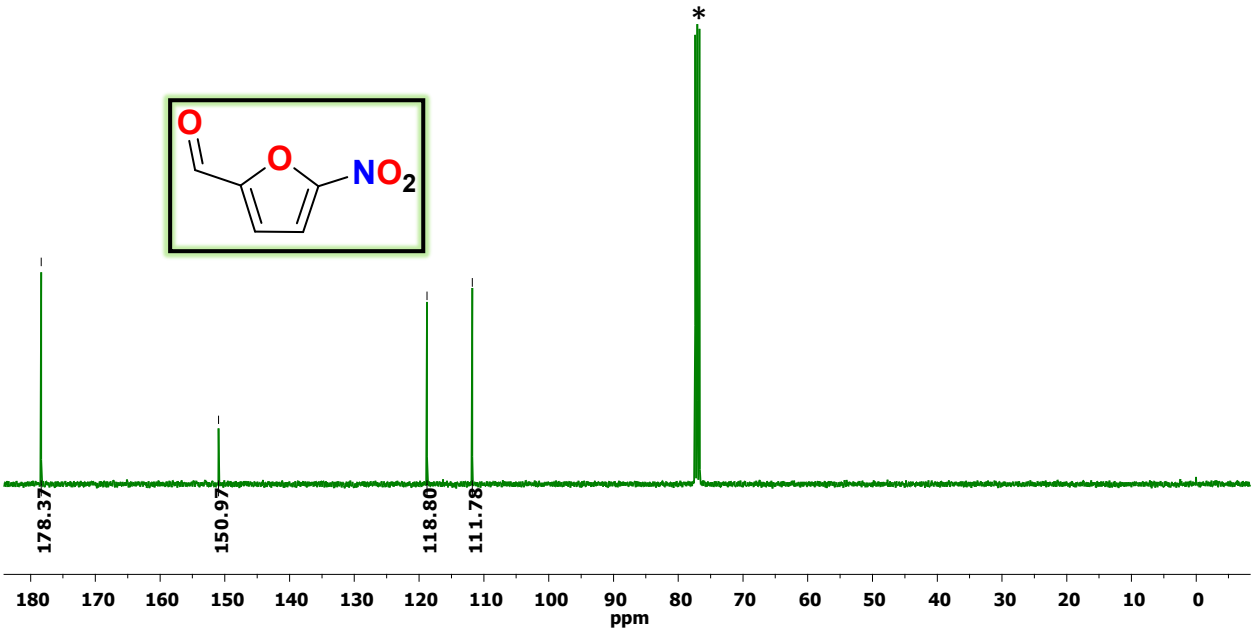

Fig. S73 ^{13}C NMR spectrum of 5-nitro-2-furaldehyde in $CDCl_3$ solvent where * represents the residual solvent and/or adventitious water peaks.

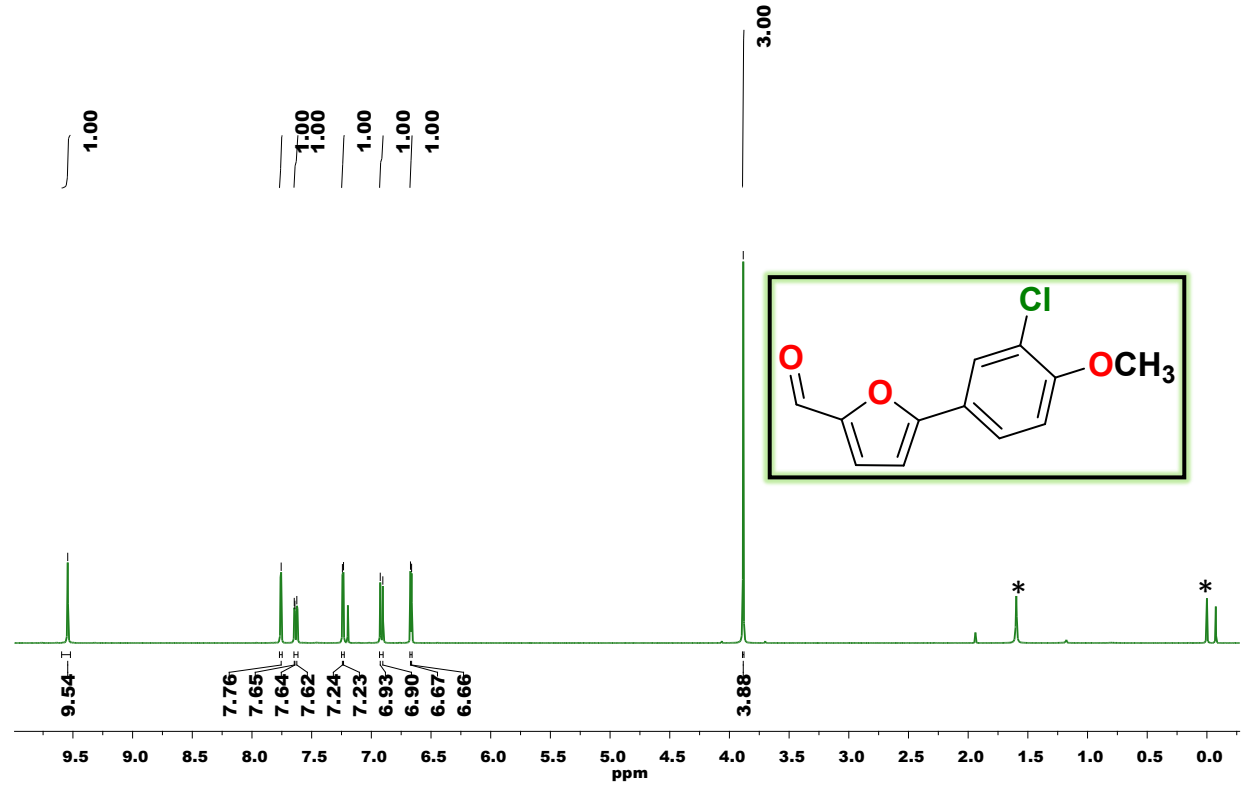

Fig. S74 ^{1}H NMR spectrum of 5-(3-chloro-4-methoxyphenyl)furan-2-carbaldehyde in $CDCl_3$ solvent where * represents the residual solvent and/or adventitious water peaks.

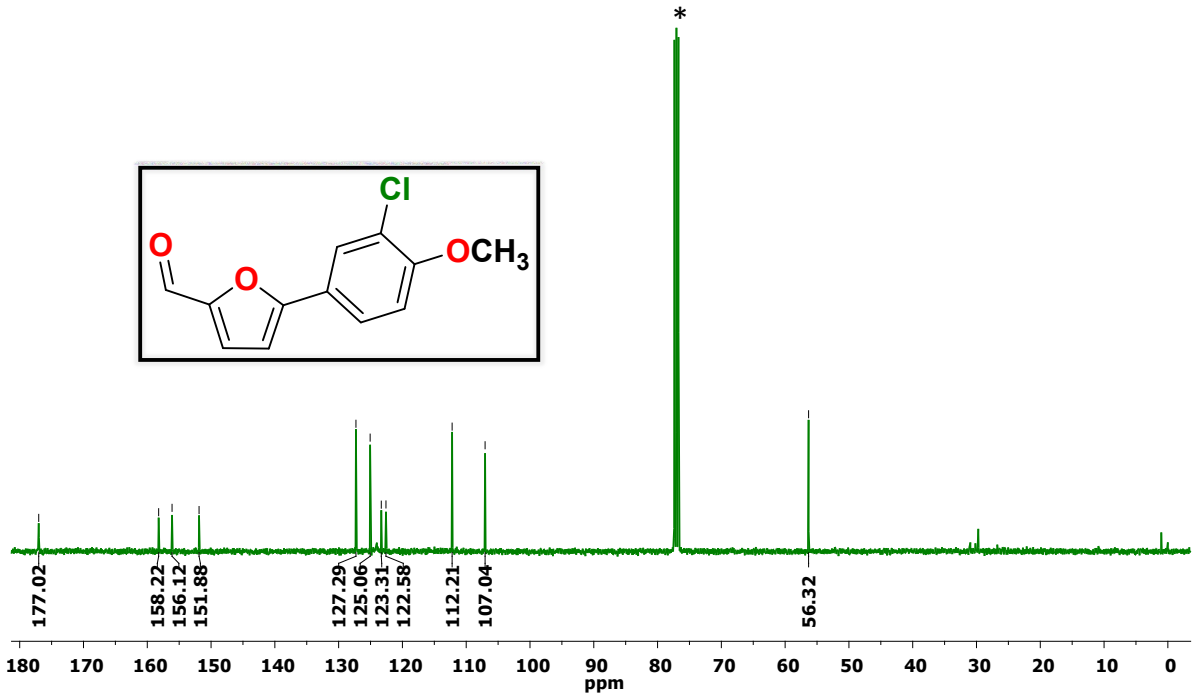

Fig. S75 ^{13}C NMR spectrum of 5-(3-chloro-4-methoxyphenyl)furan-2-carbaldehyde in $CDCl_3$ solvent where * represents the residual solvent and/or adventitious water peaks.

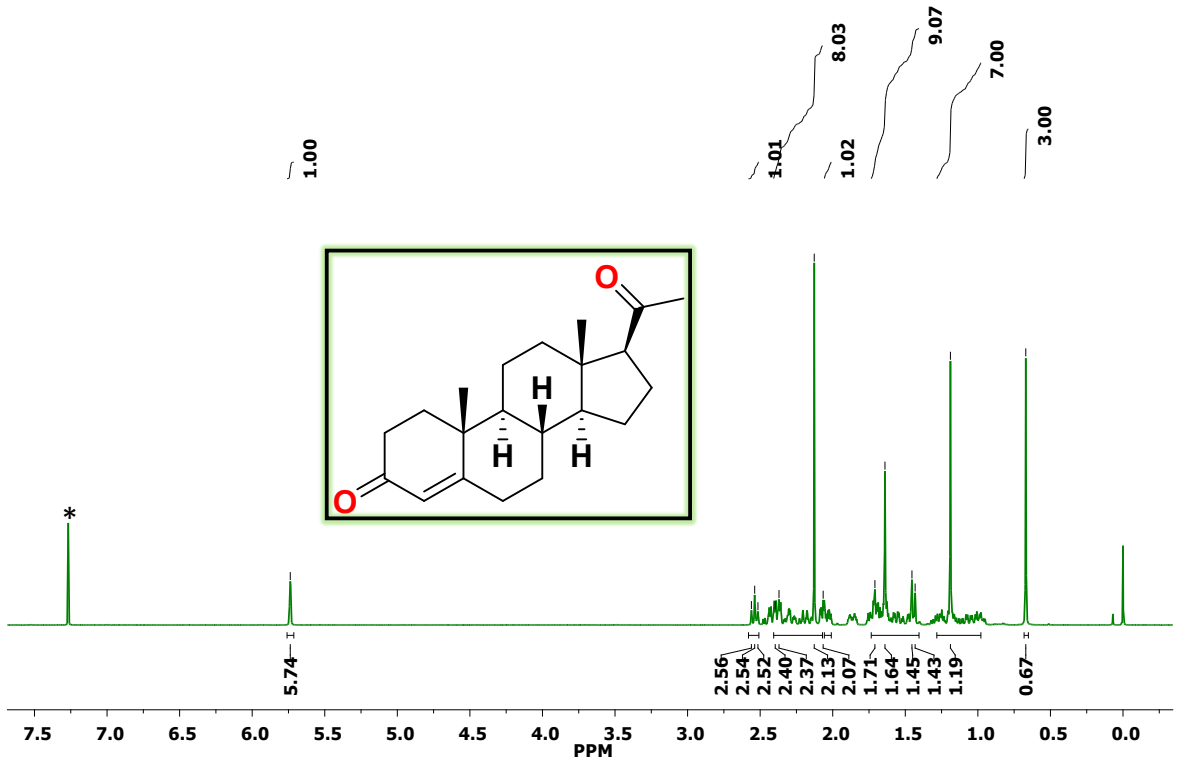

Fig. S76 ^{1}H NMR spectrum of Progesterone in $CDCl_3$ solvent where * represents the residual solvent and/or adventitious water peaks.

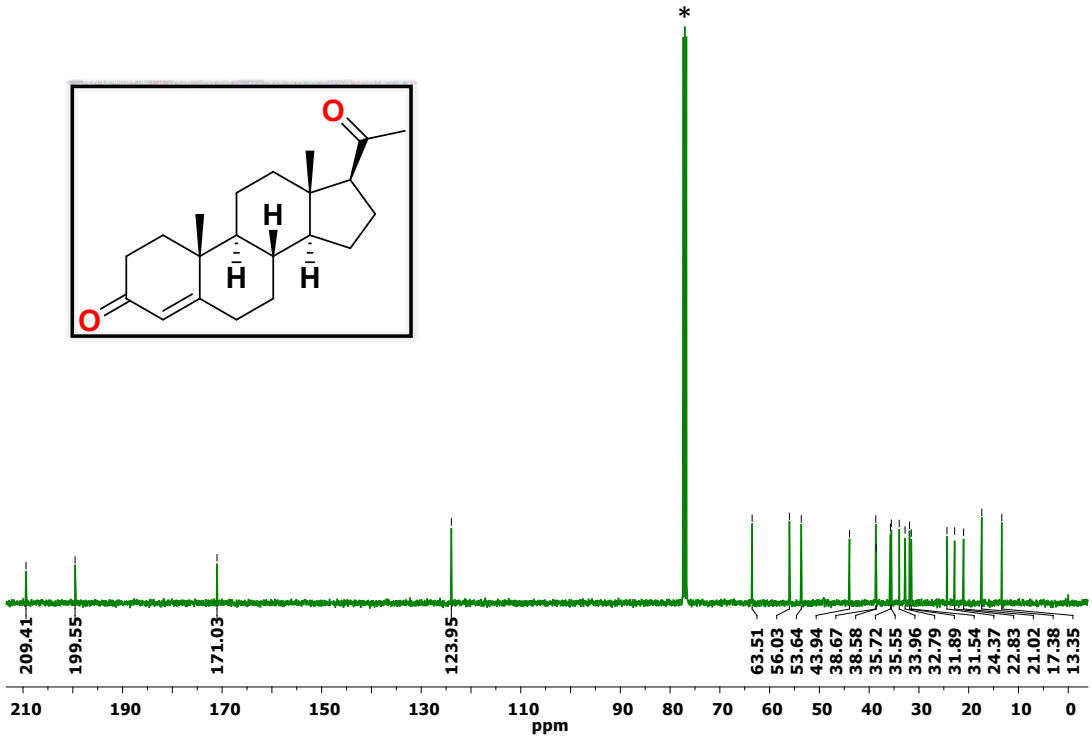

Fig. S77 ^{13}C NMR spectrum of Progesterone in $CDCl_3$ solvent where * represents the residual solvent and/or adventitious water peaks.

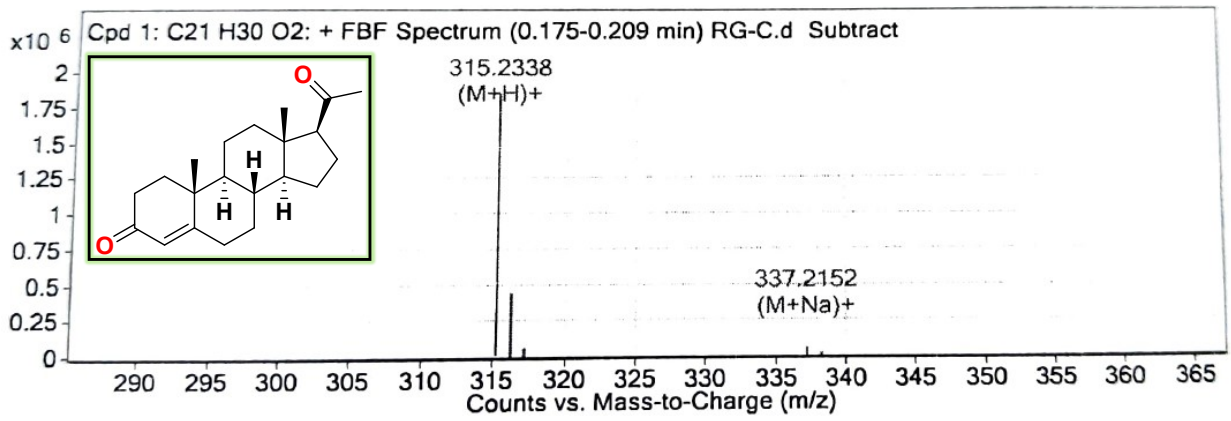

Fig. S78 ESI-MS spectrum of progesterone in $CHCl_3$.

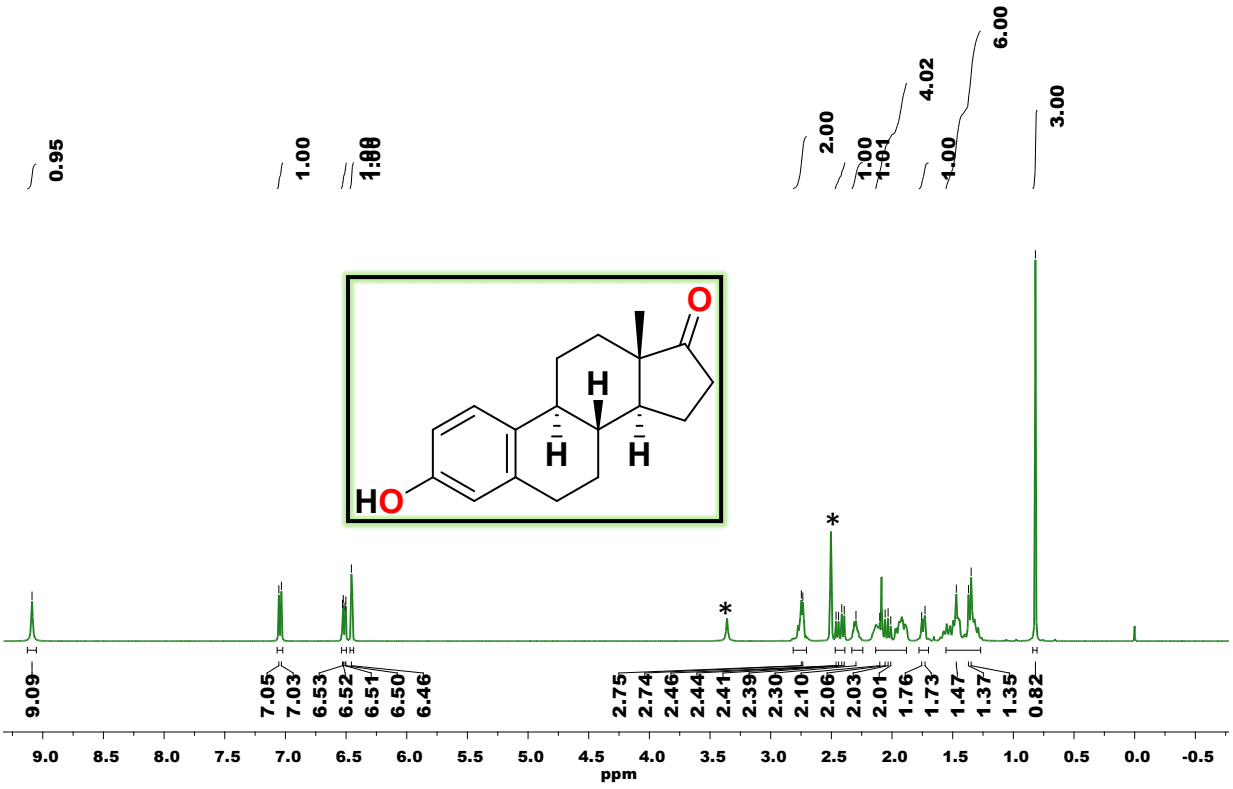

Fig. S79 ^{1}H NMR spectrum of estrone in $CDCl_3$ solvent where * represents the residual solvent and/or adventitious water peaks.

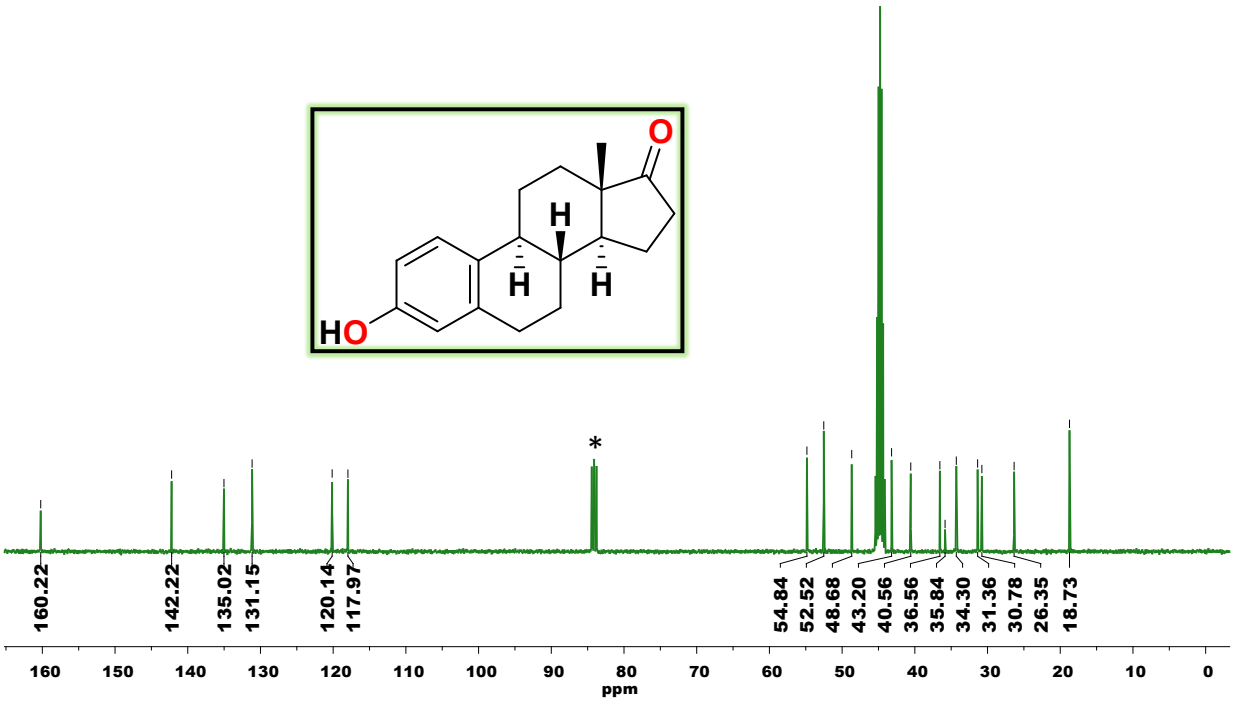

Fig. S80 ^{13}C NMR spectrum of estrone in $CDCl_3$ solvent where * represents the residual solvent and/or adventitious water peaks.

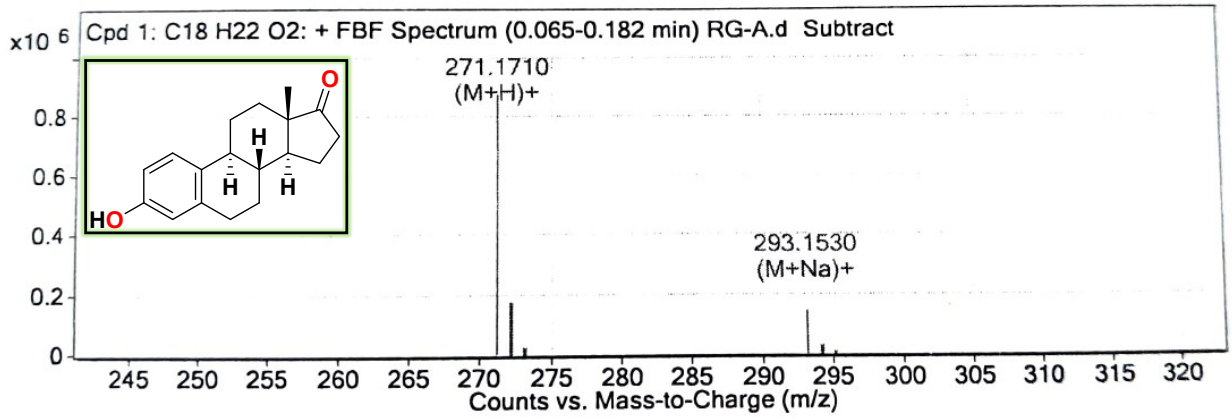

Fig. S81 ESI-MS spectrum of estrone in $CHCl_3$.

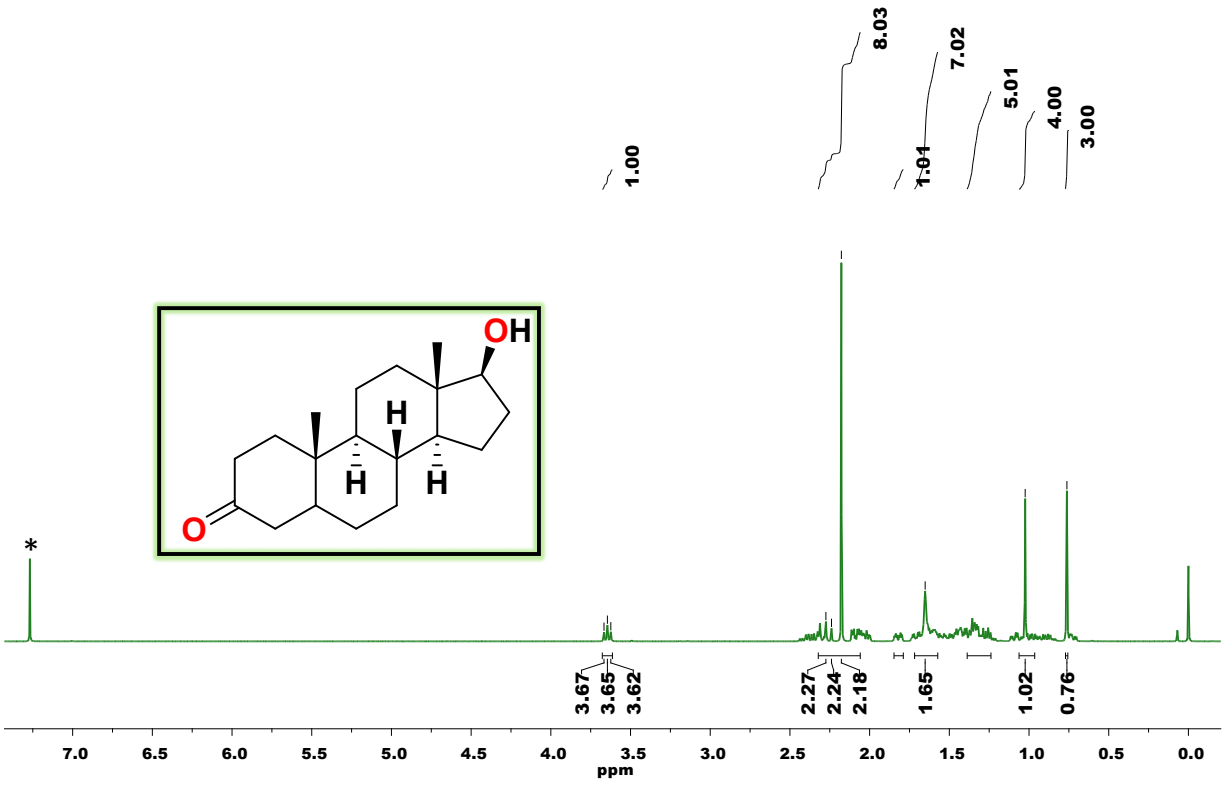

Fig. S82 ^{1}H NMR spectrum of stanolone in $CDCl_3$ solvent where * represents the residual solvent and/or adventitious water peaks.

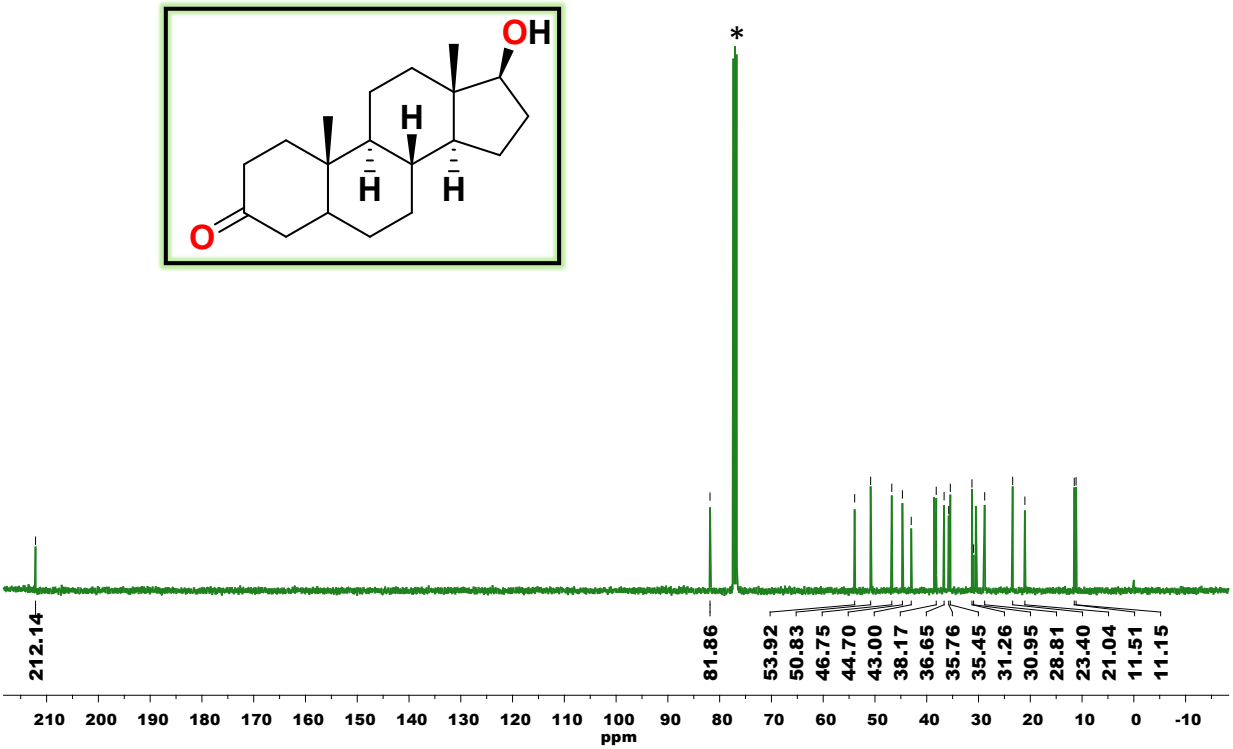

Fig. S83 ^{13}C NMR spectrum of stanolone in $CDCl_3$ solvent where * represents the residual solvent and/or adventitious water peaks.

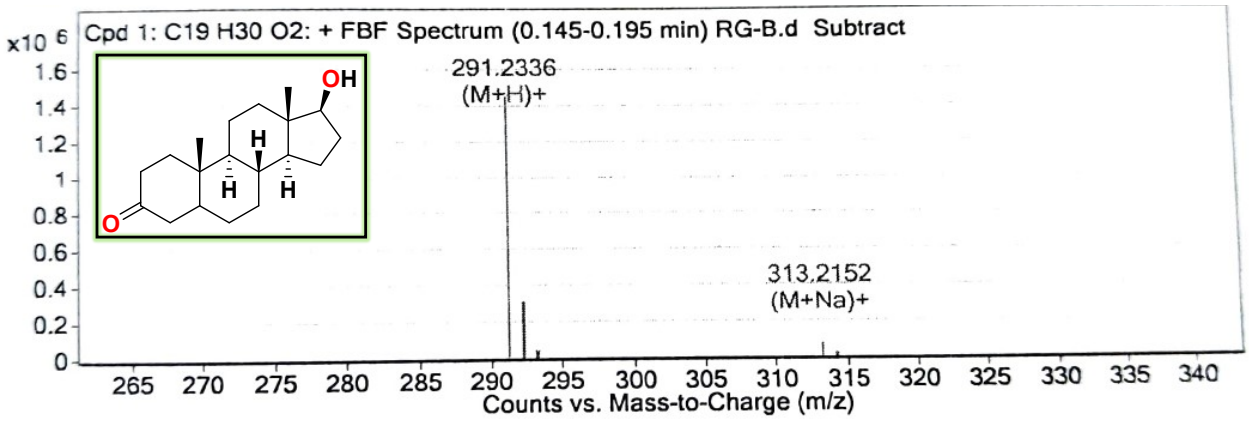

Fig. S84 ESI-MS spectrum of stanolone in $CHCl_3$.

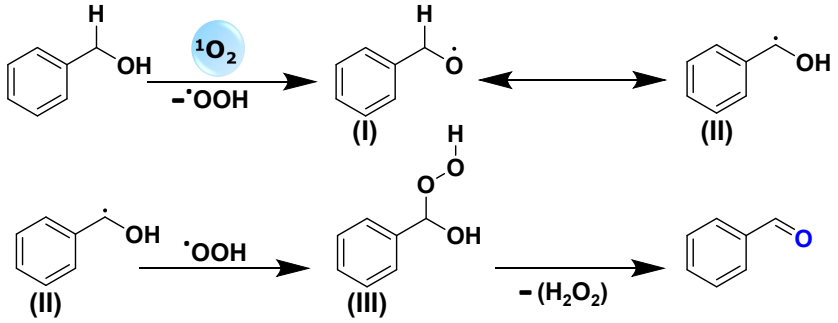

Fig. S85 Proposed reaction mechanism for the selective oxidation of benzyl alcohol using Ln-MOFs as the photocatalyst.

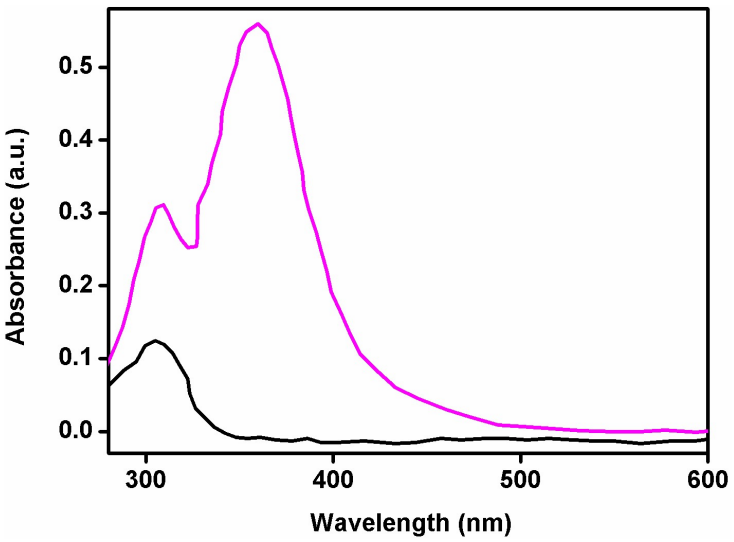

Fig. S86 UV-Vis spectra of the tri-iodide ion formed by H_2O_2 oxidation.

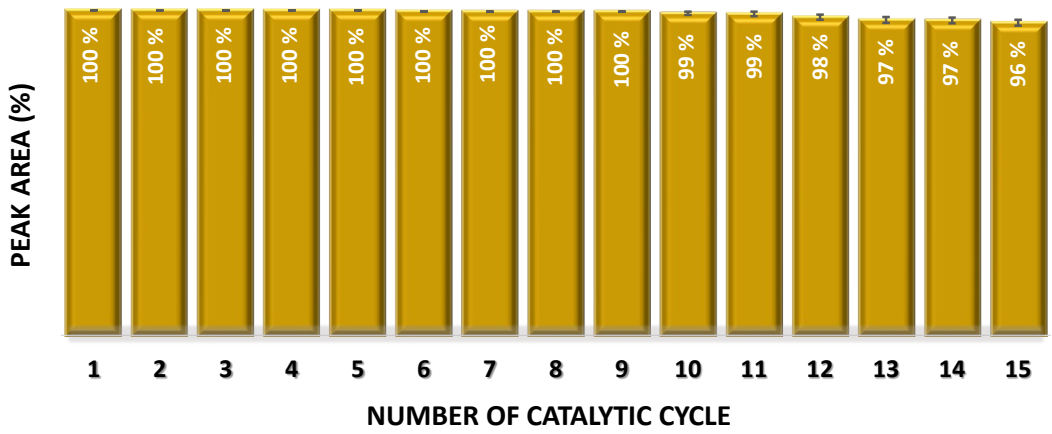

Fig. S87 A bar graph displaying the recyclability of **1-Tb** for fifteen consecutive catalytic cycles for the photo-oxidation of benzyl alcohol.

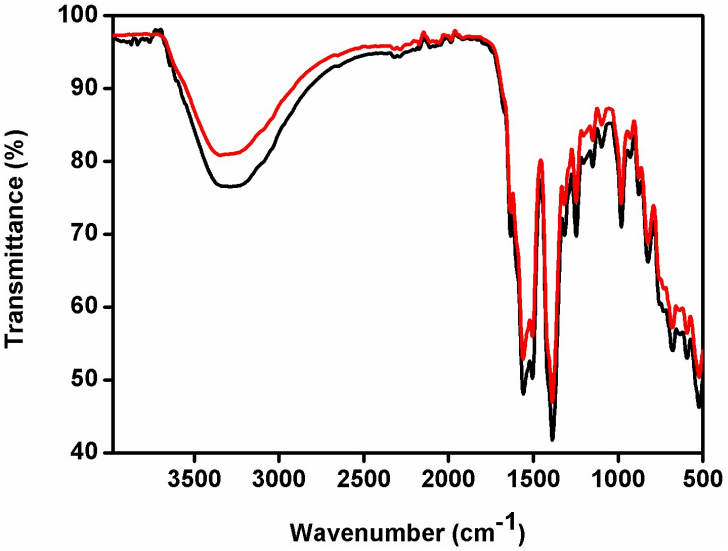

Fig. S88 FTIR spectra of as-synthesized **1-Tb** (black trace) and after the photocatalytic oxidation of benzyl alcohol (red trace).

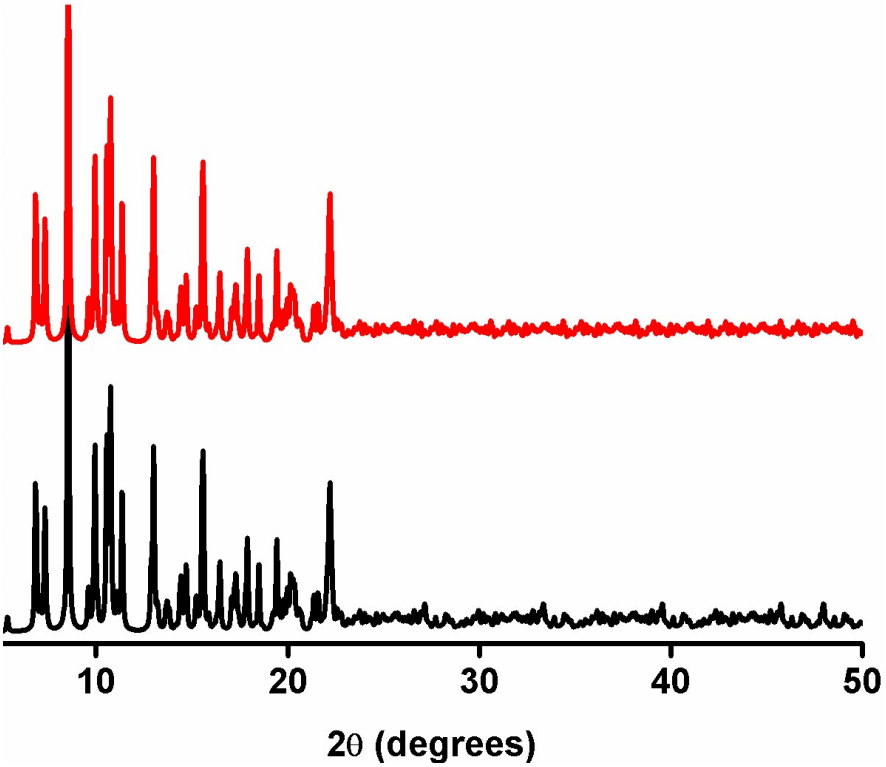

Fig. S89 Powder X-ray diffraction patterns for as-synthesized **1-Tb** (black trace) and after the photocatalytic oxidation of benzyl alcohol (red trace).

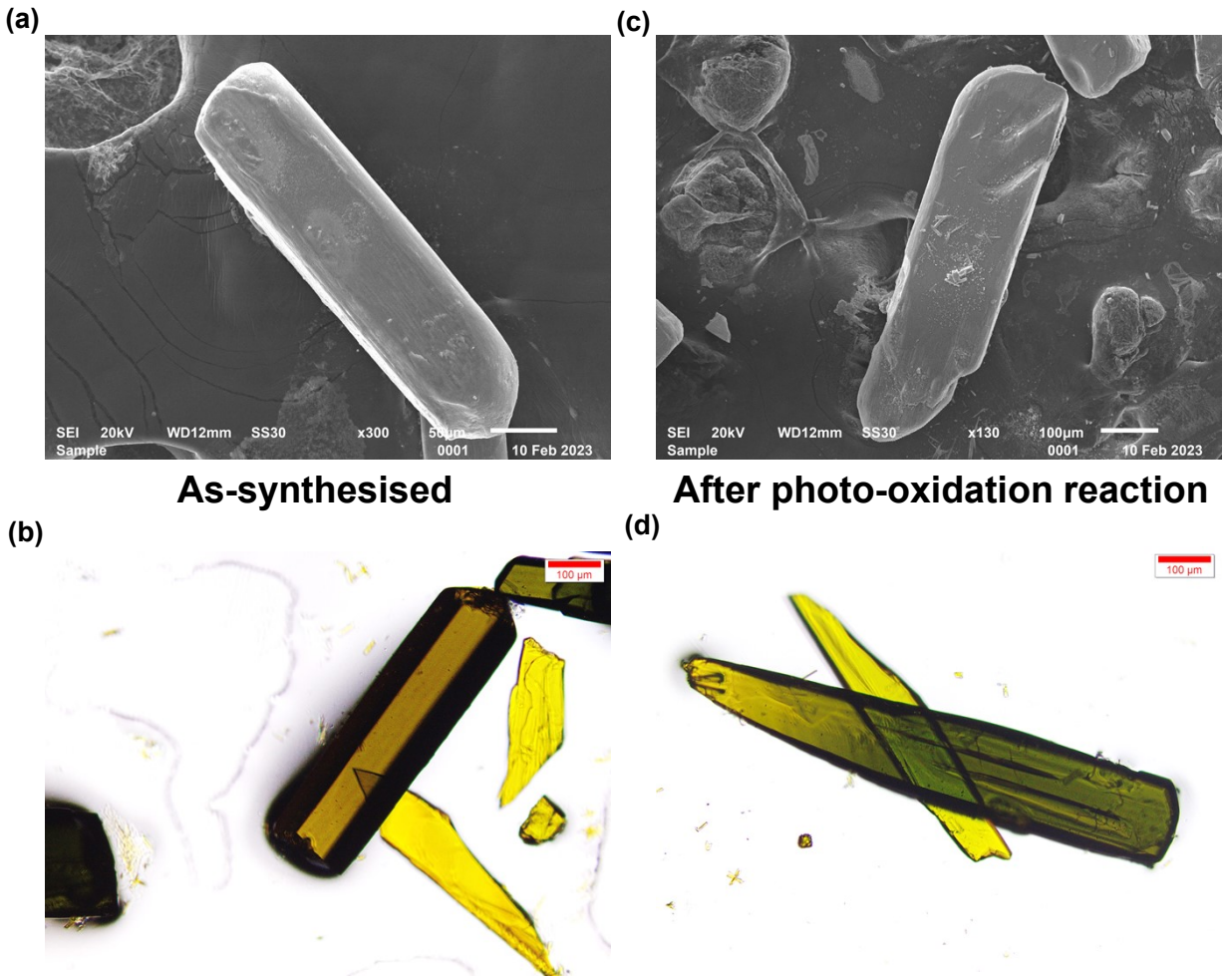

Fig. S90 (a, c) SEM images of as-synthesized **1-Tb** and after fiffteen cycles of photocatalytic oxidation of benzyl alcohol. (b, d) Optical images of as-synthesized **1-Tb** and after fiffteen cycles of photocatalytic oxidation of benzyl alcohol.

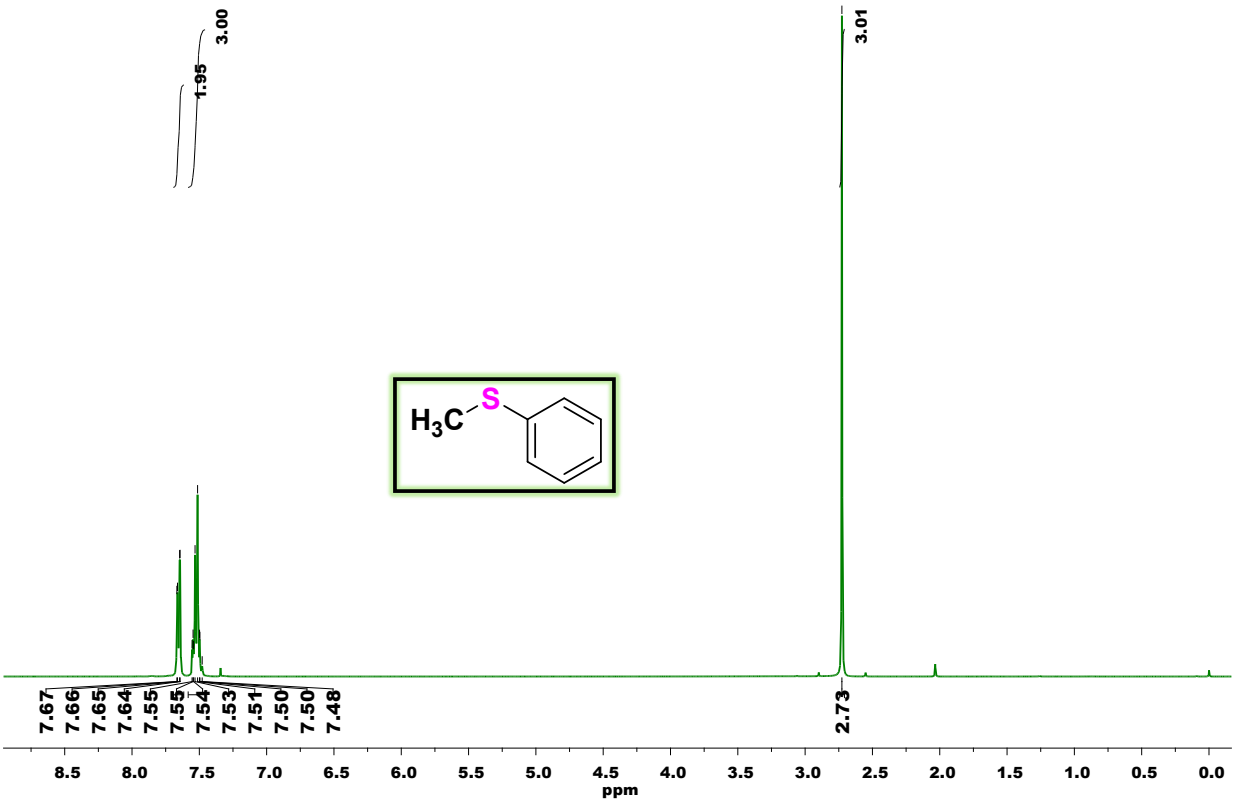

Fig. S91 ^{1}H NMR spectrum of (methylsulfinyl)benzene in $CDCl_3$ solvent where * represents the residual solvent and/or adventitious water peaks.

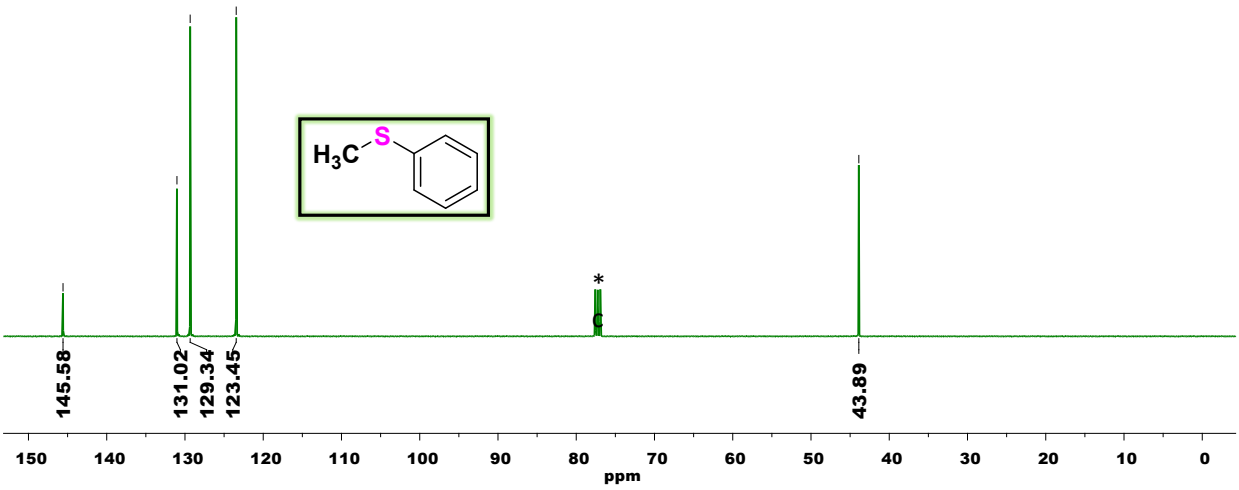

Fig. S92 ^{13}C NMR spectrum of (methylsulfinyl)benzene in $CDCl_3$ solvent where * represents the residual solvent and/or adventitious water peaks.

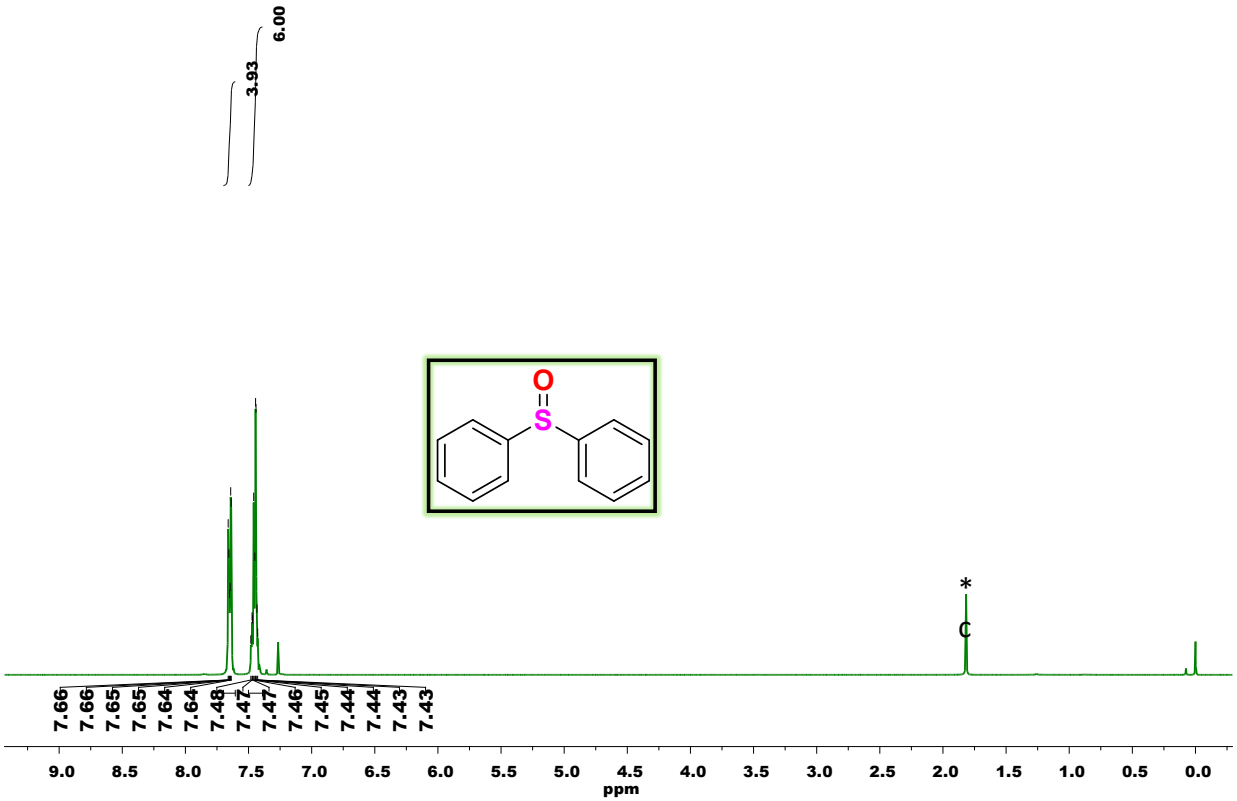

Fig. S93 ^{1}H NMR spectrum of sulfinyldibenzene in $CDCl_3$ solvent where * represents the residual solvent and/or adventitious water peaks.

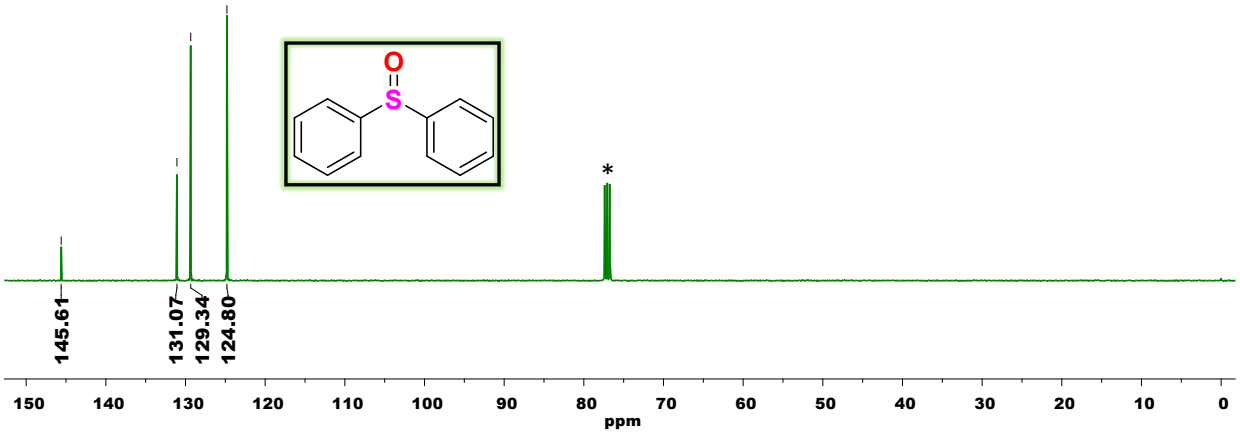

Fig. S94 ^{13}C NMR spectrum of sulfinyldibenzene in $CDCl_3$ solvent where * represents the residual solvent and/or adventitious water peaks.

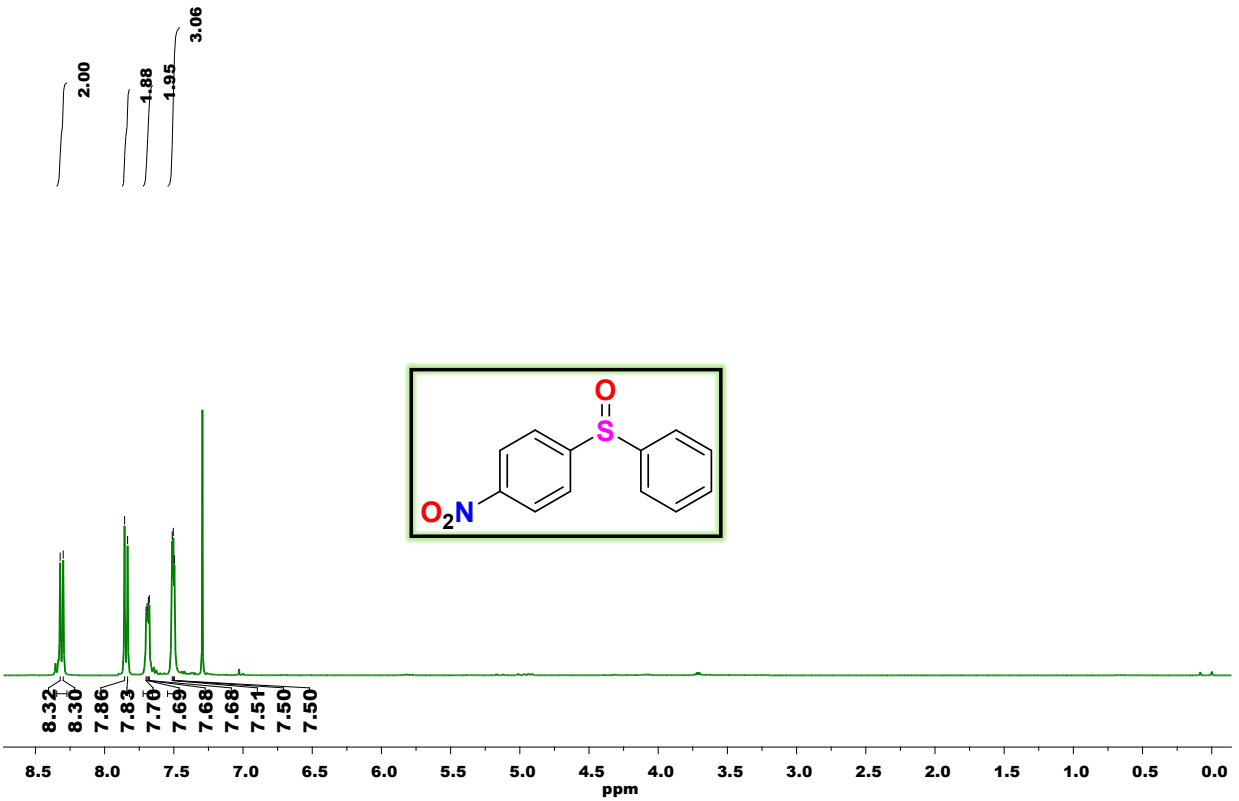

Fig. S95 ^{1}H NMR spectrum of 1-nitro-4-(phenylsulfinyl)benzene in $CDCl_3$ solvent where * represents the residual solvent and/or adventitious water peaks.

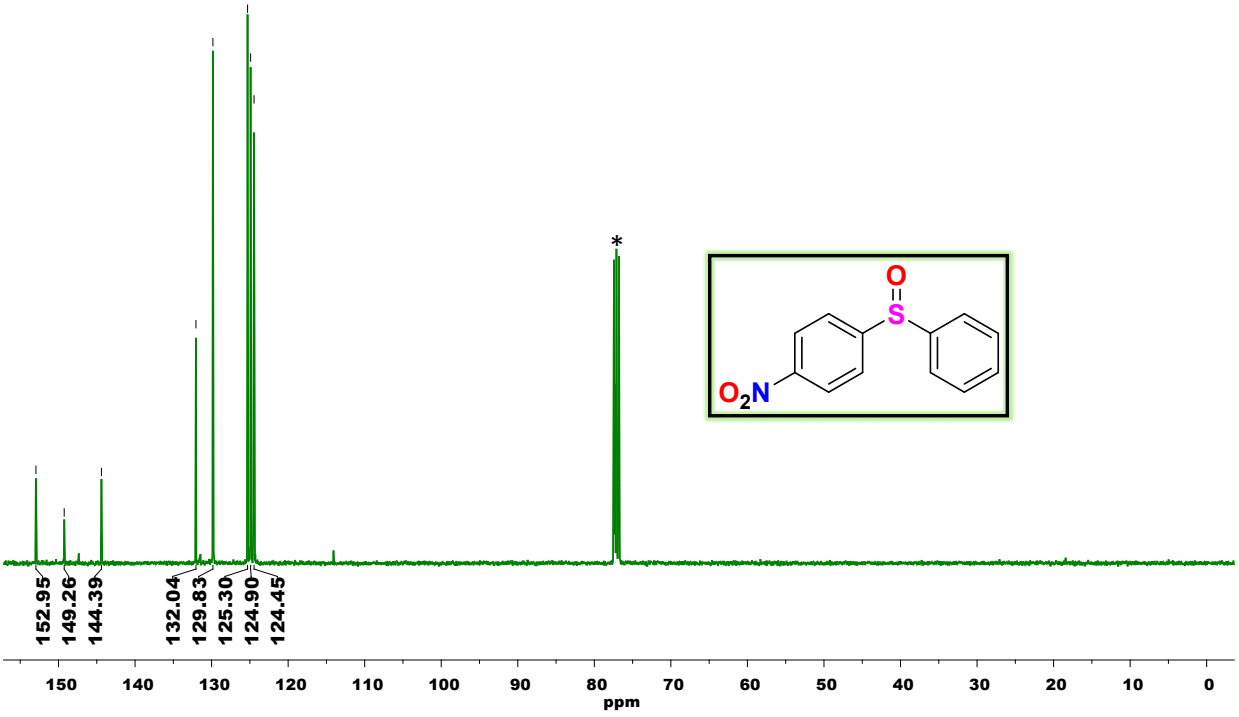

Fig. S96 ^{13}C NMR spectrum of 1-nitro-4-(phenylsulfinyl)benzene in $CDCl_3$ solvent where * represents the residual solvent and/or adventitious water peaks.

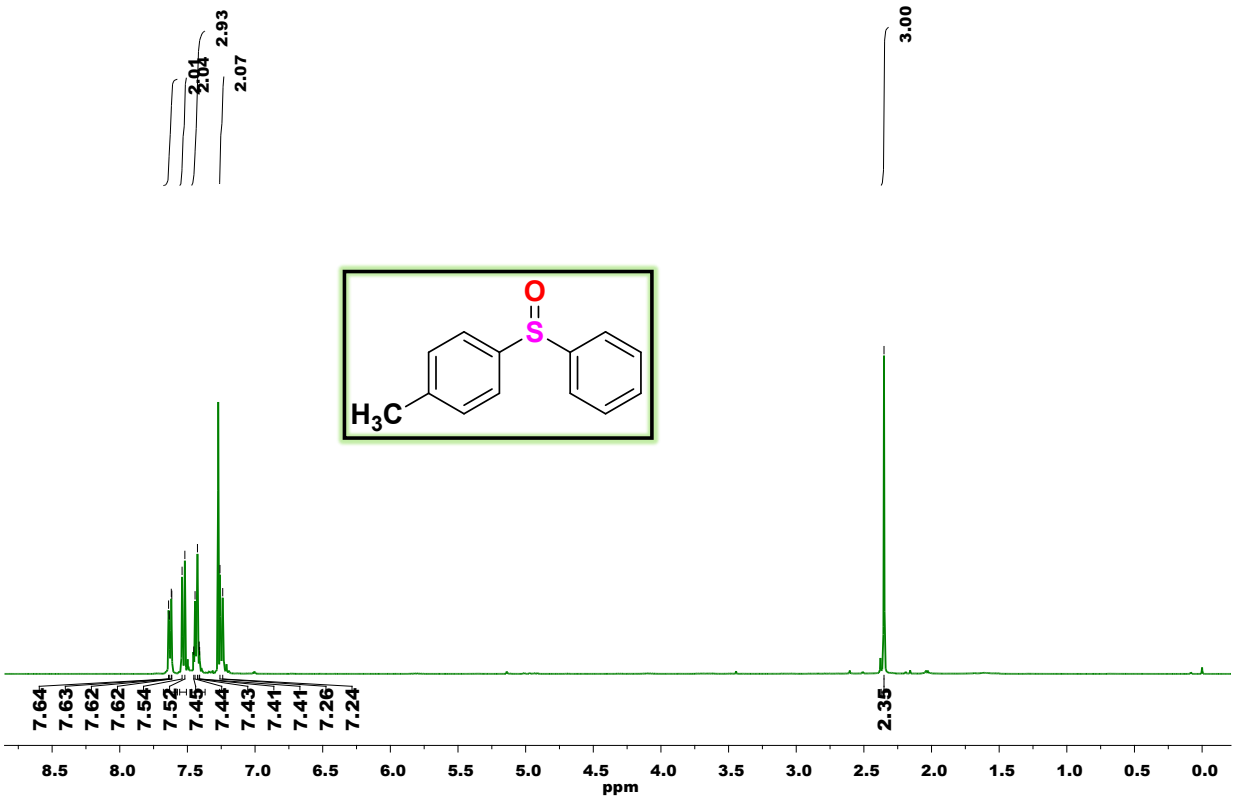

Fig. S97 ^{1}H NMR spectrum of 1-methyl-4-(phenylsulfinyl)benzene in $CDCl_3$ solvent where * represents the residual solvent and/or adventitious water peaks.

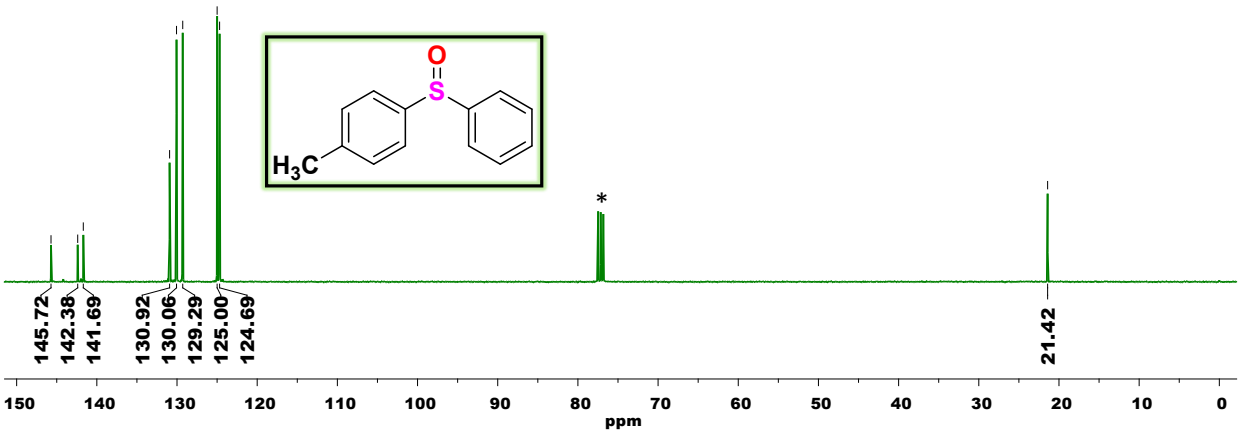

Fig. S98 ^{13}C NMR spectrum of 1-methyl-4-(phenylsulfinyl)benzene in $CDCl_3$ solvent where * represents the residual solvent and/or adventitious water peaks.

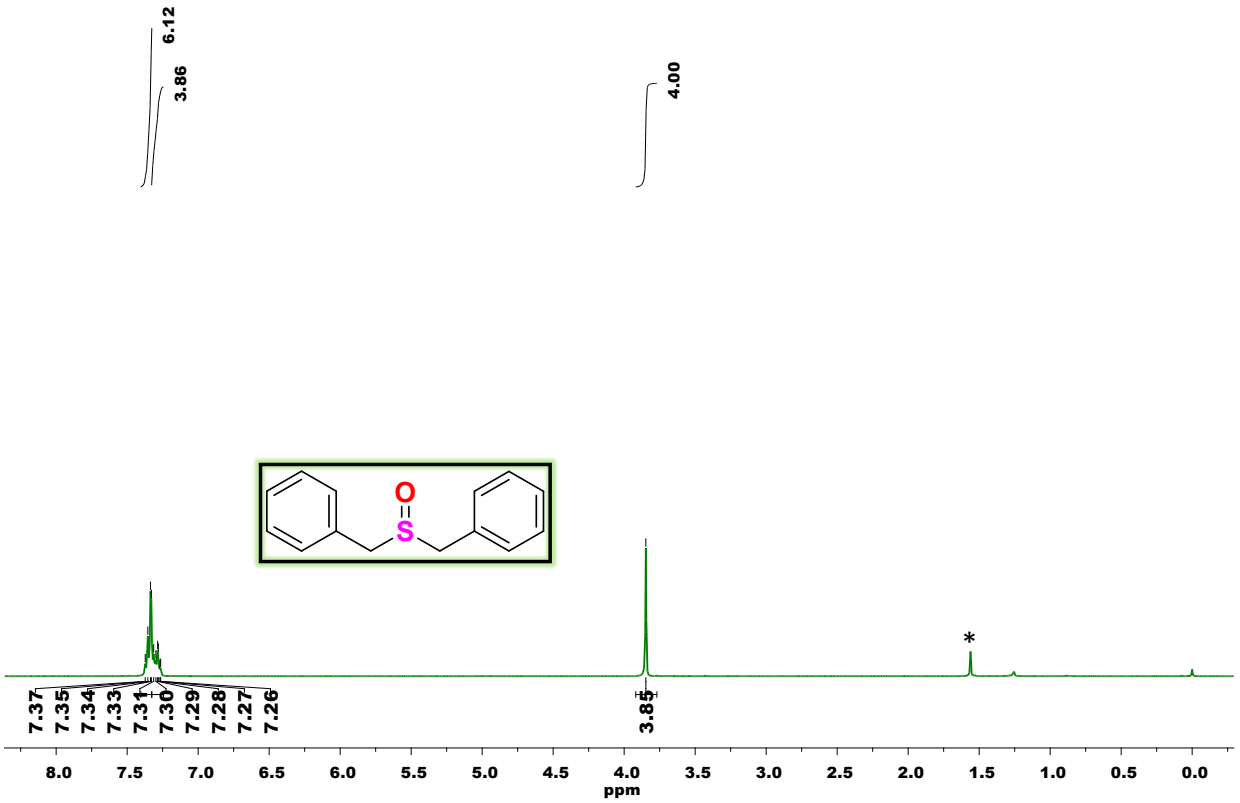

Fig. S99 ^{1}H NMR spectrum of (sulfinylbis(methylene))dibenzene in $CDCl_3$ solvent where * represents the residual solvent and/or adventitious water peaks.

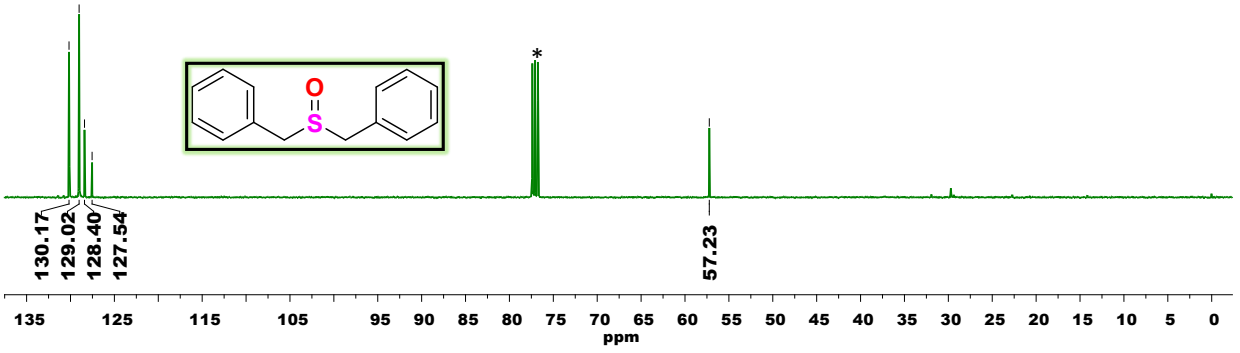

Fig. S100 ^{13}C NMR spectrum of (sulfinylbis(methylene))dibenzene in $CDCl_3$ solvent where * represents the residual solvent and/or adventitious water peaks.

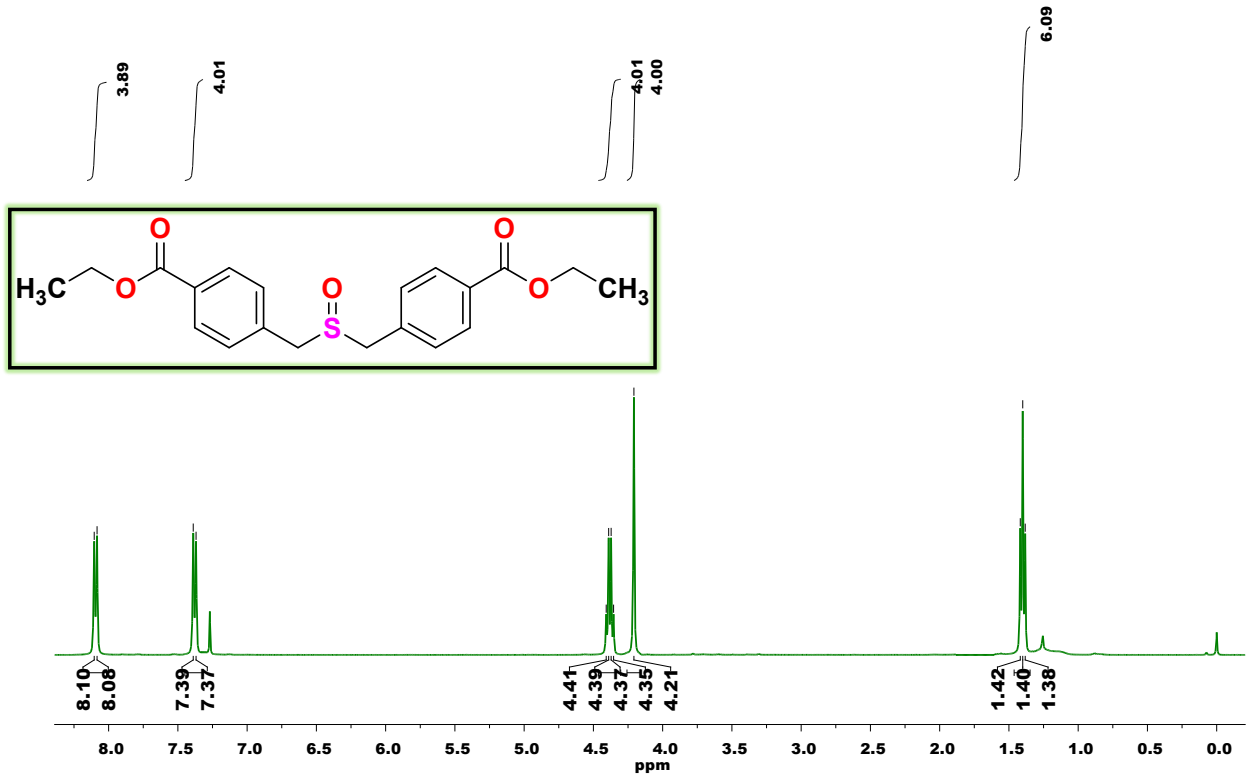

Fig. S101 ^{1}H NMR spectrum of diethyl-4,4'-(sulfinylbis(methylene))dibenzoate in $CDCl_3$ solvent where * represents the residual solvent and/or adventitious water peaks.

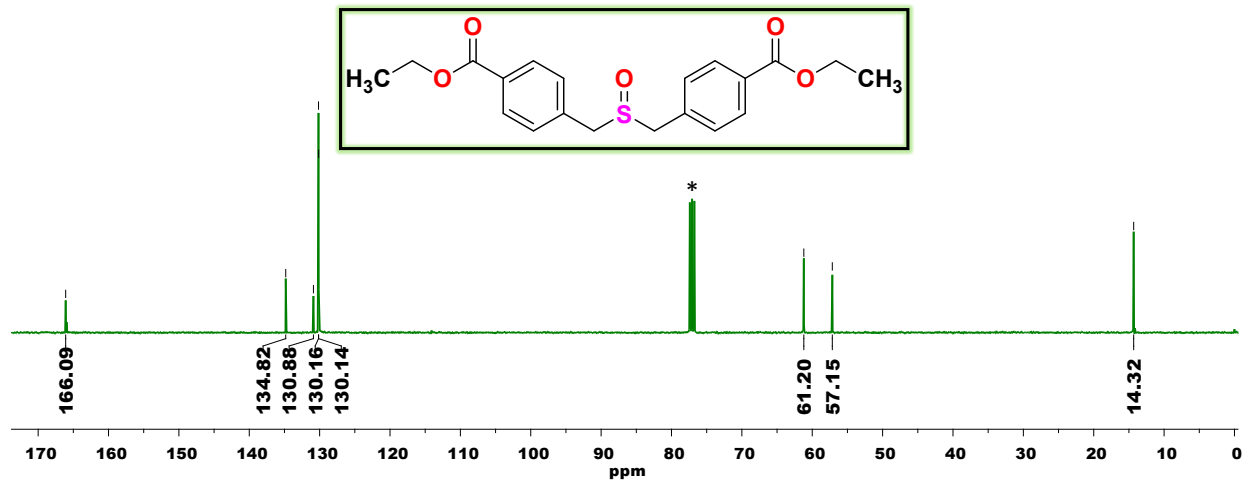

Fig. S102 ^{13}C NMR spectrum of diethyl-4,4'-(sulfinylbis(methylene))dibenzoate in $CDCl_3$ solvent where * represents the residual solvent and/or adventitious water peaks.

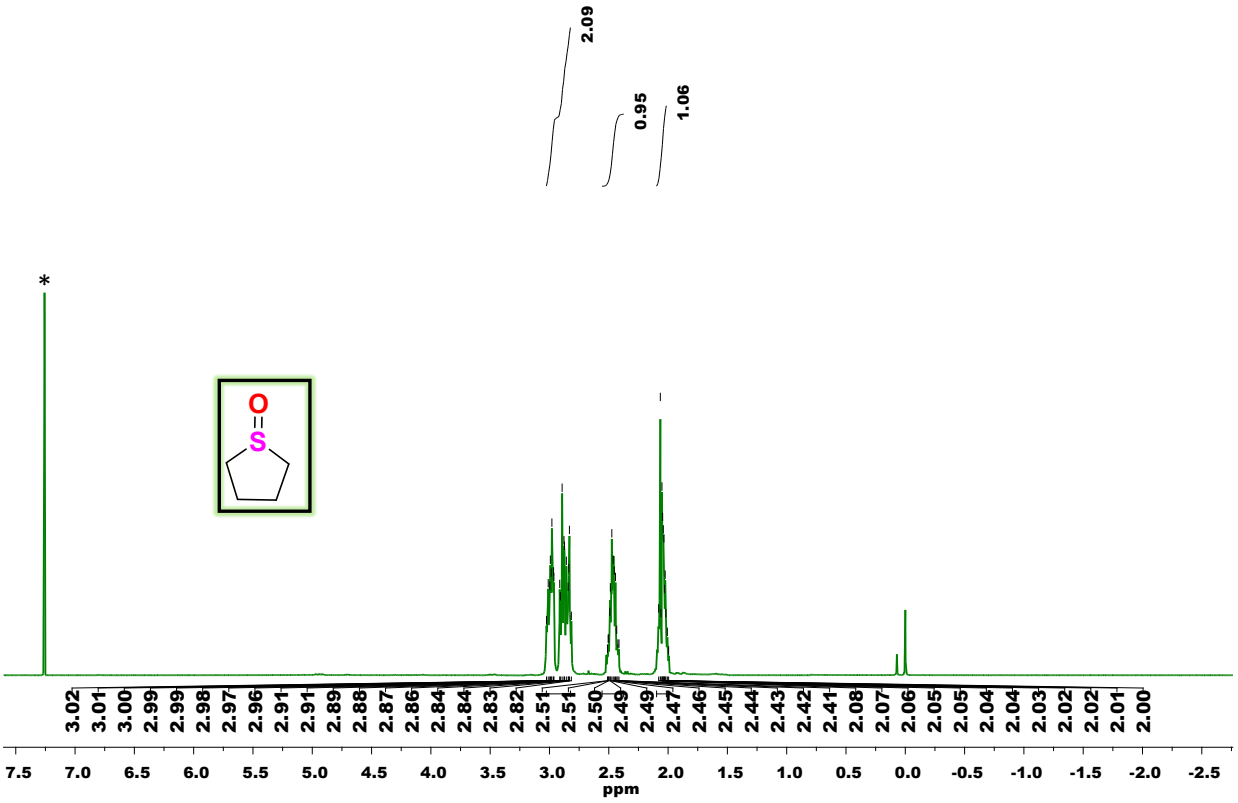

Fig. S103 ^{1}H NMR spectrum of tetrahydrothiophene-1-oxide in $CDCl_3$ solvent where * represents the residual solvent and/or adventitious water peaks.

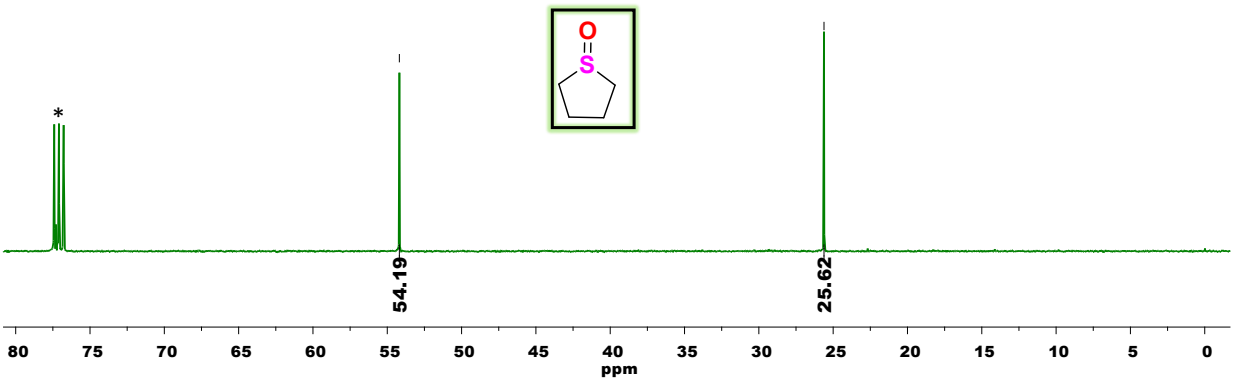

Fig. S104 ^{13}C NMR spectrum of tetrahydrothiophene-1-oxide in $CDCl_3$ solvent where * represents the residual solvent and/or adventitious water peaks.

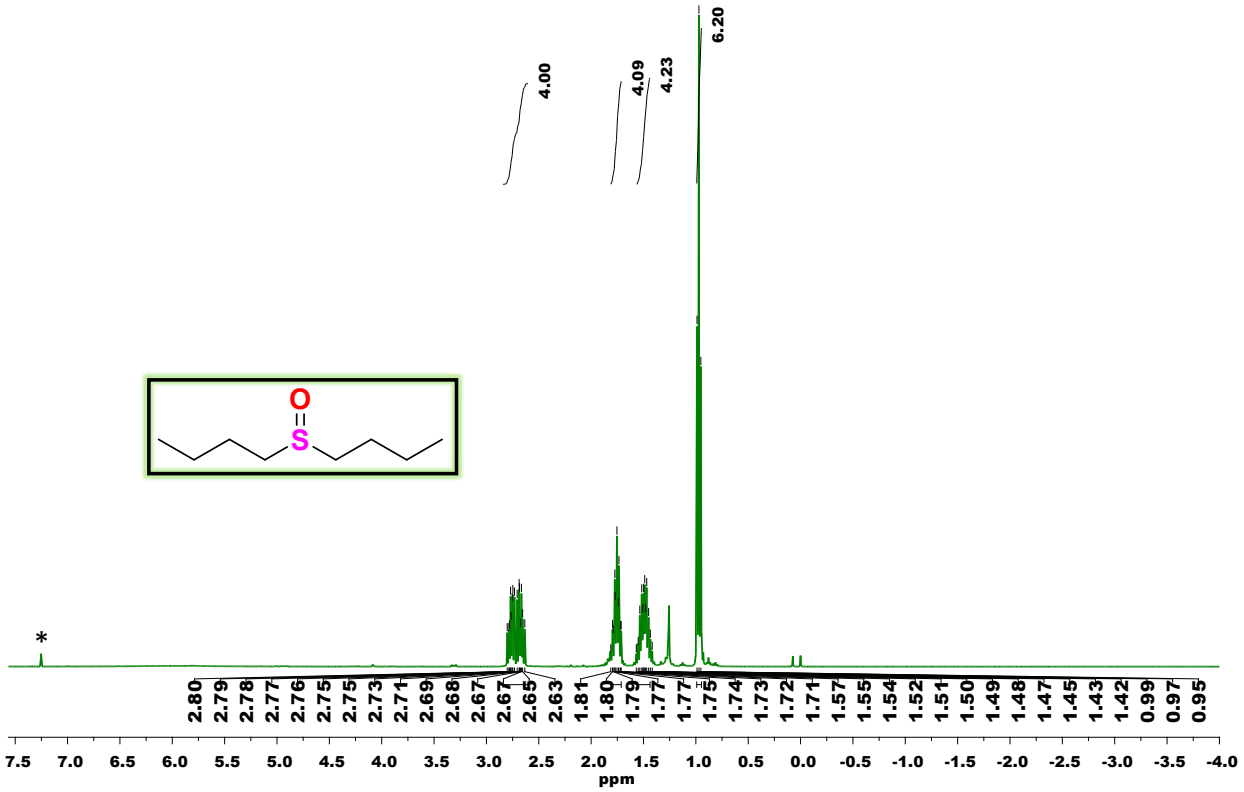

Fig. S105 ^{1}H NMR spectrum of 1-(butylsulfinyl)butane in $CDCl_3$ solvent where * represents the residual solvent and/or adventitious water peaks.

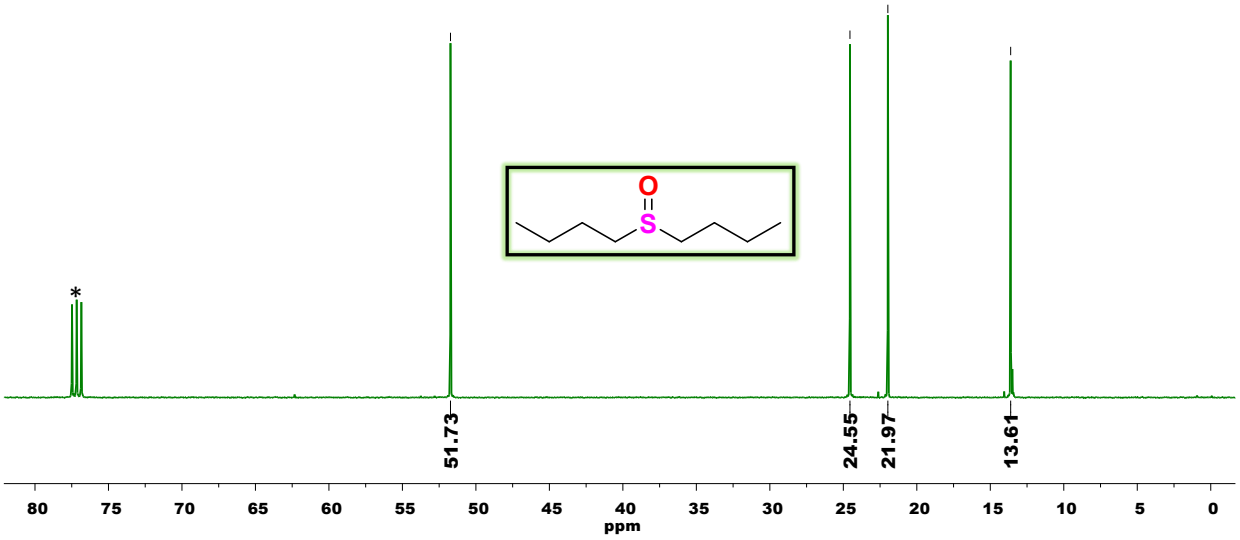

Fig. S106 ^{13}C NMR spectrum of 1-(butylsulfinyl)butane in $CDCl_3$ solvent where * represents the residual solvent and/or adventitious water peaks.

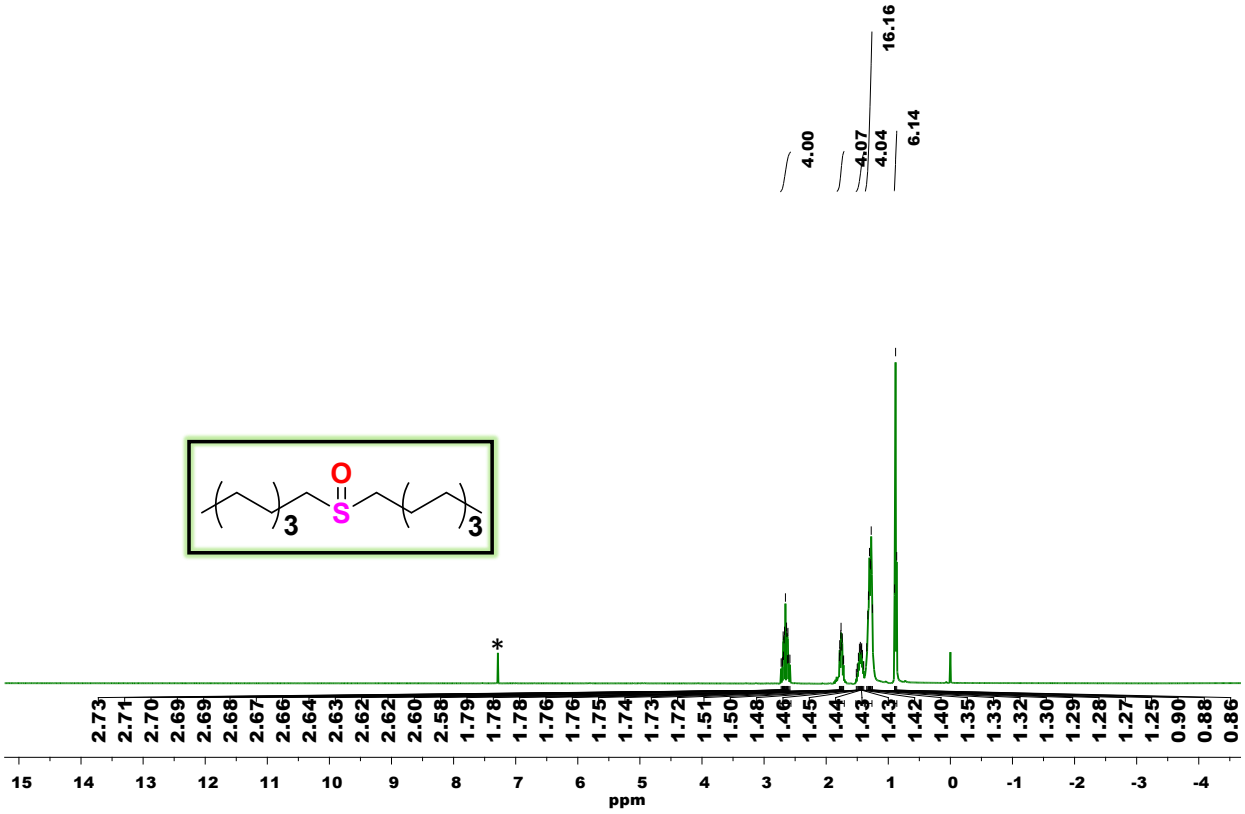

Fig. S107 ^{1}H NMR spectrum of 1-(octylsulfinyl)octane in $CDCl_3$ solvent where * represents the residual solvent and/or adventitious water peaks.

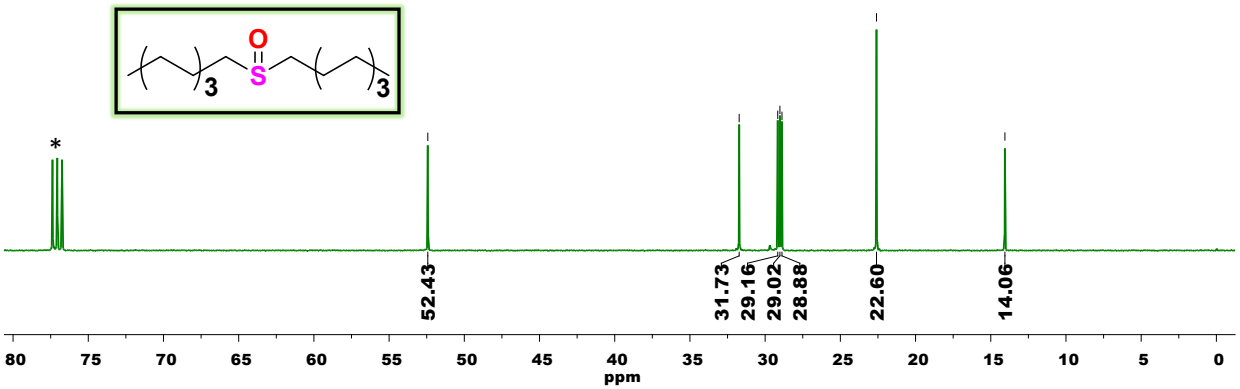

Fig. S108 ^{13}C NMR spectrum of 1-(octylsulfinyl)octane in $CDCl_3$ solvent where * represents the residual solvent and/or adventitious water peaks.

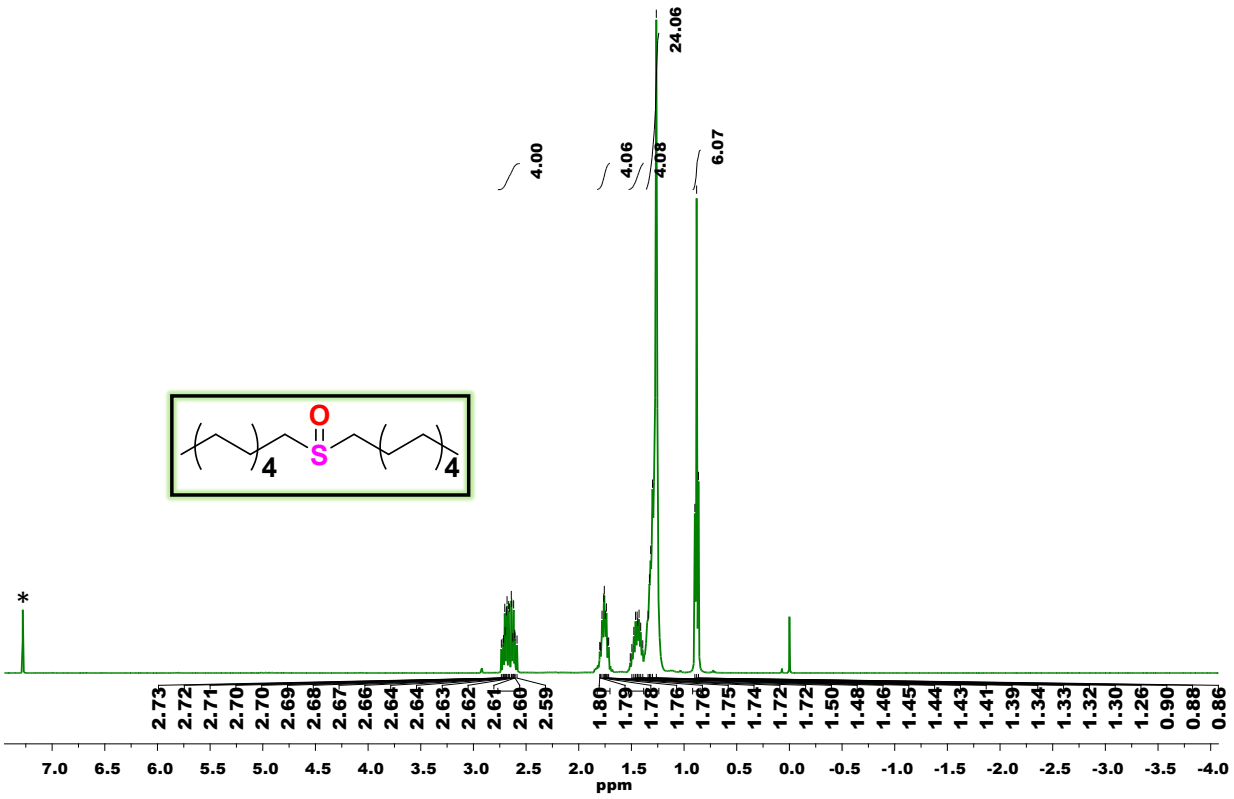

Fig. S109 ^{1}H NMR spectrum of 1-(decylsulfinyl)decane in $CDCl_3$ solvent where * represents the residual solvent and/or adventitious water peaks.

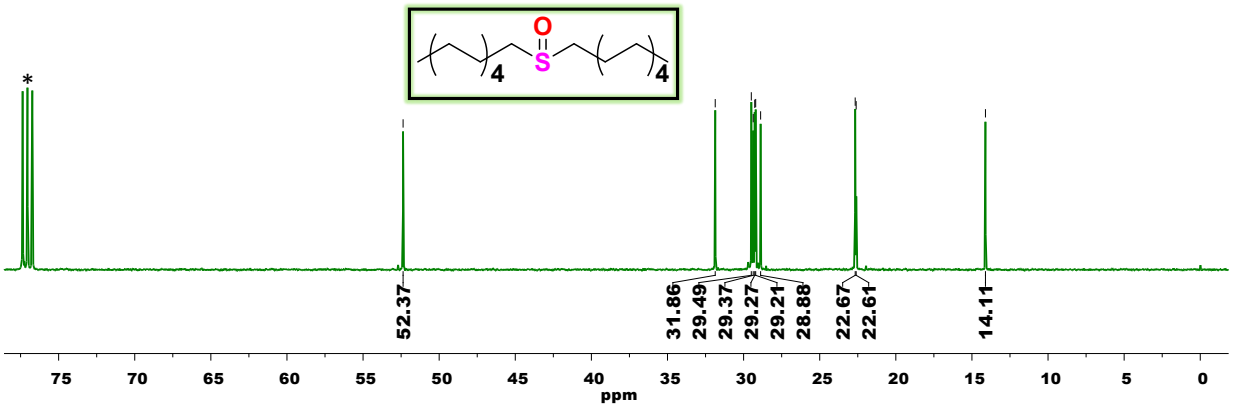

Fig. S110 ^{13}C NMR spectrum of 1-(decylsulfinyl)decane in $CDCl_3$ solvent where * represents the residual solvent and/or adventitious water peaks.

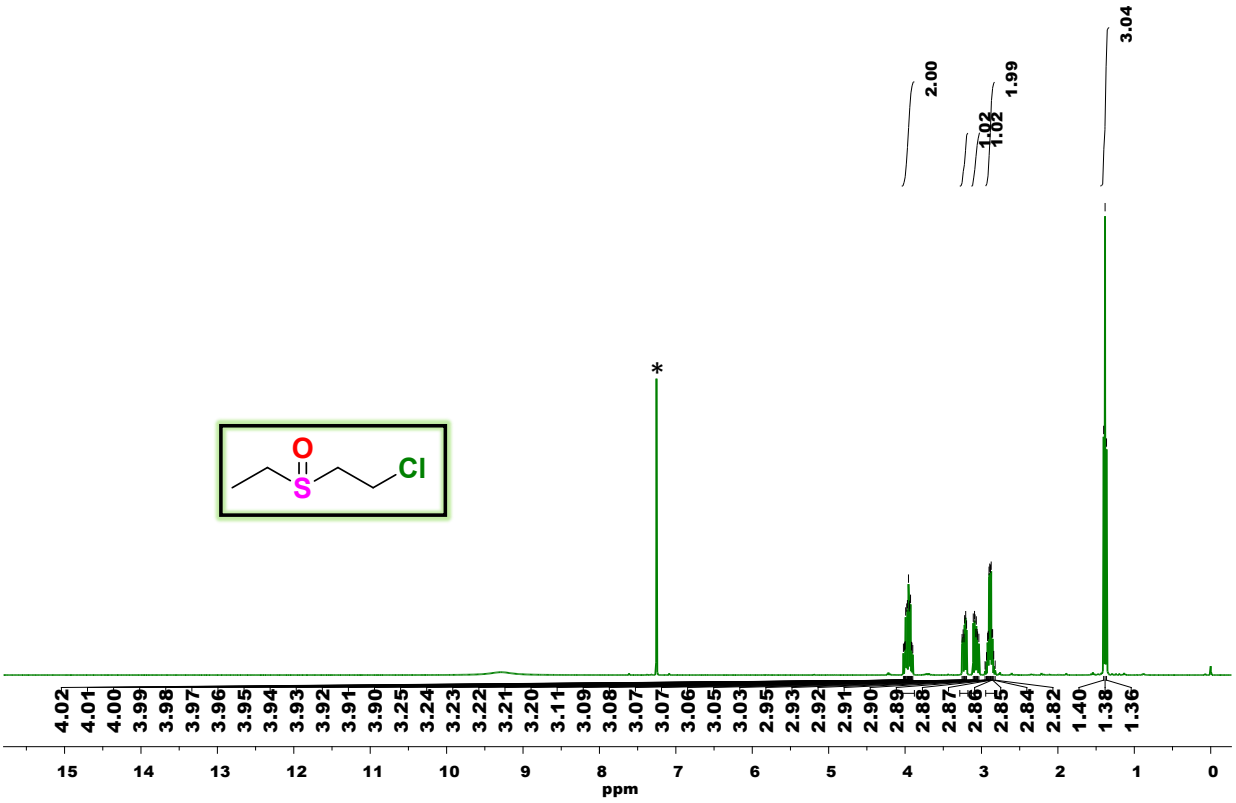

Fig. S111 ^{1}H NMR spectrum of 1-chloro-2-(ethylsulfinyl)ethane in $CDCl_3$ solvent where * represents the residual solvent and/or adventitious water peaks.

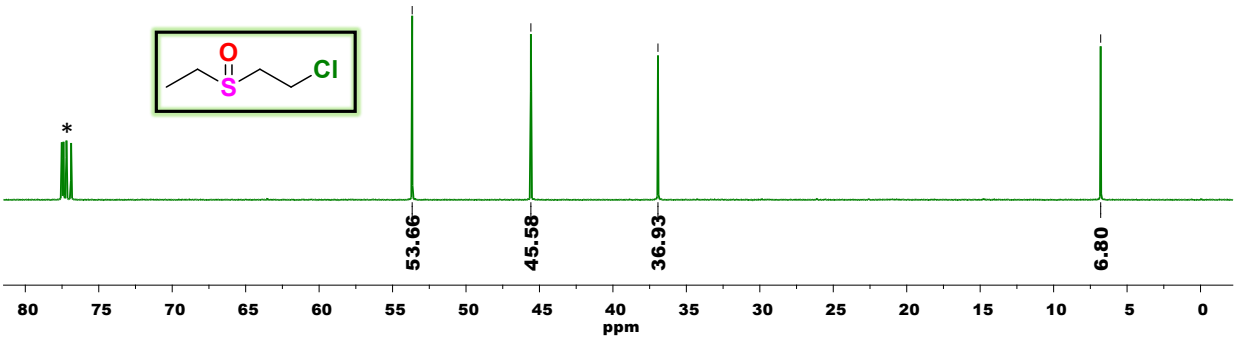

Fig. S112 ^{13}C NMR spectrum of 1-chloro-2-(ethylsulfinyl)ethane in $CDCl_3$ solvent where * represents the residual solvent and/or adventitious water peaks.

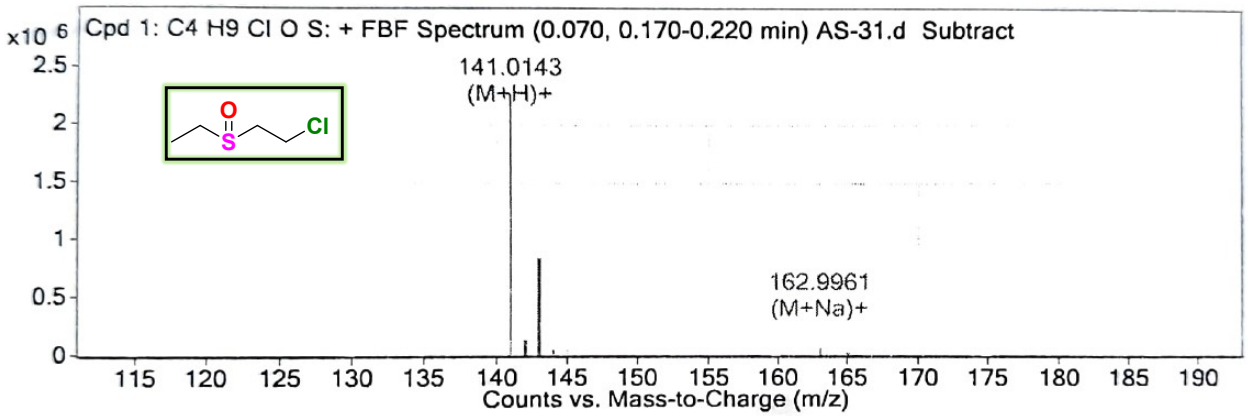

Fig. S113 ESI$^+$-MS spectrum of 1-chloro-2-(ethylsulfinyl)ethane in MeOH.

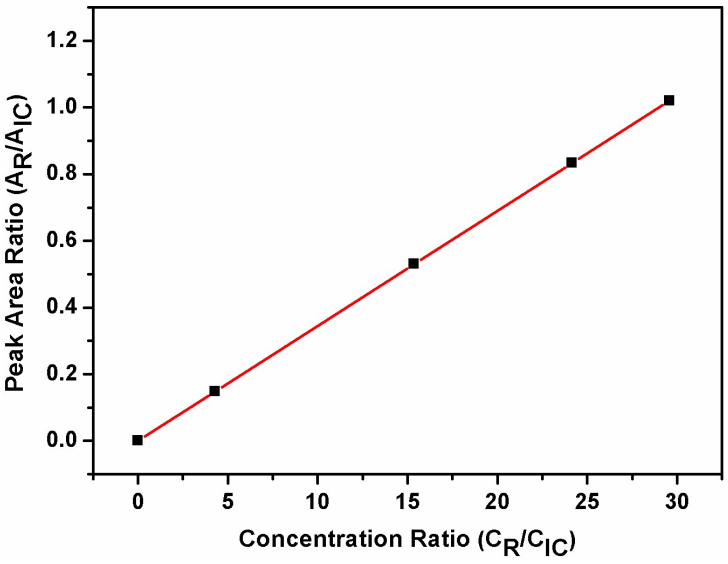

Fig. S114 Calibration plot for the gas chromatographic studies using thioanisole as the substrate and dimethylsulfide as the internal standard, where 'R' represents reactant (thioanisole) and 'IC' refers to internal used (dimethylsulfide).

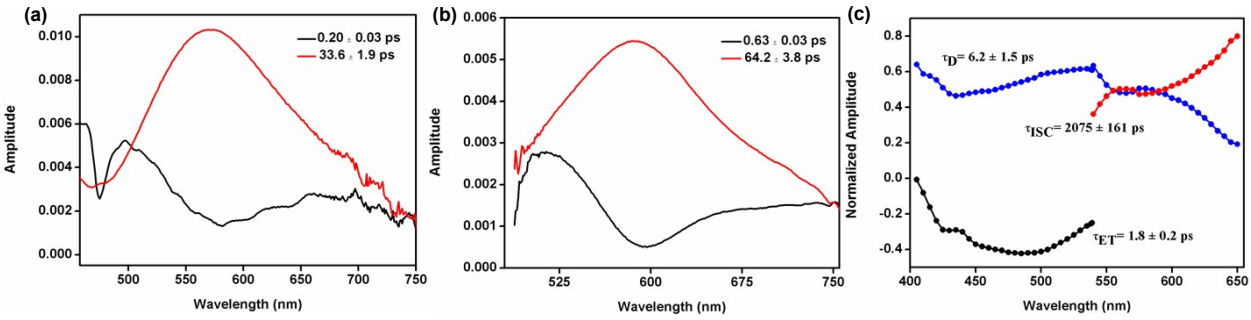

Fig. S115 Global analyses of (a) **L**, (b) **1** and (c) **1-Tb** obtained from the Glotaran and Surface Xplorer software (τ_{ET} = Timescale of electron transfer, τ_D = timescale of intramolecular vibrational relaxation, and τ_{ISC} = timescale of inter-system crossing).

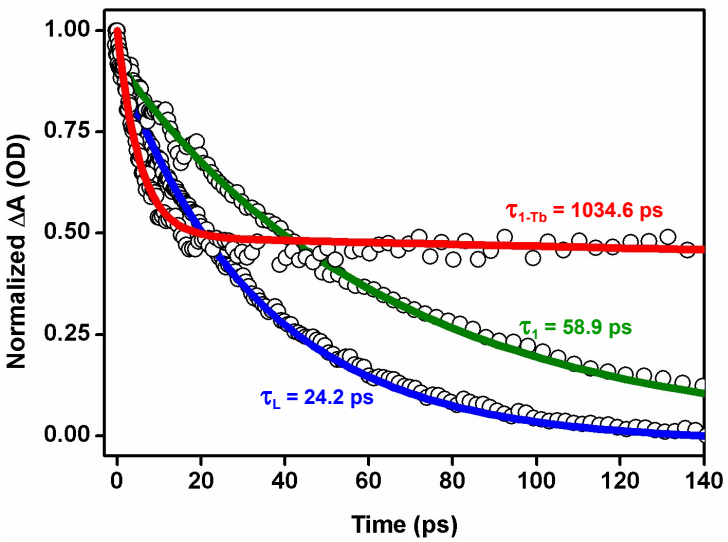

Fig. S116 Combined decay kinetics (probed at the maximum of the excited state absorption spectra) of **L** at 565 nm, **1** at 590 nm and **1-Tb** at 560 nm.

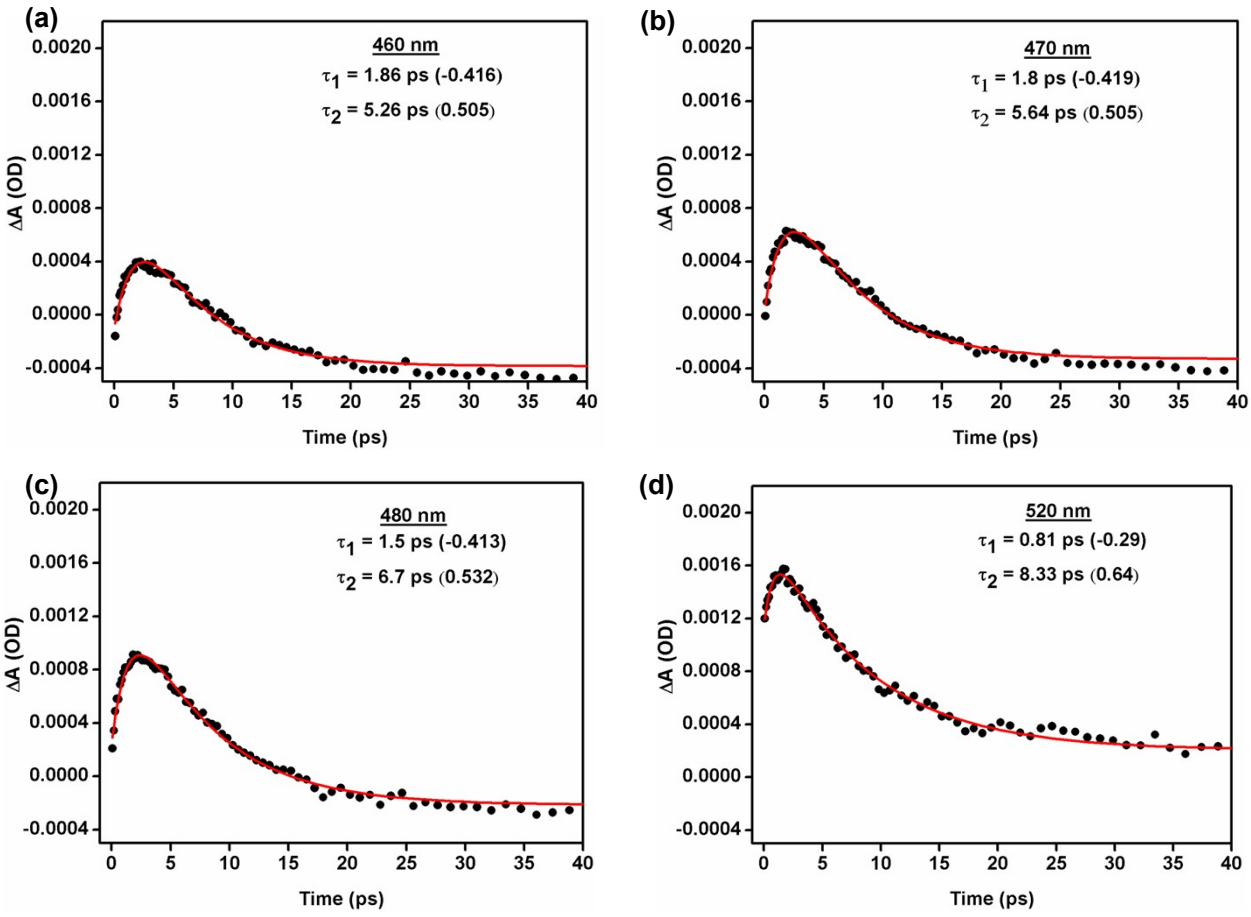

Fig. S117 (a-d) Decay kinetics of **1-Tb** at different probe wavelengths indicating the rise trend.

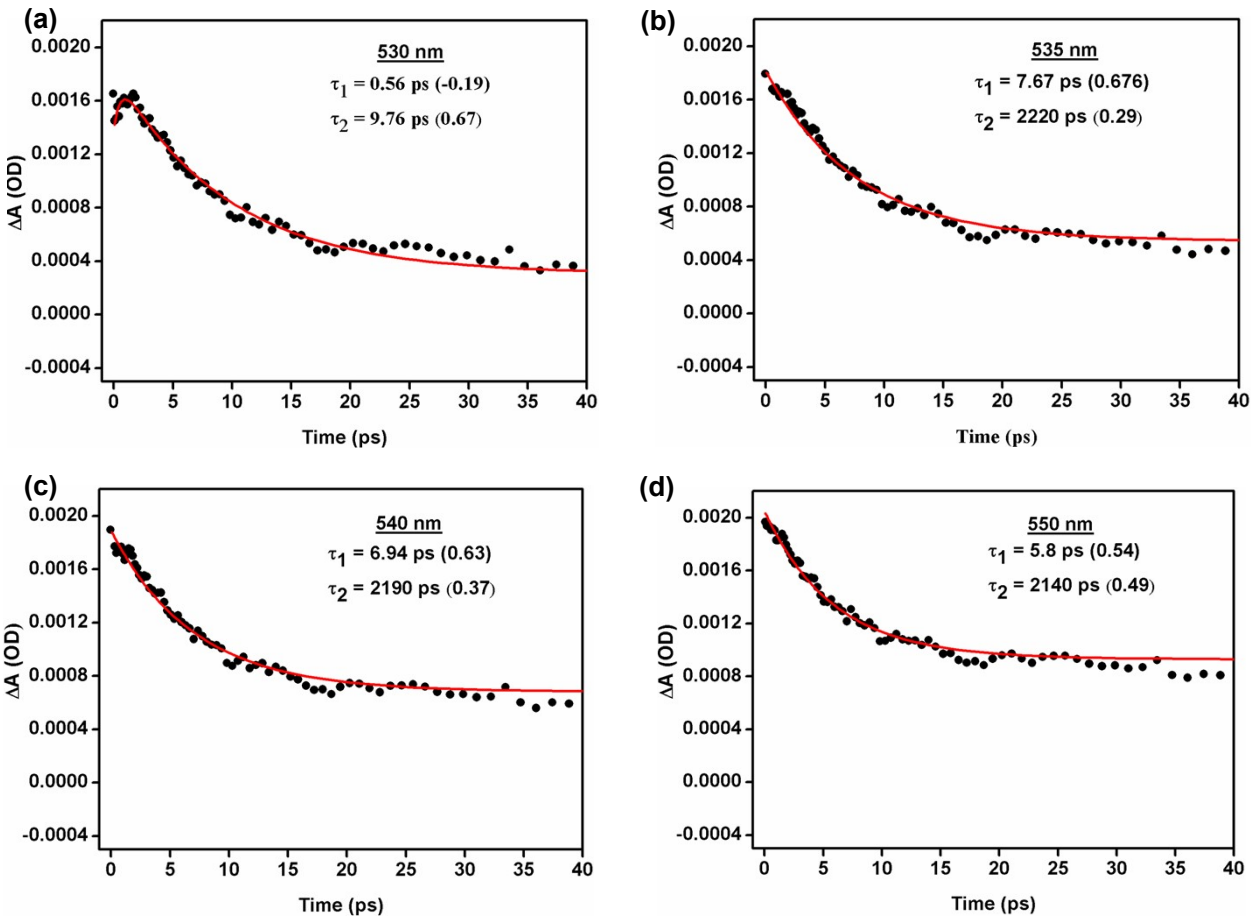

Fig. S118 (a-d) Decay kinetics of **1-Tb** at different probe wavelengths indicating the decay-only trend.

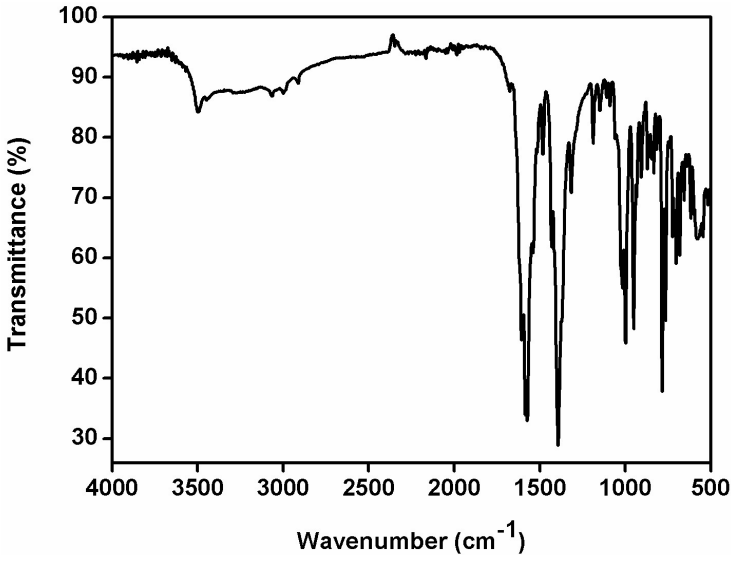

Fig. S119 FTIR spectrum of **1-Zn**.

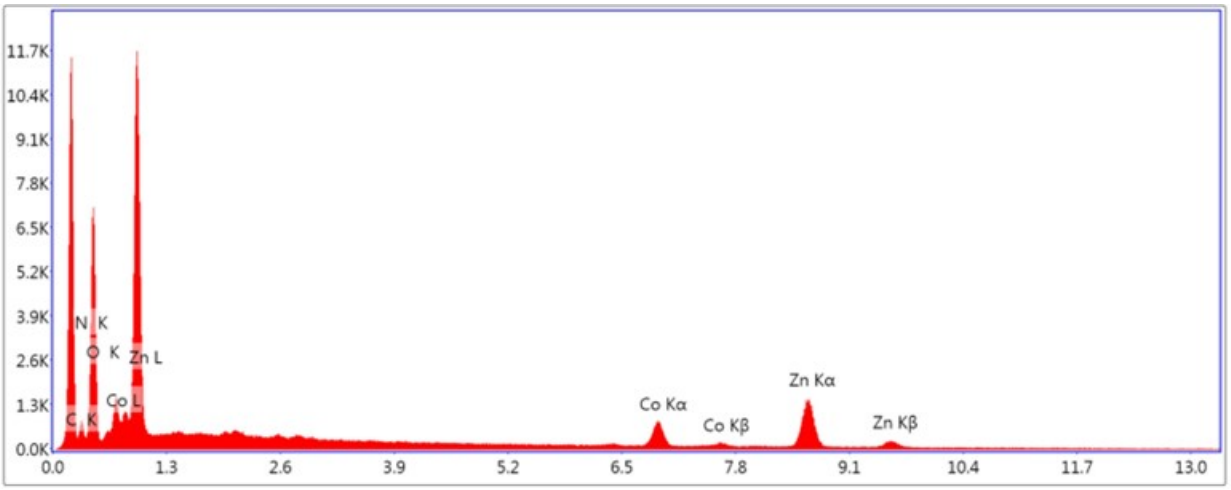

Fig. S120 EDX spectrum of **1-Zn**.

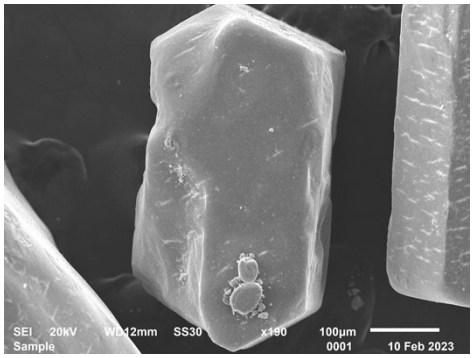

Fig. S121 SEM image of **1-Zn**.

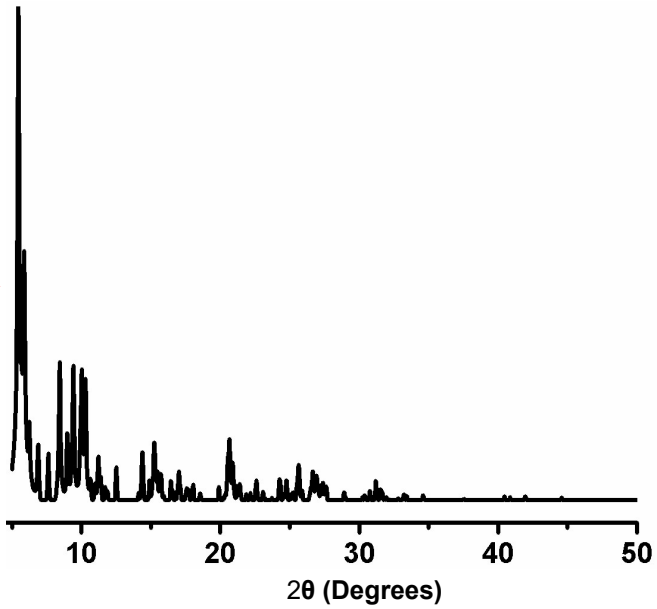

Fig. S122 Powder X-ray diffraction pattern for **1-Zn**.

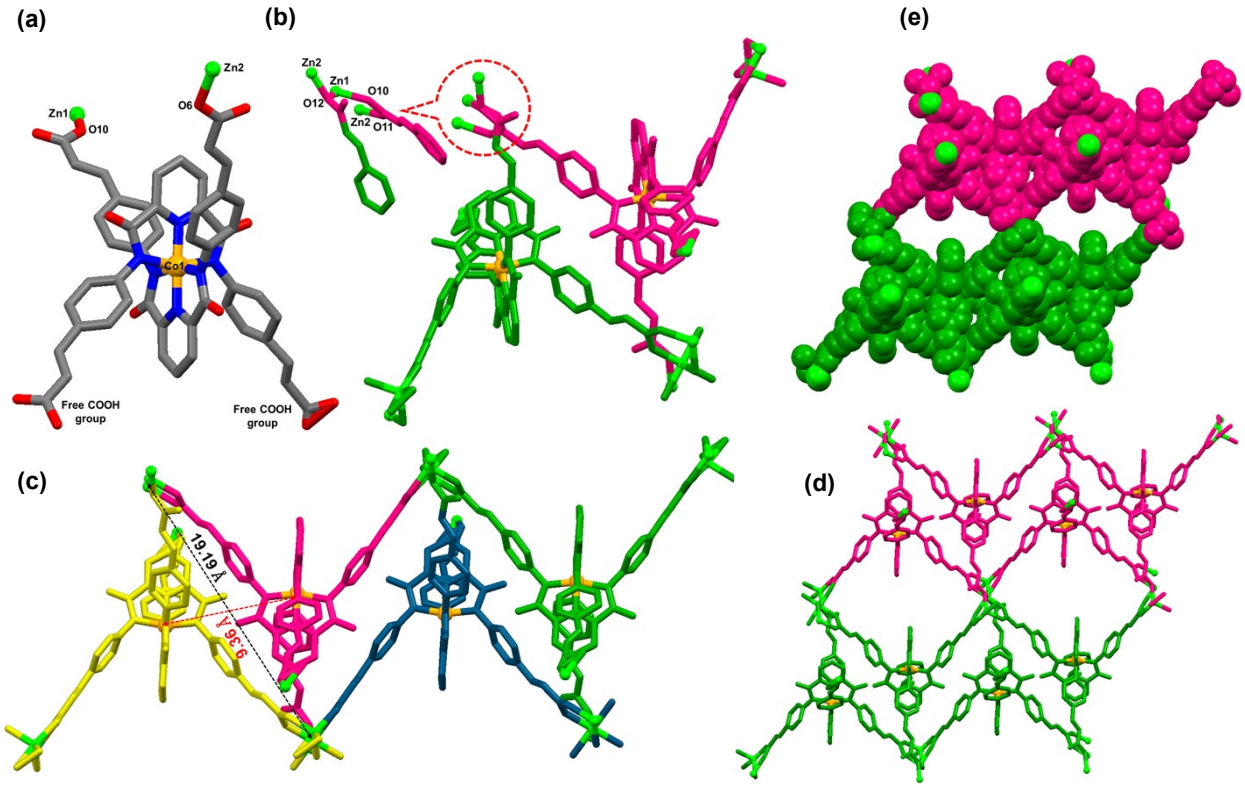

Fig. S123 (a) Stick representation of the preliminary crystal structure of **1-Zn**. Color code: Orange, Co; green, Zn; pink, S; blue, N; red, O; gray, C. Hydrogen atoms and solvent molecules have been omitted for clarity. (b) Preliminary crystal structure of **1-Zn** displaying arrangements of metalloligands (shown in pink and green colors) and Zn^{2+} ions generating a double chain when viewed along *b* axis. (c) Preliminary crystal structure of **1-Zn** displaying arrangements of metalloligands (shown in pink, green, olive and dark blue colors) and Zn^{2+} ions generating the double chains when viewed along *a* axis. (d) A view of 2D network connecting various double chains (shown in pink and green colors). (e) Spacefill diagram of **1-Zn** when viewed along *a* axis.

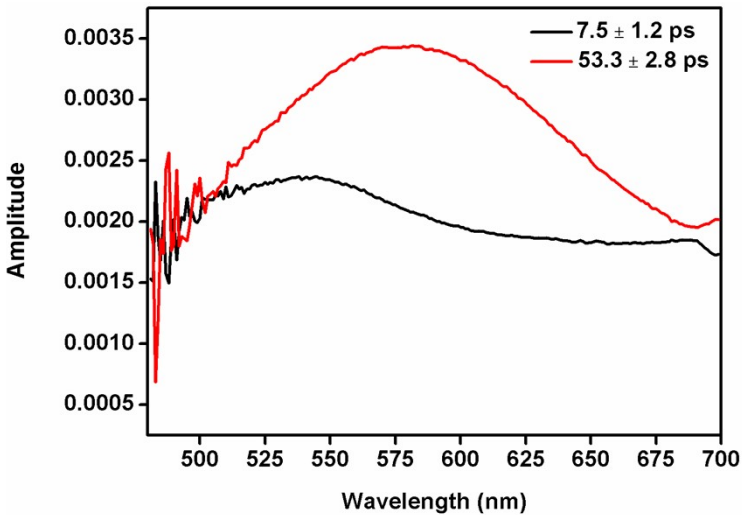

Fig. S124 Global analysis of **1-Zn** obtained from the Glotaran and Surface Xplorer software.

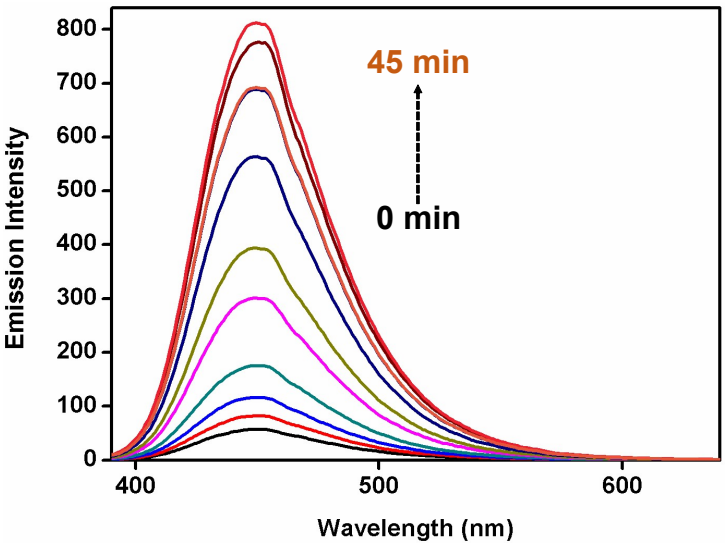

Fig. S125 Emission spectrum for the generation of 7-hydroxycoumarin from coumarin during a photocatalysis experiment in the presence of **1-Zn** under visible light irradiation at different time (0-45 min at an interval of 5 min).

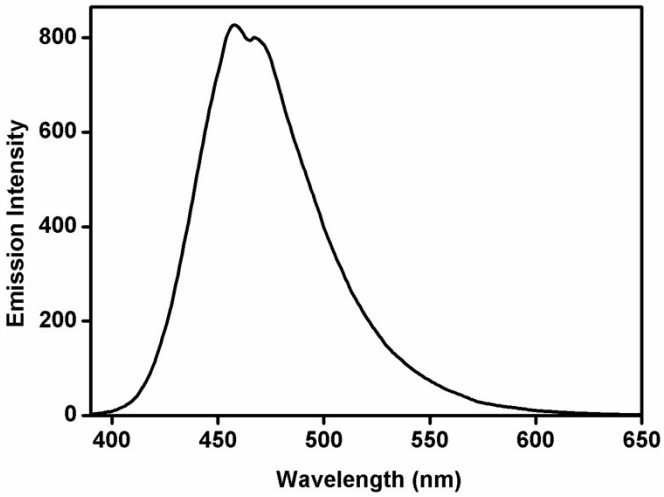

Fig. S126 Emission spectrum of a standard sample of 7-hydroxycoumarin.

Table S1 Crystallographic data collection and structure refinement parameters for **1-Tb** and **1-Eu**.

Coordination Polymer	**1-Tb**	**1-Eu**
Empirical formula	$C_{54}H_{61}CoN_6O_{25}S_2Tb$	$C_{51}H_{41}CoN_6O_{17}SEu$
Formula weight	1476.07	1252.86
Temperature/ K	273.15	298.15
Radiation Wavelength/ Å	0.71073	0.71073
Crystal system	Triclinic	Triclinic
Space group	$P\bar{1}$	$P\bar{1}$
a/ Å	13.609(8)	12.760(10)
b/ Å	13.904(8)	16.813(14)
c/ Å	18.595(11)	17.885(14)
α/°	68.205(2)	64.977(3)
β/°	70.537(2)	78.609(3)
γ/°	81.543(2)	87.398(3)
Volume/ Å^3	3079.7(3)	3405.6(5)
Z	2	2
ρ_{calc}Mg/m^3	1.592	1.222
μ/mm^{-1}	1.563	1.246
F(000)	1502	1262
Crystal size/ mm^3	0.09 x 0.06 x 0.02	0.08 x 0.06 x 0.01
2Θ range for data collection/°	4.416 to 56.746	4.304 to 56.594
Reflections collected	15412	16924
Data/ restraints/ parameters	15370/ 1/ 835	16853/ 0/ 714
Goodness-of-fit on F^2	1.102	1.046
Final *R* indices [I>2sigma(I)]	R_1 = 0.0650, wR_2 = 0.1682	R_1 = 0.0936, wR_2 = 0.2608
R indices (all data)	R_1 = 0.0822, wR_2 = 0.1871	R_1 = 0.1238, wR_2 = 0.2873
Largest diff. peak and hole/ e.Å^{-3}	4.55 and -1.85	7.90 and -2.18
CCDC No.	2288468	2288469

Table S2 Selected bond distances (Å) for **1-Tb**.

Bond	**Distance (Å)**
Tb(1)-O(16)	2.329(5)
Tb(1)-O(6)	2.257(4)
Tb(1)-O(12)^1	2.477(4)
Tb(1)-O(15)	2.421(4)
Tb(1)-O(14)	2.507(5)
Tb(1)-O(4)^2	2.249(4)
Tb(1)-O(11)^1	2.392(4)
Tb(1)-O(13)	2.405(4)
Tb(1)-C(41)^1	2.805(6)
Co(1)-N(3)	1.954(5)
Co(1)-N(4)	1.868(5)
Co(1)-N(2)	1.969(5)
Co(1)-N(6)	1.974(5)
Co(1)-N(5)	1.952(5)
Co(1)-N(1)	1.864(5)

Table S3 Selected bond distances (Å) for **1-Eu**.

Bond	Distance (Å)
Eu(1)-Eu(1)[1]	4.2562(8)
Eu(1)-O(5)	2.479(6)
Eu(1)-O(11)[2]	2.444(6)
Eu(1)-O(11)[3]	2.568(5)
Eu(1)-O(14)	2.451(6)
Eu(1)-O(6)	2.436(6)
Eu(1)-O(12)[3]	2.446(6)
Eu(1)-C(41)[3]	2.890(8)
Eu(1)-O(13)	2.445(7)
Eu(1)-C(32)	2.826(9)
Eu(1)-O(15)	2.427(8)
Co(1)-N(6)	1.968(7)
Co(1)-N(1)	1.858(6)
Co(1)-N(4)	1.854(6)
Co(1)-N(5)	1.936(6)
Co(1)-N(2)	1.959(6)
Co(1)-N(3)	1.948(6)

Table S4 Selected bond angles (°) for **1-Tb**.

Atom-Atom-Atom	Angle (°)
O(16)-Tb(1)-O(12)[1]	80.80(15)
O(16)-Tb(1)-O(15)	143.67(17)
O(16)-Tb(1)-O(14)	127.33(16)
O(16-Tb(1)-O(11)[1]	132.18(15)
O(16)-Tb(1)-O(13)	69.32(16)
O(16)-Tb(1)-C(41)[1]	105.61(17)
O(6)-Tb(1)-O(16)	81.45(16)
O(6)-Tb(1)-O(12)[1]	162.17(16)
O(6)-Tb(1)-O(15)	77.41(15)
O(6)-Tb(1)-O(14)	72.93(17)
O(6)-Tb(1)-O(11)[1]	142.65(16)
O(6)-Tb(1)-O(13)	96.28(17)
O(6)-Tb(1)-C(41)[1]	167.16(17)
O(12)[1]-Tb(1)-O(14)	117.32(16)
O(12)[1]-Tb(1)-C(41)[1]	26.44(16)
O(15)-Tb(1)-O(12)[1]	118.70(15)
O(15)-Tb(1)-O(14)	73.43(16)
O(15)-Tb(1)-C(41)[1]	101.24(16)
O(14)-Tb(1)-C(41)[1]	94.38(17)
O(4)[2]-Tb(1)-O(16)	76.54(16)
O(4)[2]-Tb(1)-O(6)	95.55(17)
O(4)[2]-Tb(1)-O(12)[1]	81.99(15)
O(4)[2]-Tb(1)-O(15)	76.50(17)
O(4)[2]-Tb(1)-O(14)	149.46(16)

O(4)^{2}-Tb(1)-O(11)^{1}	106.80(16)
O(4)^{2}-Tb(1)-O(13)	141.58(16)
O(4)^{2}-Tb(1)-C(41)^{1}	96.54(16)
O(11)^{1}-Tb(1)-O(12)^{1}	53.61(14)
O(11)^{1}-Tb(1)-O(15)	79.21(15)
O(11)^{1}-Tb(1)-O(14)	72.70(16)
O(11)^{1}-Tb(1)-O(13)	84.60(16)
O(11)^{1}-Tb(1)-C(41)^{1}	27.34(16)
O(13)-Tb(1)-O(12)^{1}	75.78(16)
O(13)-Tb(1)-O(15)	141.84(17)
O(13)-Tb(1)-O(14)	68.80(15)
O(13)-Tb(1)-C(41)^{1}	76.78(17)
N(3)-Co(1)-N(2)	163.1(2)
N(3)-Co(1)-N(6)	90.7(2)
N(4)-Co(1)-N(3)	94.8(2)
N(4)-Co(1)-N(2)	102.1(2)
N(4)-Co(1)-N(6)	81.7(2)
N(4)-Co(1)-N(5)	81.2(2)
N(2)-Co(1)-N(6)	92.9(2)
N(5)-Co(1)-N(3)	91.6(2)
N(5)-Co(1)-N(2)	89.8(2)
N(5)-Co(1)-N(6)	162.9(2)
N(1)-Co(1)-N(3)	81.4(2)
N(1)-Co(1)-N(4)	176.0(2)
N(1)-Co(1)-N(2)	81.7(2)
N(1)-Co(1)-N(6)	99.8(2)
N(1)-Co(1)-N(5)	97.4(2)
S(1)-O(16)-Tb(1)	134.1(3)
C(32)-O(6)-Tb(1)	166.1(4)
C(41)-O(12)-Tb(1)^{3}	91.6(4)
C(13)-O(4)-Tb(1)^{2}	164.3(4)
C(6)-N(3)-Co(1)	116.4(4)
C(15)-N(3)-Co(1)	124.3(4)
C(41)-O(11)-Tb(1)^{3}	94.4(3)
C(10)-N(4)-Co(1)	118.5(4)
C(11)-N(4)-Co(1)	119.0(4)
C(24)-N(2)-Co(1)	126.9(4)
C(7)-N(2)-Co(1)	115.0(4)
C(13)-N(6)-Co(1)	114.4(4)
C(33)-N(6)-Co(1)	128.3(4)
C(14)-N(5)-Co(1)	116.1(4)
C(42)-N(5)-Co(1)	122.6(4)
C(3)-N(1)-Co(1)	118.4(4)
C(4)-N(1)-Co(1)	118.4(4)
O(12)-C(41)-Tb(1)^{3}	62.0(3)
O(11)-C(41)-Tb(1)^{3}	58.2(3)
C(40)-C(41)-Tb(1)^{3}	170.1(4)

Table S5 Selected bond angles (°) for **1-Eu**.

Atom-Atom-Atom	Angle (°)
O(5)-Eu(1)-Eu(1)^{1}	72.42(12)
O(5)-Eu(1)-O(11)^{2}	77.56(18)
O(5)-Eu(1)-C(41)^{2}	79.8(2)
O(5)-Eu(1)-C(32)	27.0(2)
O(11)^{2}-Eu(1)-Eu(1)^{1}	31.01(12)
O(11)^{3}-Eu(1)-Eu(1)^{1}	32.78(12)
O(11)^{3}-Eu(1)-O(5)	72.57(19)
O(11)^{3}-Eu(1)-O(11)^{2}	63.79(19)
O(11)^{3}-Eu(1)-O(14)	72.5(2)
O(11)^{3}-Eu(1)-O(12)^{2}	113.6(2)
O(11)^{2}-Eu(1)-C(41)^{2}	25.83(19)
O(11)^{3}-Eu(1)-C(41)^{2}	89.2(2)
O(11)^{3}-Eu(1)-O(13)	143.7(3)
O(11)^{3}-Eu(1)-C(32)	70.8(2)
O(11)^{2}-Eu(1)-C(32)	100.6(2)
O(14)-Eu(1)-Eu(1)^{1}	70.09(15)
O(14)-Eu(1)-O(5)	141.9(2)
O(14)-Eu(1)-O(11)^{2}	73.85(19)
O(14)-Eu(1)-C(41)^{2}	85.1(2)
O(14)-Eu(1)-C(32)	141.1(2)
O(6)-Eu(1)-Eu(1)^{1}	99.96(17)
O(6)-Eu(1)-O(5)	53.21(18)
O(6)-Eu(1)-O(11)^{2}	122.9(2)
O(6)-Eu(1)-O(11)^{3}	74.3(2)
O(6)-Eu(1)-O(14)	128.2(2)
O(6)-Eu(1)-O(12)^{2}	130.4(2)
O(6)-Eu(1)-C(41)^{2}	132.8(2)
O(6)-Eu(1)-O(13)	74.5(3)
O(6)-Eu(1)-C(32)	26.2(2)
O(12)^{2}-Eu(1)-Eu(1)^{1}	81.53(16)
O(12)^{2}-Eu(1)-O(5)	81.4(2)
O(12)^{2}-Eu(1)-O(11)^{2}	51.26(19)
O(12)^{2}-Eu(1)-O(14)	99.2(2)
O(12)^{2}-Eu(1)-C(41)^{2}	25.5(2)
O(12)^{2}-Eu(1)-C(32)	106.8(3)
C(41)^{2}-Eu(1)-Eu(1)^{1}	56.54(16)
O(13)-Eu(1)-Eu(1)^{1}	141.2(2)
O(13)-Eu(1)-O(5)	74.1(3)
O(13)-Eu(1)-O(11)^{2}	121.7(2)
O(13)-Eu(1)-O(14)	143.2(3)
O(13)-Eu(1)-O(12)^{2}	74.7(2)
O(13)-Eu(1)-C(41)^{2}	98.7(2)
O(13)-Eu(1)-C(32)	73.0(3)
C(32)-Eu(1)-Eu(1)^{1}	85.54(17)

O(11)-C(41)-Eu(1)^{4}	62.7(4)
O(12)-C(41)-Eu(1)^{4}	57.0(4)
C(40)-C(41)-Eu(1)^{4}	174.3(6)
O(5)-C(32)-Eu(1)	61.3(4)
O(6)-C(32)-Eu(1)	59.2(4)
C(32)-Eu(1)-C(41)^{2}	106.7(2)
O(15)-Eu(1)-Eu(1)^{1}	130.7(3)
O(15)-Eu(1)-O(5)	141.3(3)
O(15)-Eu(1)-O(11)^{3}	144.9(3)
O(15)-Eu(1)-O(11)^{2}	107.6(3)
O(15)-Eu(1)-O(14)	72.5(3)
O(15)-Eu(1)-O(6)	128.5(3)
O(15)-Eu(1)-O(12)^{2}	74.0(3)
O(15)-Eu(1)-C(41)^{2}	89.6(3)
O(15)-Eu(1)-O(13)	70.9(3)
O(15)-Eu(1)-C(32)	142.2(3)
N(1)-Co(1)-N(6)	100.1(3)
N(1)-Co(1)-N(5)	97.0(3)
N(1)-Co(1)-N(2)	81.7(3)
N(1)-Co(1)-N(3)	81.8(3)
N(4)-Co(1)-N(6)	81.4(3)
N(4)-Co(1)-N(1)	178.4(3)
N(4)-Co(1)-N(5)	81.5(3)
N(4)-Co(1)-N(2)	99.0(3)
N(4)-Co(1)-N(3)	97.6(3)
N(5)-Co(1)-N(6)	162.9(3)
N(5)Co(1)-N(2)	89.9(3)
N(5)-Co(1)-N(3)	92.2(3)
N(2)-Co(1)-N(6)	93.0(3)
N(3)-Co(1)-N(6)	89.8(3)
N(3)-Co(1)-N(2)	163.5(3)
C(32)-O(5)-Eu(1)	91.7(5)
Eu(1)^{3}-O(11)-Eu(1)^{4}	116.21(19)
C(41)-O(11)-Eu(1)^{4}	91.5(5)
C(41)-O(11)-Eu(1)^{3}	150.2(5)
C(32)-O(6)-Eu(1)	94.6(5)
C(13)-N(6)-Co(1)	116.0(5)
C(33)-N(6)-Co(1)	125.0(5)
C(3)-N(1)-Co(1)	118.8(5)
C(4)-N(1)-Co(1)	118.7(5)
C(10)-N(4)-Co(1)	118.1(5)
C(11)-N(4)-Co(1)	118.7(5)
C(42)-N(5)-Co(1)	123.3(5)
C(31)-C(32)-Eu(1)	179.7(7)
S(1)-O(15)-Eu(1)	140.2(7)
C(14)-N(5)-Co(1)	117.0(5)
C(24)-N(2)-Co(1)	123.0(5)
C(7)-N(2)-Co(1)	115.6(5)

C(41)-O(12)-Eu(1)[4]	97.4(5)
C(15)-N(3)-Co(1)	122.8(5)
C(6)-N(3)-Co(1)	116.0(5)

Table S6 Kinetic parameters for the photo-oxidation of 1,5-dihydroxynapthalene in the presence of different photocatalysts and the present Ln-MOF **1-Tb**.

Entry	Photocatalyst	$k \times 10^{-2}$ (min^{-1})	Reference
1	Ir-1	0.62	9
2	Ir-2	0.95	9
3	Ir-3	3.05	9
4	Ir-4	2.40	9
5	CTC-1	1.50	15
6	**1-Tb**	**5.42**	**This work**

Table S7 Comparison of photo-oxidation of benzyl alcohol with different photocatalysts and the present Ln-MOF **1-Tb**.

Entry	Photocatalyst	Time (h)	Yield (%)	Conditions/Remarks	Reference
1	Cu(I)W−DPNDI	16	75	EtOH/H_2O, H_2O_2	16
2	Pt/PCN-224(Zn)	0.83	99	H_2O, O_2	8
3	Pt/PCN-224(Ni)	1	97	H_2O, O_2	8
4	Pt/PCN-224(Co)	1	83	H_2O, O_2	8
5	Pt/PCN-224(Mn)	1	81	H_2O, O_2	8
6	0.1%Cu@UiO-66	3	50	MeCN, O_2, low conversion	17
7	Zn-OFDC	12	90	DMSO, O_2, low conversion with other substrates	18
8	Bi-TATB	5	38	Hexane, O_2, low conversion	19
9	**1-Tb**	**0.25**	**99**	**H_2O, O_2**	**This work**

Table S8 Control experiments for the photocatalytic oxidation of thioanisole.

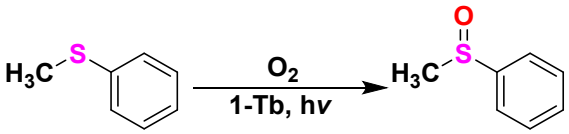

Entry[a]	Solvent	Isolated Yield (%)
1	DMF	62
2	CH_3CN	68
3	THF	78
4	H_2O	84
5	MeOH-H_2O	92
6	**CH_3OH**	**>99**
7	C_2H_5OH	>99

[a]Reaction conditions: thioanisole (0.80 mmol), photocatalyst (1 mol%), MeOH (2 mL), temperature (25 ºC).

Table S9 Comparison of photo-oxidation of thioanisole with different photocatalysts and the present Ln-MOF **1-Tb**.

Entry	Photocatalyst	Time (h)	Yield (%)	Remarks	Reference
1	CTC-1	8	99	EtOH/H_2O, air	15
2	$Ir(ppy)_3$	8	7	EtOH/H_2O, air	15
3	Oxidized g-C_3N_4 (CNO)	8	99	MeCN, O_2	20
4	Zr-TCA	10	100	MeOH, air, low selectivity with other substrates	21
5	CPOP-29	10	99	MeOH/air	22
6	**1-Tb**	**0.25**	**99**	**MeCN, O_2**	**This work**

Table S10 The bi-exponential fitting parameters of decay kinetics probed at a single wavelength (at maximum of the excited state absorption spectra) of **L**, **1**, **1-Tb** and **1-Zn**.

Component	a_1	τ_1 (ps)	a_2	τ_2 (ps)	τ_{av} (ps)
L	0.28	0.22	0.72	34.0	24.5
1	0.09	0.48	0.91	64.2	58.9
1-Tb	0.52	5.34	0.48	2150.0	1034.6
1-Zn	0.33	7.94	0.67	52.9	38.1

References

1. T. Ghosh, Reductive Heck Reaction: An Emerging Alternative in Natural Product Synthesis, *ChemistrySelect*, 2019, **4**, 4747–4755.
2. CrysAlisPro, v 1.171.33.49b, Oxford Diffraction Ltd., 2009.
3. L. Farrugia, WinGX, version 1.80.05, University of Glasgow: Glasgow, Scotland, 2009.
4. O. V. Dolomanov, L. J. Bourhis, R. J. Gildea, J. A. K. Howard and H. Puschmann, OLEX2: A Complete Structure Solution, Refinement and Analysis Program, *J. Appl. Cryst.*, 2009, **42**, 339–341.
5. H. Zhao, Q. Xia, H. Xing, D. Chen and H. Wang, Construction of Pillared-Layer MOF as Efficient Visible-Light Photocatalysts for Aqueous Cr(VI) Reduction and Dye Degradation, *ACS Sustain. Chem. Eng.*, 2017, **5**, 4449–4456.
6. V. Leandri, J. M. Gardner and M. Jonsson, Coumarin as a Quantitative Probe for Hydroxyl Radical Formation in Heterogeneous Photocatalysis, *J. Phys. Chem. C*, 2019, **123**, 6667–6674.

7. R. Liu, S. Fu, H. Zhan and L. A. Lucia, General Spectroscopic Protocol to Obtain the Concentration of the Superoxide Anion Radical, *Ind. Eng. Chem. Res.*, 2009, **48**, 9331–9334.

8. Y.-Z. Chen, Z. U. Wang, H. Wang, J. Lu, S.-H. Yu and H.-L. Jiang, Singlet Oxygen-Engaged Selective Photo-Oxidation over Pt Nanocrystals/Porphyrinic MOF: The Roles of Photothermal Effect and Pt Electronic State. *J. Am. Chem. Soc.*, 2017, **139**, 2035–2044.

9. J. Sun, J. Zhao, H. Guo and W. Wu, Visible-Light Harvesting Iridium Complexes as Singlet Oxygen Sensitizers for Photooxidation of 1,5-Dihydroxynaphthalene, *Chem. Commun.*, 2012, **48**, 4169–4171.

10. W. Huang, B. C. Ma, H. Lu, R. Li, L. Wang, K. Landfester and K. A. I. Zhang, Visible-Light-Promoted Selective Oxidation of Alcohols Using a Covalent Triazine Framework, *ACS Catal.*, 2017, **7**, 5438–5442.

11. Y. Wei, J. Zhang, Q. Zheng, J. Miao, PedroJ. J. Alvarez and M. Long, Quantification of Photocatalytically-Generated Hydrogen Peroxide in the Presence of Organic Electron Donors: Interference and Reliability Considerations. *Chemosphere*, 2021, **279**, 130556.

12. Z.-H. Yan, M.-H. Du, J. Liu, S. Jin, C. Wang, G.-L. Zhuang, X.-J. Kong, L.-S. Long and L.-S. Zheng, Photo-Generated Dinuclear $\{Eu(II)\}_2$ Active Sites for Selective CO_2 Reduction in a Photosensitizing Metal-Organic Framework. *Nat. Commun.*, 2018, **9**, 3353.

13. I. H. M. Van Stokkum, D. S. Larsen and R. Van Grondelle, Global and Target Analysis of Time-Resolved Spectra. *Biochim et Biophy Acta- Bioenerg.,* 2004, **1657**, 82–104.

14. C. Consani, O. Bräm, F. Van Mourik, A. Cannizzo and M. Chergui, Energy Transfer and Relaxation Mechanisms in Cytochrome c. *Chem Phys*, 2012, **396**, 108–115.

15. R.-Q. Xia, J. Zheng, R.-J. Wei, J. He, D.-Q. Ye, M.-D. Li, G.-H. Ning and D. Li, Strong Visible Light-Absorbing BODIPY-Based Cu(I) Cyclic Trinuclear Sensitizer for Photocatalysis. *Inorg. Chem. Front.*, 2022, **9**, 2928–2937.

16. C. Si, X. Liu, T. Zhang, J. Xu, J. Li, J. Fu and Q. Han, Constructing a Photocatalyst for Selective Oxidation of Benzyl Alcohol to Benzaldehyde by Photo-Fenton-like Catalysis. *Inorg. Chem.*, 2023, **62**, 4210–4219.

17. L. Xiao, Q. Zhang, P. Chen, L. Chen, F. Ding, J. Tang, Y.-J. Li, C.-T. Au and S.-F. Yin, Copper-Mediated Metal-Organic Framework as Efficient Photocatalyst for the Partial Oxidation of Aromatic Alcohols under Visible-Light Irradiation: Synergism of Plasmonic Effect and Schottky Junction. *Appl. Catal., B*, 2019, **248**, 380–387.

18. Z. Wang, L. Zeng, C. He and C. Duan, Photocatalytic C–H Activation with Alcohol as a Hydrogen Atom Transfer Agent in a 9-Fluorenone Based Metal–Organic Framework. *ACS Appl. Mater. Interfaces*, 2021, **13**, 25898–25905.

19. R. Zhang, Y. Liu, Z. Wang, P. Wang, Z. Zheng, X. Qin, X. Zhang, Y. Dai, M.-H. Whangbo and B. Huang, Selective Photocatalytic Conversion of Alcohol to Aldehydes by Singlet Oxygen over Bi-Based Metal-Organic Frameworks under UV–Vis Light Irradiation. *Appl. Catal., B*, 2019, **254**, 463–470.

20. H. Wang, S. Jiang, S. Chen, D. Li, X. Zhang, W. Shao, X. Sun, J. Xie, Z. Zhao, Q. Zhang, Y. Tian and Y. Xie, Enhanced Singlet Oxygen Generation in Oxidized Graphitic Carbon Nitride for Organic Synthesis. *Adv. Mater.*, 2016, **28**, 6940–6945.

21. D. Zhang, X.-N. Zou, X.-G. Wang, J. Su, T.-X. Luan, W. Fan, P.-Z. Li and Y. Zhao, Highly Effective Photocatalytic Radical Reactions Triggered by a Photoactive Metal–Organic Framework. *ACS Appl. Mater. Interfaces*, 2022, **14**, 23518–23526.

22. H.-P. Liang, Q. Chen and B.-H. Han, Cationic Polycarbazole Networks as Visible-Light Heterogeneous Photocatalysts for Oxidative Organic Transformations. *ACS Catal.*, 2018, **8**, 5313–5322.